Doctor of Engineering

Advanced diseases diagnostic platform using cost-affordable functional biomaterials

The Graduate School
of the University of Ulsan

Department of Medical Science
Bonhan Koo

Advanced diseases diagnostic platform using cost-affordable functional biomaterials

Supervisor: Sung-Han Kim

A Dissertation

Submitted to
the Graduate School of the University of Ulsan
In partial Fulfillment of the Requirements
for the Degree of

Doctor of Engineering

by

Bonhan Koo

Department of Medical Science
University of Ulsan, Republic of Korea
August 2021

Advanced diseases diagnostic platform using cost-affordable functional biomaterials

This certifies that the dissertation

of Bonhan Koo is approved.

Committee Chair Dr. Jun Ki Kim

Committee Member Dr. Sung-Han Kim

Committee Member Dr. In Kyong Shim

Committee Member Dr. Eunsung Jun

Committee Member Dr. Yong Shin

Department of Medical Science
University of Ulsan, Republic of Korea
August 2021

ABSTRACT

Background

A rapid and accurate disease diagnosis based on identifying cancer and emerging infectious diseases is essential for preventing further infection, monitoring patients, and proper treatment. In particular, since individual symptom patterns are different depending on the severity of cancer mutations and infections, it is necessary to accurately diagnose diseases and proceed with treatment optimized for each patient. Recently, various diagnostic methods were reported for better diagnostics, but most of these techniques are time-consuming, complex, require large equipment, low sensitivity, and lack multiple-target detection specificity. To overcome these limitations, we reported sample preparation platform using cost-affordable functional biomaterials and advanced bio-optical sensing platform.

Method

In Section 1, sample preparation platform using cost-affordable functional biomaterials, we reported a rapid and simple cfNAs sampling using bio-composite and microfluidic platform, and pathogen enrichment/NAs extraction using microfluidic platform. We analyzed a total of 366 clinical samples for sample preparation; cfDNA sampling using 13 blood plasma samples consisting of 3 colorectal and 10 pancreatic cancers in bio-composite platform, cfDNA sampling using 81 blood plasma samples consisting of 34 confirmed TB, 6 probable TB, and 41 not TB, and pathogen enrichment/DNAs extraction using 272 oral swab samples consisting of 128 TB and 144 not TB.

In Section 2, advanced bio-optical sensing platform, we reported SMR biosensor based on an isothermal, label-free, one-step DNA/RNA amplification and detection, improved bio-optical sensing platform by combining CRISPR/dCas9, and novel arch-shaped multiple-target sensing. We analyzed a total of 61 clinical samples for bio-optical sensing; 35 blood plasma samples consisting of 16 Q fever and 19 other febrile diseases patients in SMR biosensor, 6 blood plasma samples consisting of 3 ST and 3 SFTS patients in

CRISPR/dCas9-mediated biosensor, and 20 nasopharyngeal samples consisting of 11 MERS-CoV and 9 HCoV patients.

Result

In sample preparation, the bio-composite platform showed high capture efficiency (86.78–90.26%) with genomic DNA and amplified DNA products (777, 525 and 150 bp). The bio-composite platform allowed the isolation of high purity and quantity cfDNA from the blood plasma of 13 cancer patients (3 colorectal and 10 pancreatic cancer samples) without requiring a lysis step and special equipment. The cfDNA sampling in microfluidic platform showed high sensitivity (80.0%) and specificity (78.1%) using the blood plasma of 34 confirmed TB, 6 probable TB, and 41 not TB. These results showed that the sensitivity of cfDNA is higher than acid-fast bacilli microscopy (31.6%), Xpert MTB/RIF (61.1%), and mycobacterial culture (65.8%) results. While the sensitivity and specificity of cfDNA were similar with those of IGRA (sensitivity 80.6% and specificity 71.4%), the combined sensitivity and specificity of the two assays was 94.4% and 64.3%, respectively, which can be used to rule out TB. The pathogen enrichment/DNA extraction showed high sensitivity (65.6%) and specificity (86.1%) using the oral swab of 128 TB and 144 not TB. These results showed that the sensitivity of DNA is higher than sputum-based Xpert MTB/RIF (sensitivity 43.4% and specificity 100%).

In bio-optical sensing, the SMR biosensor showed high sensitivity (87.5%) and specificity (89.5%) using the blood plasma of 16 Q fever and 19 other febrile diseases within 10 min. By using CRISPR/dCas9-mediated biosensor, these results showed single molecule sensitivity for the detection of ST (0.54 aM) and SFTS (0.63 aM); this sensitivity is 100 times more sensitive than that of real-time PCR. The CRISPR/dCas9-mediated biosensor allowed the clearly distinguish between ST and SFTS in plasma samples within 20 min. The arch-shaped multiple-target biosensor showed high sensitivity with T7 RNA of MERS (10 copies), ZIKV (100 copies), EBOV (10 copies), and HCoV (10 copies) and simultaneously distinguished between Middle East respiratory syndrome and human coronavirus in clinical specimens within 20 min.

Conclusion

In this study, advanced diseases diagnostic platform using cost-affordable functional biomaterials was proposed. This platform consists of two sections of sample preparation using bio-composite and microfluidic chip, and bio-optical sensing using SMR biosensor, CRISPR/dCas9-mediated biosensor, and arch-shaped multiple-target biosensor. We expect that these techniques can provide rapid, sensitive, and accurate diagnoses of cancer and emerging infectious diseases in clinical applications.

CONTENTS

LIST OF FUGURES

Chapter 6. CRISPR/dCas9-mediated bio-optical sensor

Chapter 7. Arch-shaped multiple-target bio-optical sensor

LIST OF TABLES

ABBREVIATIONS

AD	Amine-modified diatomaceous earth
AFB	Acid-fast bacilli
APDMS	3-aminopropyl(diethoxy)methylsilane
APTES	3-aminopropyltriethoxysiane
BRC	Bio Resource Center
CB[6]	Cucurbit[6]uril
cfDNA	Cell-free DNA
cfNA	Cell-free nucleic acid
CRC	Colorectal cancer
CRISPR	Combining a RNA-guided clustered regularly interspaced short palindromic repeats
CRISPR/dCas9	Combining a RNA-guided clustered regularly interspaced short palindromic repeats/inactivated Cas9 protein
CSF	Cerebrospinal fluid
CT	Chest computed tomography
C_T	Cycle threshold
CTC	Circulating tumor cell
ctDNA	Circulating tumor DNA
dCas9	Catalytically inactivated Cas9 protein
DE	Diatomaceous earth
DMP	Dimethyl pimelimidate dihydrochloride
dNTP	Deoxynucleotide triphosphate
DTBP	Dimethyl 3,3′-dithiopropionimidate dihydrochloride
DTT	Dethiothreitol
EBOV	Ebola virus
EDTA	Ethylenediaminetetraacetic acid
ELISA	Enzyme-linked immunosorbent assay
EMSA	Electrophoretic mobility shift assay
EtBr	Ethidium bromide
FT-IR	Fourier transform-infrared spectroscopy
GAD	Glutaraldehyde

gRNA	Guide RNA
HCoV	Human coronavirus
HDP	High-density plasma
HI	Homobifunctional imidoester
HIV	Human immunodeficiency virus
IFA	Immunofluorescence assay
IGRA	Interferon-gamma releasing assay
IL	Insertion loss
IPTG	Isopropyl β-d-1-thiogalactopyranoside
IRB	Institutional Review Board
KatG	Catalase-peroxidase
LB	Luria-Bertani
LTBI	Latent TB infection
MERS	Middle East respiratory syndrome
MgAc	Magnesium acetate
MTB	Mycobacterium tuberculosis
NTA	Ni-nitrilotriacetic acid
NTM	Nontuberculous mycobacterium
PAM	Protospacer adjacent motif
POCT	Point-of-care testing
RBC	Red blood cells
RDT	Rapid diagnostic testing
RNP	Ribonucleoprotein
RPA	Recombinase polymerase amplification
RPA-RT	RPA-reverse transcription
SDS	Sodium dodecyl sulfate
SEM	Scanning electron microscope
SFTS	Severe fever with thrombocytopenia syndrome
sgRNA	Single guide RNA
SMR	Silicon microring resonator
SOI	Silicon on insulator
ST	Scrub typhus
T7 RNA	T7 in vitro transcribed RNA

TB	Tuberculosis
TEC	Thermoelectric cooler
UV	Ultraviolet
WHO	World Health Organization
ZIKV	Zika virus

INTRODUCTION

Today, despite outstanding and various advances in the medical field, our world is still vulnerable to various diseases. Cancer is the second leading cause of death worldwide, and the prevalence and cancer-related mortality rates are increasing. In addition, cancer is a complicated heterogeneous disease with unique genomic and protein characteristics between individual patients, tumor sites, and cancer types. Infectious diseases are caused by living pathogens such as bacteria, viruses, and parasites. They can be quickly transmitted and infected between human or animal carriers by direct contact and airborne infectious agents. Recently, since newly emerging infectious diseases are increasing, rapid diagnosis and appropriate response are essential.

Diagnostic tests for cancer and emerging infectious diseases are commonly performed in local hospitals and large laboratories. Sample concentration phenomenon to these centralized facilities is time-consuming due to sample delivery and waiting for orders. In addition, rather than reactive medicine that aims to treat patients, it is developing into preventive medicine and personalized medicine focusing on prevention, early diagnosis, and disease monitoring. These changes can provide timely diagnostic information for better diagnosis and treatment decisions by detection an increasingly diverse cancer and infectious disease in the patient setting.

We are developing platforms for diagnosing early and accurate cancer and infectious diseases using various clinical specimens. Especially, we are focus on a POCT following the WHO guidelines (ASSURED: affordable, sensitive, specific, user friendly, rapid and robust, equipment-free, and deliverable). It is an emerging theme for global health that is gradually integrated into the modern medical field. POCT has been developed in many applications by providing decentralized diagnostics in a patient-centered resource-efficient manner at low cost. In this study, advanced diseases diagnostic platform using cost-affordable functional biomaterials was proposed that nearly meets the WHO guidelines for use as a POCT device and complements the limitations of existing diagnostic methods.

SECTION 1.

Sample preparation platform using cost-affordable functional biomaterials

Chapter 1. General information for sample preparation

1.1. Significance and goal of study

The diagnosis and monitoring of cancer and infectious diseases using liquid biopsy samples is an emerging field in diagnostics because it can overcome the limitations of conventional tissue biopsy sampling, including its invasive nature, risks, and difficult reproducibility [1-3]. Liquid biopsy samples also provide important information on genomic mutations, tumor burden, extend of infection and drug resistance [1-4].

Among several biomarkers in liquid biopsy samples, cell-free nucleic acids (cfNAs), which were first described in 1948, are released to the blood or other body fluids, and are important biomarkers for clinical diagnosis [5, 6]. In cancer diagnosis, circulating tumor DNAs (ctDNAs) are small DNA fragments derived from tumor tissues and tumor necrosis, which yield DNAs of varying sizes in contrast to uniform DNAs resulting from apoptosis of normal cells [7-9]. Cell-free DNA (cfDNA) exists at low concentrations of approximately 3–22 ng per 1 mL in plasma. The ratio of ctDNA to cfDNA varies from extremely low (< 0.01%) to high (60%), according to tumor type and stage [10-12]. Although the concentration of cfDNA is higher in cancer and infectious diseases patients due to tumor necrosis and apoptosis of infected macrophages than in healthy controls, the development of efficient isolation techniques to obtain high quality cfDNA in sufficient quantities is important [13-15]. In addition, contamination of gDNA derived from normal cells in the plasma can occur upon isolation of cfDNA, and reduces the sensitivity and specificity of ctDNA detection.

Circulating tumor cells (CTCs) and infectious pathogens are present in liquid biopsy samples of cancer and infectious diseases patients, and they exist in various concentrations depending on the progress of the patient as is cfNAs. In general, clinically distinct patients contain high concentration of CTC and infectious agent in the blood or other body fluids.

However, early diagnosis of cancer and infectious diseases is difficult and there is a limit to detection using CTCs and infectious agents in a limited volume of samples.

Recently, novel cfNAs and NAs extraction techniques based on spin columns and magnet beads were recently developed [16-18]. However, these methods require limited sample volume and special equipment such as a centrifuge, vacuum pump, thermo–regulator, and specific component to trigger the next step. Moreover, the limited volume leads to low sensitivity by reducing the chance of detecting low concentration of pathogen, and use of cell lysis buffer, which increases the yield of nucleic acids for cfNAs extraction, can amplify the genetic background of noncancerous cells.

Here, the sample preparation platform using cost-affordable functional biomaterials for cfDNAs sampling and pathogen enrichment/DNAs extraction from liquid biopsy samples was proposed. We reported a rapid and simple cfDNAs sampling using bio-composite [19] and microfluidic chip, and pathogen enrichment/DNAs extraction using microfluidic chip. To validate our sample preparation platform, optimization was performed using cell lines and bacteria, and clinical utility was confirmed using plasma samples of pancreatic cancer, colorectal cancer (CRC), and *Mycobacterium tuberculosis* (MTB) infected patients and oral swab samples of MTB infected patients. These low-cost and high yield cfDNAs and pathogen enrichment/DNA extraction sampling platforms could be useful for early diagnosis, monitoring, and determining treatment outcomes.

1.2. Components for bio-composite platform

For fabrication of bio-composite, we used calcined diatomaceous earth (DE, D3877-500G), 3-aminopropyl(diethoxy)methylsilane (APDMS, 371890-50ML), cucurbit[6]uril hydrate (CB[6], 94544-1G-F) from Sigma-Aldrich. For washing of DE, amine-modified DE (AD), and bio-composite, we uesd ethyl alcohol 99.9% (Ducksan Co.), UltraPure™ DNase/RNase-Free Distilled Water (Invitrogen), and 1x PBS pH 7.4 (Gibco). The produced bio-composite was stored at room temperature (RT) until use. In process of cfDNAs sampling, we used vortex-mixer and mini-microcentrifuge for mixing samples and collecting bio-composite. For cfDNAs extraction, we used sodium bicarbonate (S5761-500G) and 10M sodium hydroxide solution (NaOH, 72068-100ML) from Sigma-Aldrich. The cfDNAs were

extracted by a high pH (pH 10.4) elution buffer containing 10 mM sodium bicarbonate in bio-composite platform.

1.3. Components for microfluidic platform

For fabrication of microfluidic chip, we used hydrophilic thin films (HNW-100, COVEME, 100 μm) and double coated tape (300LSE-9495LE, 3M, 100 μm). The middle layer of microfluidic chip was consisted of attaching double coated tape on the top and bottom of the thin film. The middle layer of microfluidic chip and thin film was designed by AutoCAD (Autodesk) and cut by VLS3.50 Desktop laser platforms (Universal Laser Systems). The microfluidic chip (85 mm × 70 mm × 0.5 mm) was manufactured by assembling a thin film constituting the top and bottom of the chip and middle layer constituting the channel. For modification of microfluidic chip, we used O2 plasma treatment system (CUTE, Femto Science Inc.) and APDMS. For washing of microfluidic chip, we used UltraPure™ DNase/RNase-Free Distilled Water, and 1x PBS pH 7.4. The produced microfluidic chip was stored at RT until use. In process of DNAs sampling, we used vortex-mixer and mini-microcentrifuge for mixing and centrifugation of samples, and legato 101 dual syringe pump (KD Scientific) for injection of samples. For enrichment of pathogen and DNAs, we used dimethyl 3,3′-dithiopropionimidate dihydrochloride (DTBP, D2388-100MG) and dimethyl pimelimidate dihydrochloride (DMP, D8388-5G) as homobifunctional imidoesters (HIs) from Sigma-Aldrich. For pathogen lysis, we used 1M Tris-HCl, 10% sodium dodecyl sulfate (SDS), and 0.5M ethylenediaminetetraacetic acid (EDTA) from Bioneer. For extraction of DNAs, we used sodium bicarbonate and 10M NaOH solution from Sigma-Aldrich. The NAs were extracted by a high pH (pH 10.4) elution buffer containing 10 mM sodium bicarbonate in microfluidic platform.

1.4. Conventional DNA extraction

We used QIAamp DNA Mini Kit (51306, Qiagen) for extraction of DNA and QIAamp Circulating Nucleic Acid Kit (55114, Qiagen) for extraction of cfDNA. All DNA and cfDNA extraction processes were carried out according to the manufacturer's instructions.

Approximately 100 μL of DNA and cfDNA was extracted. The extracted DNA and cfDNA was screened by real-time PCR and stored at −20°C until use.

1.5. Conventional and real-time PCR

Conventional assays, such as end-point and real-time PCR, were used with the sample preparation platforms to test its utility. The forward and reverse primers were synthesized at the usual length of 24 bp (Table 1.1). A Taq PCR Core Kit (201225, Q1iagen) was used to produce amplified DNAs for further use. The end-point PCR process consisted of an initial denaturation step at 95°C for 15 min; 40–45 cycles of 95°C for 30 s, 57–62°C for 30 s, and 72°C for 30 s; and a final elongation step at 72°C for 10 min. A volume of 5 μL DNA was amplified in a total volume of 25 μL containing 10x PCR buffer, 2.5 mM MgCl, 0.25 mM deoxynucleotide triphosphate (dNTP), 25 pmol of each primer, and 1 unit of Taq DNA polymerase. Gel electrophoresis was performed to separate PCR products on a 2% agarose gel containing LoadingSTAR (A750, Dyne Bio Inc.). The gel was visualized using a ChemiDoc XRS + system (Bio-Rad).

The real-time PCR procedure used was modified from the Bio-Rad CFX96 Instrument protocol. Briefly, 5 μL DNA was amplified in a total volume of 20 μL containing 2x brilliant III SYBR Green QPCR Master Mix (600882, Agilent Technologies) and 25 pmol of each primer. Results of real-time PCR were used to produce a standard curve in which the template concentration was unknown, and measure cfDNA integrity (*Alu* 247/115 ratio) and cellular DNA background (β-actin 400 bp). For *Alu* elements, the amplification protocol consisted of an initial denaturation step at 95°C for 10 min, 35 cycles of 30 s at 95°C, 30 s at 62°C, 30 s at 72°C, and a cooling step at 40°C for 30 s. The absolute equivalent amount of cfDNA in each sample was determined using a calibration curve with serial dilutions of genomic DNA obtained from healthy donors. For others, the amplification protocol consisted of an initial denaturation step at 95°C for 15 min, 40–45 cycles of 10 s at 95°C, 20 s at 57–62°C, and 20 s at 72°C, and a cooling step at 40°C for 30 s. The amplified products with SYBR Green signals were obtained using a CFX96 Real-time PCR System (Bio-Rad).

Table 1.1. Primer sequences for conventional and real-time PCR in Section 1.

Assay		Primer	sequence (5'–3')
Conventional & real-time PCR	β-actin	102 bp F	ATC GCC GAC AGG ATG CA
		102 bp R	CGT ACT CCT GCT TGC TGA TCC
		400 bp F	GCA CCA CAC CTT CTA CAA TGA
		400 bp R	TGT CAC GCA CGA TTT CCC
	KRAS	133 bp F	GCT GTA TCG TCA AGG CAC TCT T
		133 bp R	ACC TTA TGT GTG ACA TGT TCT AAT ATA GTC
		150 bp F	GCA GAA CAG CAG TCT GGC TAT TT
		150 bp R	CAG TTG ACT GCA GAC GTG TAT CG
		777 bp F	TAG CCG CCG CAG AAC AGC AGT C
		777 bp R	TCA CAA TAC CAA GAA ACC CAT AAA
	Q fever	203 bp F	GAG CGA ACC ATT GGT ATC G
		203 bp R	CTT TAA CAG CGC TTG AAC GT
		525 bp F	CGG GTT AAG CGT GCT CAG TAT GTA
		525 bp R	TGC CAC CGC TTT TAA TTC CTC CTC
	Alu segment	247 bp F	GTG GCT CAC GCC TGT AAT C
		247 bp R	CAG GCT GGA GTG CAG TGG
		115 bp F	CCT GAG GTC AGG AGT TCG AG
		115 bp R	CCC GAG TAG CTG GGA TTA CA

1.6. Cell free DNA integrity and cellular DNA background

To compare the clinical utility of the conventional assay and the bio-composite platform, cfDNA integrity and cellular DNA background from the clinical samples were measured using *Alu* element primers (247 and 115 bp products), and *β*-actin primer (400 bp product)[22]. The C_T values for each clinical specimen were converted to DNA concentration,and cfDNA integrity was measured at *Alu* 247/115 ratio. A ratio close to 1.0 indicated that the cfDNAs were not truncated, whereas that close to 0 indicated that cfDNAs were truncated[22]. The C_T values of *β*-actin present cellular DNA background. Extracted cfDNA contaminated with cellular DNA has a lower C_T value than uncontaminated cfDNA[22]

Chapter 2. Sample preparation using bio-composite platform

2.1. Introduction

Pancreatic cancer is a severe and lethal malignancy, and the poor prognosis of patients with pancreatic cancer is mainly attributed to its frequent diagnosis at advanced stages [20-22]. The clinical use of cfDNA as a biomarker for early detection and monitoring of metastasis and treatment outcomes may improve the survival rate and prognosis of cancers, including pancreatic cancer[25]. Recent studies show a high correlation between cfDNA level and cancer stage, supporting the value of cfDNA as a biomarker for the diagnosis and monitoring of human malignancies [23, 24]. However, there is no standard method of cfNA sampling and analysis for clinical application.

In this study, we report a simple, low-cost cfNA sampling platform for the rapid and accurate diagnosis and monitoring of cancer patients using patient-derived plasma. This platform is based on the use of a novel bio-composite of DE and CB[6]. DE consists of porous silica microparticles of 1–200 μm [25]. CB[6] is composed of n-glycoluril units, negatively charged carbonyl groups and a cavity [26-28]. We synthesized the bio-composites by coating the amine groups on the surface of DE with CB[6]. This bio-composite platform allowed the effective isolation of DNA when genomic DNA (> 1 kb) and amplified products (777, 525 and 150 bp) were used. The clinical utility of the bio-composite platform for cfDNA sampling from plasma was validated in three patients with CRC and ten patients with pancreatic cancer. The bio-composite platform allowed rapid (< 20 min) isolation of cfDNA from clinical specimens. The results suggest that the bio-composite platform can be used for cfNA sampling from liquid biopsy specimens for various clinical applications.

2.2. Materials and methods

2.2.1. Fabrication and operation of the bio-composite platform

For cfNA sampling using DE, AD was fabricated in three steps as follows. (1) *DE washing step*: 3 g DE was added to 150 mL DW while stirring at 550 rpm for 10 min at RT. The stirring was stopped for 1 min, and the supernatant was discarded. The precipitate was then washed twice with 150 mL DW under the same conditions. After washing, the mixture was divided into 50 mL conical tubes, centrifuged at 14,000 rpm for 1 min, the supernatant was discarded, and the precipitate was stored. (2) *APDMS functionalization step*: 3 mL APDMS was added to 150 mL ethanol-DW (95:5, v/v) solution while stirring at 550 rpm for 3 min at RT. The pure DE precipitate was mixed with a 95% ethanol solution with APDMS and stirred at 550 rpm for 4 h at RT. The precipitate was washed three times with 95% ethanol to remove the remaining APDMS. After washing, the mixture was divided into 50 mL conical tubes and centrifuged at 14,000 rpm, and the supernatant was discarded. (3) *Dry step*: the pure AD was dried for 2 days at RT in a vacuum chamber until all remaining ethanol was evaporated. The bio-composite for cfDNA sampling was prepared as follows: 50 mg AD was added into a 1 mL of CB[6] solution containing 0.1, 0.01, or 0.001 mg of CB[6], and incubated at RT for 2, 4, or 6 h to make bio-composite with shaking for 1 min at 30 min intervals. 1 mL of the bio-composite mixture containing 50 mg of AD and 0.001 mg of CB[6] was prepared for cfDNA sampling. For the capture of amplified DNA and cfDNA, 40 μL of the prepared bio-composite was added to 500 μL of blood plasma or 500 μL of solution containing amplified DNA, and then incubated at RT for 10 min with shaking for 30 s at 2 min intervals. After the capture, the supernatant was discarded by centrifugation at 5,500 rpm for 1 min, and the precipitate was washed by pipetting with the addition of 1 mL PBS. Then, the precipitate was washed two more times with 1 mL PBS under the same conditions. Finally, 100 μL elution buffer (pH 10.4) was added to collect the captured amplified DNA or cfDNA for further analysis. The zeta potential of the DE, AD, and bio-composite was measured by dynamic light scattering (DynaPro NanoStar). Fourier transform-infrared spectroscopy (FT-IR) results and scanning electron microscope (SEM) images of DE, AD, bio-composite, and bio-composite–cfDNA were obtained from FT-IR

Fourier Transform Infrared Spectrometer (TENSOR27) and field emission scanning electron microscope (JSM–7800F Prime, JEOL Ltd).

2.2.2. Evaluation of the bio-composite platform

To evaluate the capture efficiency of the bio-composite platform, gDNA was extracted from HCT116 human CRC cells (ATCC_CCL–247), and PCR products of 777, 525, and 150 bp were generated. The amplified PCR products were generated using clinical specimens derived from patients as described in previous studies [29-32]. The products of 777 and 150 bp consisted of part of exon 2 containing the *KRAS gene* sequence and were used as a template for nucleic acid amplification using a *KRAS* 133 and 150 bp primers. The product of 525 bp consisted of part of the *C. burnetii transposase gene* containing the *IS1111a* region and was used as a template for nucleic acid amplification using a 203 bp primer. All PCR products were stored at −20°C until use.

2.2.3. Blood plasma from colorectal cancer and pancreatic cancer patients

To validate the bio-composite platform for clinical use, blood plasma specimens from three CRC and ten pancreatic cancer patients were collected from the Bio Resource Center (BRC) of the Asan Medical Center (Seoul, Republic of Korea, No. 2016–13(125) & 2019–8(187)) after approval from the Institutional Review Board (IRB no. 2016–0809 & no. 2019–0631). All methods were carried out in accordance with relevant guidelines and regulations. The Institutional Review Board of Asan Medical Center approved the study protocol, and informed consent was obtained from all participants. The blood samples, which were obtained by colorectal and pancreatic surgery teams, were randomly selected according to the stage of cancer (Table 2.1). All blood samples were collected in a blood collection tube treated with K_2 EDTA, and plasma was transferred after centrifugation at a rate of 1,500 × *g* for 15 min (4°C), according to protocol from the previous study[22].

Table 2.1. Clinical characteristics of 3 colorectal and 10 pancreatic cancers.

	Nr.	Age	Gender	Pathologic Stage
Colorectal cancer	CRC #1	64	F	2
	CRC #2	42	M	3
	CRC #3	72	F	3
Pancreatic cancer	P #1	71	F	2
	P #2	59	M	3
	P #3	70	M	3
	P #4	64	F	2
	P #5	47	M	3
	P #6	54	M	2
	P #7	54	M	1
	P #8	56	F	2
	P #9	72	F	1
	P #10	53	M	1

2.3. Results and discussion

2.3.1. Design of the bio-composite platform

Figure 2.1 is a schematic showing the construction of the bio-composite platform based on AD coated with CB[6], and a description of the experimental procedure used to isolate cfNA from plasma specimens using the bio-composite platform. AD has amine groups on the outer and inner surface that render it chemically stable in aqueous solution. The positively charged AD interacts with the negatively charged carbonyl portals of CB[6], resulting in an electrically neutralized and stabilized complex. In addition, we confirmed that the bio-composite have several micropores, and a large surface area (Fig. 2.2A). The bio-composite has a high molecular recognition capability by the porous structure of DE and the cavity structure of CB[6], and this function enhances the capture efficiency of the bio-composite for cfDNA isolation. Furthermore, we performed FT-IR analysis to identify the properties of the bio-composite after the cfDNA binding. The wavelength peaks at 1681 cm^{-1} (C=O bonds) and 1,071 cm^{-1} (C–N bonds) were observed in the bio-composite group (Fig. 2.2B). The C=O bonds at the edge of CB[6] reacts with NH_2 of AD to act as one of the important anchoring site in the bio-composite platform. In addition, the C–N bonds indicate that the oxygen atoms, which are located along the edges of CB[6], which can bind with the amine group from the AD. Therefore, these characteristics of AD and CB[6] contribute to improve the structural stability of the bio-composite for cfDNA capturing. The bio-composite platform can be used to detect various biomarker molecules for sampling of clinical specimens. The application of the bio-composite platform includes the following steps (Fig. 2.1): (1) *Mixing blood plasma and bio-composite*: the bio-composite is mixed with blood plasma samples and shaken by hand to capture cfDNA. (2) *Binding to cfDNA*: the amine groups of the fragmented cfDNA covalently bind to the C=O of the carbonyl portal of CB[6] on the DE. The phosphate backbone of cfDNA can electrostatically bind to positively charged DE and CB[6] in the bio-composite. (3) *Washing to remove the debris*: two binding mechanisms lead to a stable combination of the bio-composites and cfDNA. (4) *Elution of isolated cfDNA*: the covalent and electrostatic bonds between the bio-composite and cfDNA are cleaved using the elution buffer (pH 10.4), resulting in high efficiency isolation of

cfDNA. The bio-composite platform enabled rapid sampling of cfDNA within 20 min, and the product obtained showed good quality and quantity.

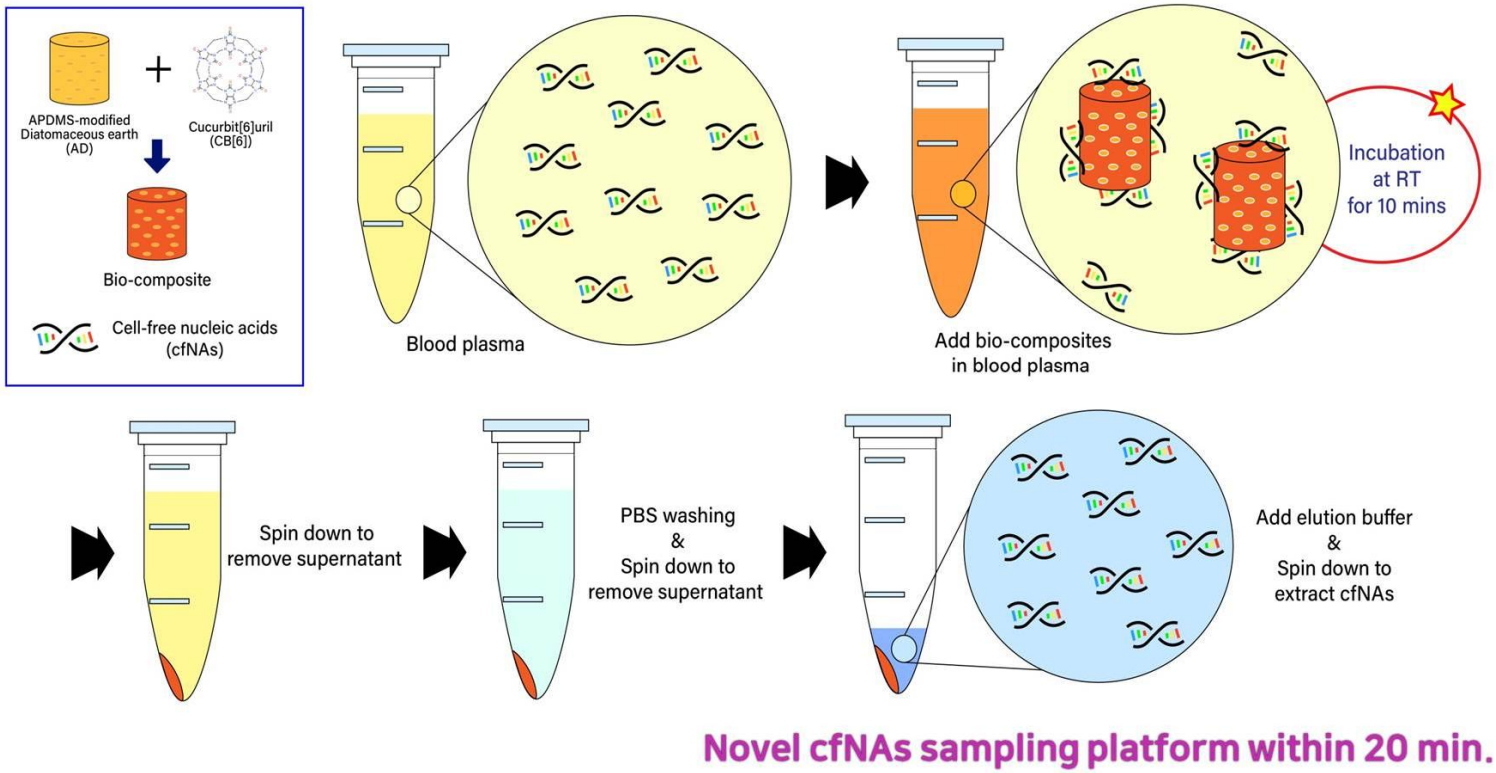
APDMS-modified Diatomaceous earth (AD)
Cucurbit[6]uril (CB[6])
Bio-composite
Cell-free nucleic acids (cfNAs)
Blood plasma
Add bio-composites in blood plasma
Incubation at RT for 10 mins
Spin down to remove supernatant
PBS washing & Spin down to remove supernatant
Add elution buffer & Spin down to extract cfNAs
Novel cfNAs sampling platform within 20 min.

Figure 2.1. Schematic representation of the process of cfNAs sampling from clinical specimens using the bio-composite platform. First, the bio-composite platform was prepared for ready-to-use cfNAs sampling. The bio-composites were added to blood plasma samples and incubated at RT for 10 min with shaking for 30 s at 2 min intervals for cfNAs capture. The solution was centrifuged to remove the supernatant containing debris, and the precipitate was washed three times with 1 mL PBS. Finally, high pH (pH 10.4) elution buffer was added and centrifuged to extract cfNAs. The bio-composite platform was able to isolate cfNAs from clinical specimens at high concentrations and purity within 20 min without requiring large equipment or a thermo-regulator.

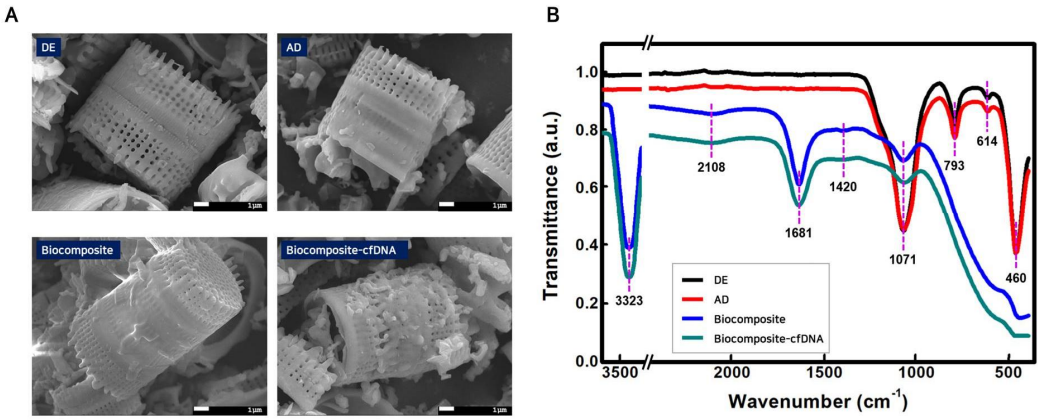

Figure 2.2. Characterization of material structure in bio-composite platform. (A) Scanning electron microscopy (SEM) images of the DE, AD, bio-composite, and bio-composite-cfDNA. (B) Visual Fourier transform-infrared spectroscopy (FT-IR) spectrum analysis of the DE, AD, bio-composite, and bio-composite-cfDNA.

2.3.2. Synthesis and optimization of the bio-composites

A protocol for the synthesis of bio-composites was designed by optimizing DE and CB[6] concentrations, incubation time, and the volume of bio-composites to produce molecules with high functionality for cfDNA sampling. To optimize the protocol for the synthesis of bio-composites, human gDNA and an amplified 777 bp DNA product were prepared. Different CB[6] concentrations (0.1, 0.01, and 0.001 mg/mL) and incubation times (2, 4, and 6 h) were tested to determine the optimal conditions for the generation of bio-composites. Determining the optimal concentration of CB[6] for coating the DE is essential to improve the efficiency of cfDNA isolation (Fig. 2.3A). High capture efficiency for 1 ng of a 777 bp product was observed using a CB[6] concentration of 0.001 mg/mL and 50 mg DE. The optimal incubation time for DE and CB[6] binding is essential to obtain stabilized bio-composites (Fig. 2.3B). An incubation time of 4 h with 50 mg DE and 0.001 mg/mL CB[6] showed high capture efficiency for 1 ng of a 777 bp product. Different volumes (20, 40, 60, 80, and 100 μL) of bio-composite were tested to identify the ideal volume yielding high quality and quantity cfDNA (Fig. 2.3C). The volume of the bio-composites is an important factor to capture high concentrations of cfDNA and reduce uncaptured cfDNA. The results showed that 40 μL of bio-composites resulted in high capture efficiency of gDNA from 10^4 cells. These optimal conditions for the synthesis of bio-composites were used for further characterization of the bio-composite platform using clinical specimens.

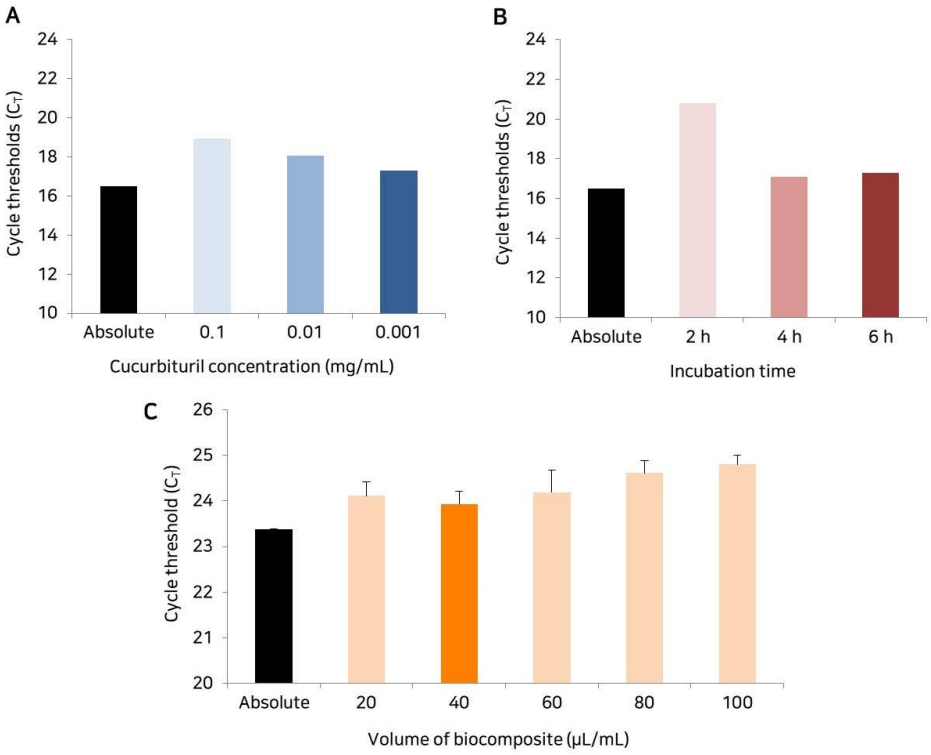

Figure 2.3. Optimization of the bio-composite platform. (A) Analysis of capture efficiency using 1 ng of amplified 777 bp DNA according to CB[6] concentration (0.1, 0.01, and 0.001 mg/mL) with 50 mg AD and 6 h of incubation time. The absolute (black) means 1 ng of amplified 777 bp DNA without CB[6]. (B) Analysis of capture efficiency using 1 ng of amplified 777 bp DNA according to incubation time (2, 4, and 6 h) for the construction of the bio-composite platform with 50 mg AD and 0.001 mg/mL CB[6]. (C) Analysis of capture efficiency using 104 cellular gDNA according to the volume of bio-composite (20, 40, 60, 80, and 100 μL/mL) with 50 mg AD, 0.001 mg/mL CB[6], and 6 h of incubation time. Colors represent results of the absolute (black) and the bio-composite platform (blue, red, and orange). Error bars indicate standard deviation from the mean based on at least three independent experiments.

2.3.3. Characterization of the bio-composite platform

The zeta potential of DE, AD, and bio-composites was measured (Fig. 2.4A, Table 2.2). The zeta potential measures the surface charge of nanoparticles, which is an indicator of the stability of colloidal dispersion because it represents the resistance between adjacent charged particles [33]. Composites with a high negative or positive zeta potential have high dispersion stability because of the lack of aggregation between particles, whereas a low zeta potential is associated with coagulation or flocculation caused by high attraction between particle. The surface charge of the bio-composite was more positive than that of pure DE and AD, indicating that the bio-composites had excellent dispersion stability (more than + 61 mV) in solution (Fig. 2.4A, Table 2.2). Therefore, cfDNAs can be captured with the positive charge of the bio-composite by the strong electrostatic interaction. Next, we tested the capture efficiency of the bio-composite platform with gDNA and amplified 777, 525, and 150 bp products. The bio-composite platform showed high capture efficiency for the 777 bp amplified DNA product without DNA loss during the PBS wash (Fig. 2.4B). As the result of real-time PCR, the C_T value of the DNAs in the supernatant collected after the PBS wash were measured. The results showed that the optimized bio-composite platform could capture most of the drifting DNA with high probability and showed strong binding that was not disrupted during the PBS washing step. Next, we examined the sensitivity of the bio-composite platform with 150 bp DNA products (Fig. 2.4C). We used serially diluted 150 bp DNA products to confirm the sensitivity of the bio-composite platform. We confirmed that the detection limit of bio-composite platform was down to 8.7 fg/mL (converted to 5.37×10^2 copies/mL). Furthermore, we examined the recovery rate of the bio-composite platform using a gDNA and fragmented DNAs (777, 525 and 150 bp), and the real ratio was calculated based on the standard curve of each sample (Fig. 2.5). The capture efficiency depends on the fragmented size of cfDNAs is important to confirm the prognosis information of clinical patients [34]. The four types of DNA obtained using the bio-composite platform showed similar C_T values before and after capture. The rate of capture according to input DNA (DNA concentration with capture/input DNA concentration × 100%) was calculated, and the capture efficiency was measured as 90.26%, 88.22%, 86.78%, and 89.09% for gDNA, 777, 525, and 150 bp DNA products, respectively (Table 2.3). These results indicate

that the bio-composite platform is a simple and rapid sampling technique that can capture cfDNA with high efficiency.

Table 2.2. Comparison of the zeta potential between DE, AD, and the bio-composite.

Zeta potential (mV)	Test #1	Test #2	Test #3	Test #4	Test #5	Test #6	**Test mean**
DE	-15.47	-14.23	-13.94	-16.36	-16.53	-14.89	**-15.24**
AD	46.73	47.48	44.04	43.09	47.37	44.04	**45.46**
Bio-composite	64.24	62.08	62.55	61.92	63.58	63.81	**63.03**

Table 2.3. Capture efficiency determined using gDNA, amplified 777, 525, and 150 bp DNA in the bio-composite platform.

Samples	Test #1 (C_T)	Test #2 (C_T)	Test #3 (C_T)	Test mean (C_T)	Absolute (C_T)	**Capture efficiency (%)**
gDNA	23.63	23.51	23.44	23.53	23.38	**90.26**
777 bp	16.81	16.94	16.72	16.82	16.64	**88.22**
525 bp	16.56	16.34	16.29	16.40	16.21	**86.78**
150 bp	14.68	14.96	14.64	14.76	14.59	**89.09**

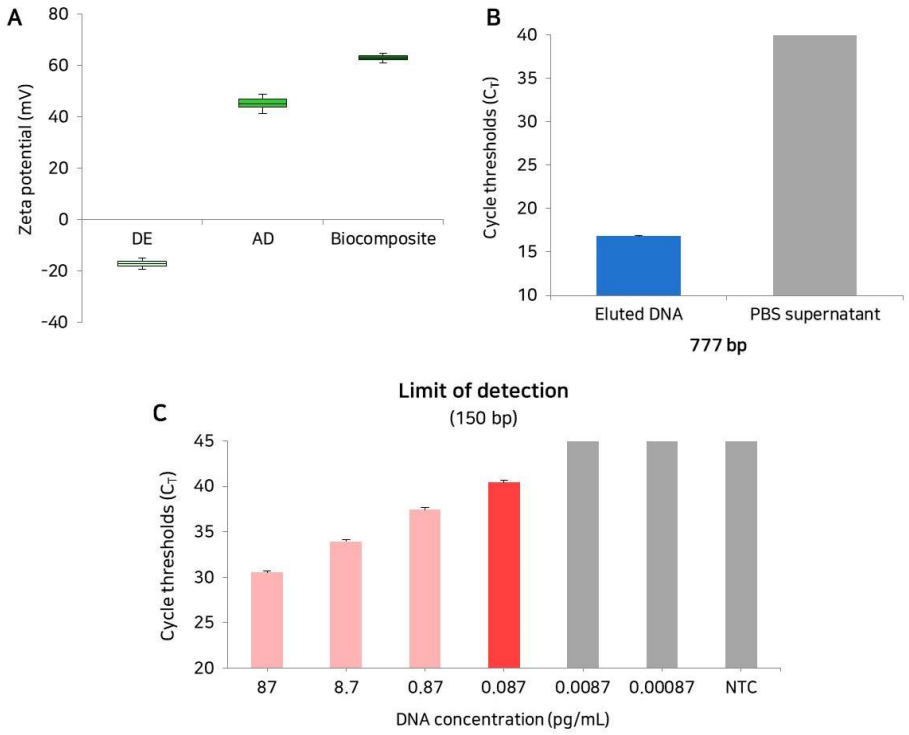

Figure 2.4. Characterization of the bio-composite platform. (A) Box plot for the comparison of zeta potential between DE, AD, and the bio-composite. (B) Confirmation of the capture efficiency of DNA using bio-composite platform-eluted DNA and the PBS supernatant after the PBS washing step. (C) Limit of detection of the bio-composite platform. The bars represent the results from the bio-composite platform depends on the concentrations of targets (red) and negative control (grey). Error bars indicate standard deviation from the mean based on at least three independent experiments.

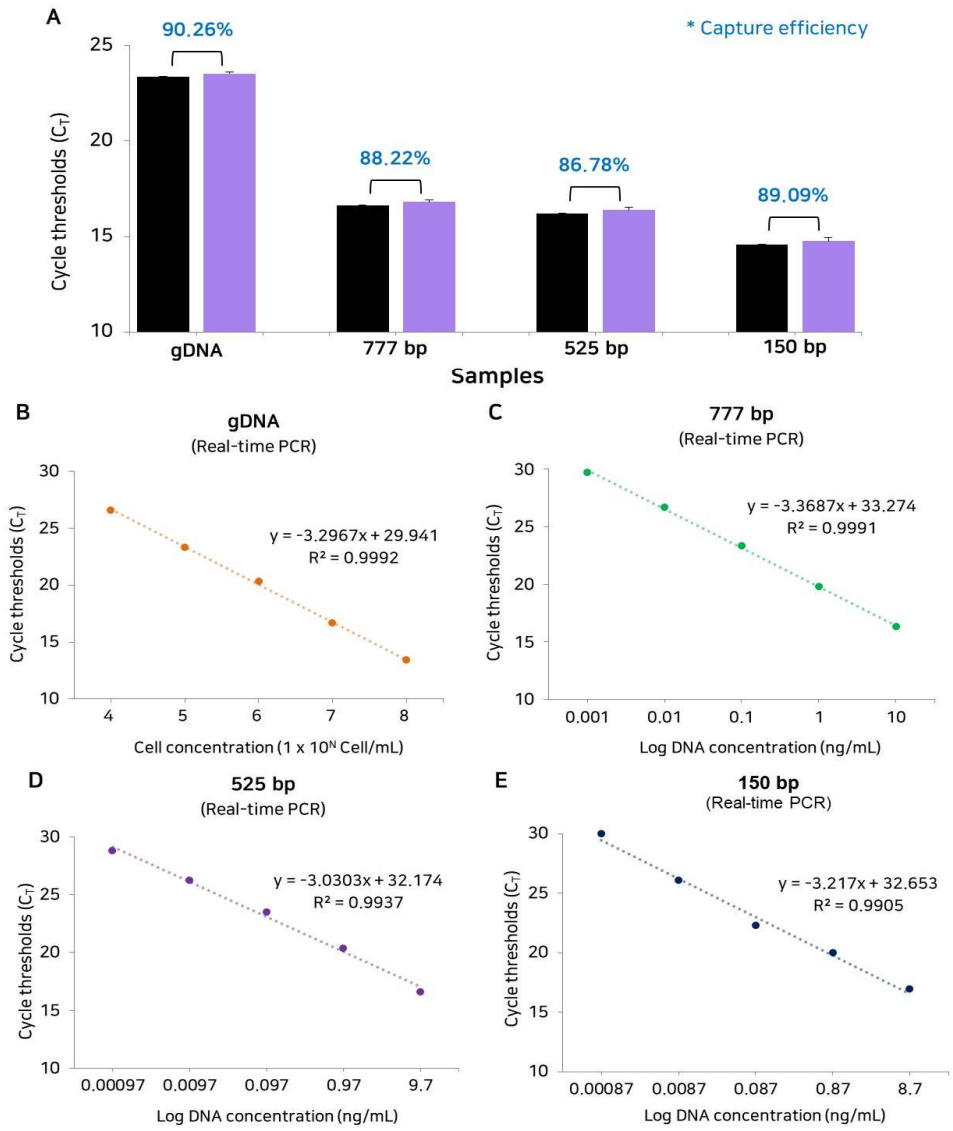

Figure 2.5. Capture efficiency of the bio-composite platform. (A) Measurement of the capture efficiency of the bio-composite platform using gDNA, amplified 777, 525, and 150 bp DNA. Colors represent results of input amount of target (black) and the bio-composite platform (violet). Error bars indicate standard deviation from the mean based on at least three independent experiments. (B) Detection of gDNA from HCT116 cells using a 102 bp primer. (C) Detection of amplified 777 bp DNA using a 133 bp primer. (D) Detection of amplified 525 bp DNA using a 203 bp primer. (E) Detection of amplified 150 bp DNA using a 150 bp primer.

2.3.4. Clinical utility of the bio-composite platform

The clinical utility of the bio-composite platform for cfDNA sampling was tested using liquid biopsy samples from 13 cancer patients. First, plasma cfDNA obtained from three patients with CRC was analyzed (Fig. 2.6A, Table 2.4). The cfDNAs isolated from the plasma were analyzed by real-time PCR using *Alu* 247 bp, *Alu* 115 bp, and *β*-actin 400 bp gene fragments. The C_T data obtained by real-time PCR allow determination of the absolute amount of longer fragments of plasma DNA, the total amount of cfDNA in plasma, and the cellular DNA background based on the standard curve of each sample (Fig. 2.7). The integrity of cfDNA was then determined using the *Alu* 247/115 ratio, which was close to zero (0). This indicated that most of the DNA was truncated as cfDNA (Fig. 2.6C). In CRC samples, the cfDNA integrity index determined using the bio-composite platform was lower (0.18) than that obtained using the conventional method (0.27). This result confirmed that the bio-composite platform easily captured the small DNA fragments, which can be regarded as reliable evidence of the whole tumor burden [35]. The cellular DNA background using the bio-composite platform, the DNAs were amplified with the *β*-actin 400 bp primer. The amplification efficiency of the bio-composite platform was higher (C_T value, 35.89) than that of the conventional method (C_T value, 28.20). This result confirmed that the bio-composite platform minimized the cellular background signal by eliminating the lysis step. In addition, the plasma cfDNA of ten pancreatic cancer patients was analyzed (Fig. 2.6B, Table 2.4). The cfDNA integrity determined by the *Alu* 247/115 ratio was 0.15–0.71 (Fig. 2.6C, Table 2.5).). The C_T value for the *β*-actin 400 bp gene was high (C_T value, 34.05) in the bio-composite platform. Taken together, the results indicate that the bio-composite platform is a useful method for capturing cfDNA from clinical specimens within 20 min, and that it can overcome the limitations of conventional approaches.

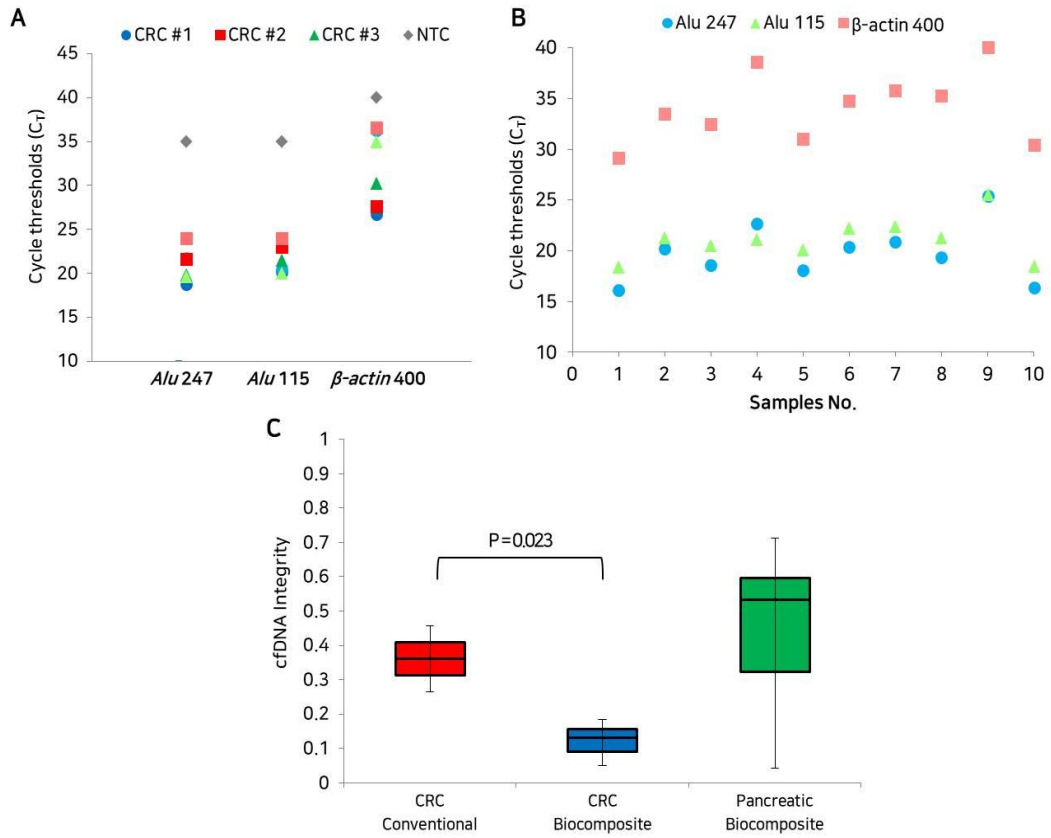

Figure 2.6. Clinical utility of the bio-composite platform. (A) Dot plots of the detection of *Alu* 247 bp, *Alu* 115 bp, and *β*-actin 400 bp using samples from three CRC patients. Circles represent CRC #1 (blue), squares represent CRC #2 (red), triangles represent CRC #3 (green), and diamonds represent negative control (NTC) samples (grey). Colors represent conventional assay (dark) and the bio-composite platform (light). (B) Dot plots of the detection of *Alu* 247 bp, *Alu* 115 bp and *β*-actin 400 bp using ten pancreatic cancer patient samples with the bio-composite platform. Light blue circles represent *Alu* 247 bp, light green triangles represent *Alu* 115 bp, and light red squares represent *β*-actin 400 bp in each sample. (C) Box plots of cfDNA integrity in three CRC and ten pancreatic cancer samples. Colors represent the conventional assay (red) in three CRC samples, the bio-composite platform (blue) in CRC samples, and the bio-composite platform (green) in pancreatic cancer samples. The p-value was evaluated by Student's *t* test.

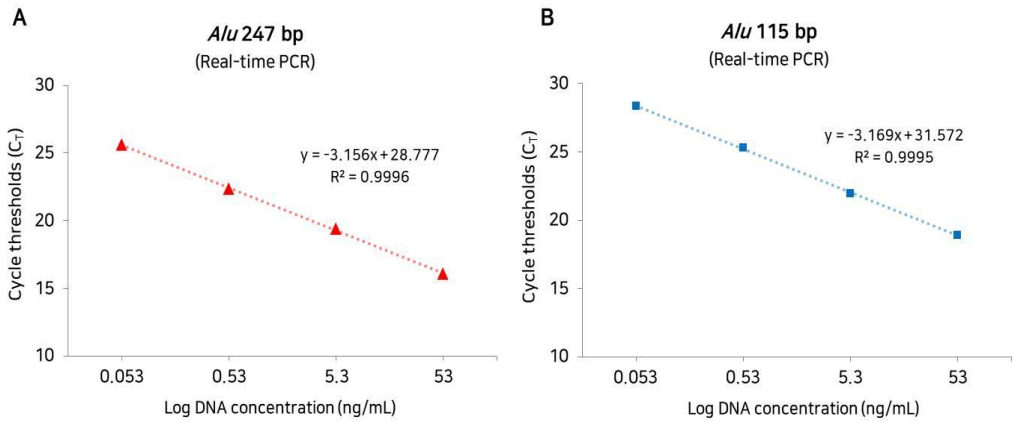

Figure 2.7. Linear relationship of the *Alu* 247 bp and *Alu* 115 bp using real-time PCR. (A) Detection of longer fragments of plasma DNA from healthy controls using the *Alu* 247 bp primer. (B) Detection of the total amount of cfDNA from healthy controls using the *Alu* 115 bp primer.

Table 2.4. Comparison of the C_T values of *Alu* 247 bp, *Alu* 115 bp, and *β*-actin 400 bp from 3 colorectal cancer specimens using the conventional assay and bio-composite platform, and from 10 pancreatic cancer specimens using the bio-composite platform.

	Nr.	***Alu* 247 bp**		***Alu* 115 bp**		***β-actin* 400 bp**	
		Conventional (C_T)	Biocomposite (C_T)	Conventional (C_T)	Biocomposite (C_T)	Conventional (C_T)	Biocomposite (C_T)
Colorectal cancer	CRC #1	18.76	20.11	20.11	20.39	26.69	36.19
	CRC #2	21.63	22.97	22.57	22.93	27.63	36.5
	CRC #3	19.83	21.51	21.51	20.02	30.29	34.98
Pancreatic cancer	P #1	.	16.09	.	18.37	.	29.11
	P #2	.	20.19	.	21.26	.	33.43
	P #3	.	18.55	.	20.49	.	32.42
	P #4	.	22.66	.	21.08	.	38.53
	P #5	.	18.05	.	20.11	.	31.00
	P #6	.	20.38	.	22.22	.	34.70
	P #7	.	20.87	.	22.41	.	35.77
	P #8	.	19.32	.	21.30	.	35.25
	P #9	.	25.34	.	25.55	.	40.00
	P #10	.	16.33	.	18.46	.	30.36

Table 2.5. Comparison of cfDNA integrity between the conventional assay and the bio-composite platform in 3 colorectal cancer specimens and the bio-composite platform in 10 pancreatic cancer specimens.

	Nr.	**cfDNA integrity index ($0 \leq X \leq 1$)**	
		Conventional	Bio-composite
Colorectal cancer	CRC #1	0.36	0.05
	CRC #2	0.27	0.13
	CRC #3	0.46	0.18
Pancreatic cancer	P #1	.	0.71
	P #2	.	0.29
	P #3	.	0.55
	P #4	.	0.04
	P #5	.	0.60
	P #6	.	0.51
	P #7	.	0.41
	P #8	.	0.57
	P #9	.	0.15
	P #10	.	0.64

2.4. Conclusion

A novel sampling platform for the simple and rapid isolation of cfDNA from liquid biopsy specimens from cancer patients with low background molecule concentrations and a high yield of cfDNA would be a useful tool for clinical use. An effective method would improve the early diagnosis of cancer and metastatic disease by detecting cancer-derived ctDNA, and it could help to predict treatment outcomes and patient prognosis [36, 37]. Many ctDNA analysis, methods were developed in recent years to increase the accuracy, sensitivity, and specificity of cfDNA detection [11, 38-40]. However, the existing methods are expensive, complex, and require high and low temperature conditions and chaotropic reagents for cell lysis. There is currently no established method for extracting cfNAs, and the analysis of cfNAs is therefore limited by low sensitivity and specificity because of the low amount and purity of cfNAs isolated. Recently, one study described for the standardized (pre)analytical work flow for cfDNA by multicenter based testing [41]. They have examined six commercialized kits for cfDNA isolation from spiked DNA in blood samples, not real samples. Although the study was given the insights regarding quantification, downstream analysis, process analysis, assay design and validation of cfDNA, the commercialized kits required several instruments for cfDNA isolation as well as there are expensive methods [41].

In this study, we report the synthesis of a bio-composite of AD and CB[6] for sampling of cfNAs that overcomes the limitations of conventional methods for clinical use. This bio-composite platform is a simple, rapid, and cost-effective cfNA sampling system. The bio-composite platform has several advantages, as follows: first, the bio-composite platform does not require large equipment. Conventional methods require specialized equipment such as vacuum pumps, high-speed centrifuges, and temperature-regulated chambers for the lysis process. On the other hand, the bio-composite platform can be used for point-of-care testing using only a mini-microcentrifuge with a built-in battery. Second, the bio-composite platform (less 3$) is more economical method than spin column based assay (over 30$ with QIAamp Circulating Nucleic Acid Kit). Third, the bio-composite platform has high capture efficiency (86.78–90.26%), as demonstrated using three types of DNA. Fourth, the bio-composite platform can extract cfNAs with high purity in the clinical

setting. There is no lysis step, which can decrease the cellular DNA background derived from normal cells. Fifth, the cfDNA isolated by the bio-composite platform showed a lower integrity ratio than that obtained by the conventional method. This method can extract high amounts of cfDNA containing lower amounts of longer DNA fragments, which contributes to the high correlation of cfNA analysis. Finally, the bio-composite platform can extract cfNAs quickly within 20 min. The bio-composite platform thus allows high efficiency cfNA sampling for early diagnosis and prognosis prediction in human cancers, including CRC and pancreatic cancer. Nevertheless, further study would be desired to optimize the protocol with a large clinical cohort for improving the sensitivity and specificity for the cfDNA isolation in clinical applications. This simple and low-cost cfNA sampling method based on the bio-composite platform could be useful for cancer diagnosis, monitoring, and determining treatment outcomes.

Chapter 3. Sample preparation using microfluidic platform

3.1. Introduction

Rapid diagnosis and treatment of tuberculosis (TB) is important for both patient clinical prognosis and infection control [42]. Thus, diagnostic tests for TB that are more rapid and sensitive than the conventional tests are needed. In 2011, the World Health Organization (WHO) endorsed the use of the Xpert MTB/RIF assay (Xpert, Cepheid), a novel, rapid, automated, cartridge-based real-time PCR method [43], for initial diagnosis of patients suspected of active PTB [44]. The Xpert assay showed a high sensitivity of 98.2% in AFB smear-positive TB cases; however, the sensitivity was shown to be as low as 72.5% in smear-negative cases [45], and data from real-world settings reported a sensitivity of around 60–74% [46, 47]. Indeed, Xpert's sensitivity for TB detection was inadequate when only a few bacilli are present in a clinical specimen. The more recently developed Xpert MTB/RIF Ultra assay showed a superior sensitivity to the Xpert assay (63% *vs* 46%) for diagnosing smear-negative PTB [48], but it was still not high enough. In addition, the Xpert assays can only be applied to sputum samples, which are occasionally hard to acquire in young children and asymptomatic patients with pauci-bacillary diseases. Furthermore, sputum collection is prone to producing potentially infectious aerosols that present a hazard for health care workers and fellow patients [49].

cfDNA from blood samples has attracted attention in various medical fields, such as prenatal fetal genetic tests and liquid biopsy methods for malignancy [50, 51]. Plasma cfDNA is released from dying cells into the bloodstream [51, 52]. Since MTB induces apoptosis of infected macrophages [53], cfDNA is expected to be detected in the plasma of the patients with active TB. Moreover, because blood samples can be drawn conveniently and less invasively from patients, plasma cfDNA detection has been expected to be a promising and new diagnostic test for TB, especially in sputum-scarce PTB and EPTB. In previous studies, the sensitivity and specificity of plasma cfDNA for diagnosing TB was 29–65% and 67–100%, respectively [54, 55]. However, these studies focused only on diagnosing smear-positive PTB in patients.

To overcome these limitations on the current TB diagnostics, we developed a novel simple cfDNA sampling and pathogen enrichment/DNA extraction platform by HIs using a microfluidic platform, followed by conventional PCR [29]. Therefore, we evaluated and compared the

diagnostic performances of plasma cfDNA and oral swab DNA detection using our novel assay with those of other conventional diagnostic tests including acid-fast bacilli (AFB) microscopy, mycobacterial culture, Xpert MTB/RIF PCR assay (Xpert, Cepheid), and interferon-gamma releasing assay (IGRA) in patients suspected to have PTB and EPTB. Moreover, to expand the clinical applicability of the microfluidic platform, we investigated its diagnostic performance for the diagnosis of PTB from oral swab samples; specifically, this real practice-based study was performed in patients with clinically suspected PTB in a country with an intermediate burden of TB and a low burden of human immunodeficiency virus (HIV).

3.2. Materials and methods

3.2.1. Study population, study design, and definition of TB for cfDNA sampling

All patients suspected to have TB and who consented the use of their blood for detecting plasma cfDNA were prospectively enrolled from January 2019 to June 2020 at a 2,700-bed tertiary-care facility in Seoul, Republic of Korea, an intermediate TB-burden country. We reviewed their demographic characteristics, underlying diseases and conditions, suspected infection sites, and the results of AFB microscopy, mycobacterial culture, Xpert, and IGRA based on their electronic medical records. Plasma cfDNA assay results were concealed from the attending physicians to avoid bias when diagnosing active TB. The study protocol was approved by the Institutional Review Board of Asan Medical Center (IRB no. 2019-0336).

We categorized the patients as confirmed, probable, possible, and not-TB groups, as described previously [56]. Confirmed TB was defined as cases where MTB was isolated from cultures of clinical specimens or where the samples tested positive using MTB PCR. Probable TB was defined as cases responding to anti-TB treatment and meeting one of the following criteria: histopathologic examination of biopsy tissue showing caseating granuloma, chest computed tomography (CT) findings compatible with active pulmonary TB, pleural, pericardial fluid or ascites analysis consistent with TB pleurisy, pericarditis or TB peritonitis, and cerebrospinal fluid analysis and radiologic findings compatible with TB meningitis. The patients were classified as possible TB if they did not fulfil the above criteria but active TB could not be excluded. Patients were classified as having ‘‘not-TB’’ when some alternative diagnosis was made or there was clinical improvement without anti-TB treatment.

3.2.2. Study population, study design, and definition of TB for pathogen enrichment/DNA extraction

Adult patients (> 18 years of age) who were clinically suspected of active PTB were prospectively enrolled in two tertiary university-affiliated hospitals in Seoul, Republic of Korea (Asan Medical Center and Severance Hospital) from May 2019 to October 2020. The suspicion of PTB was made by three respiratory and infection specialists (SHK, YAK, and SWL) who each had experience in TB treatment for more than 15 years. Patients who could not understand the study design or the instruction on the sputum exam were excluded. The institutional review

boards of Asan Medical Center (2018-0020) and Severance hospital (4-2018-0029) approved this study, and the protocols of this study were registered in clinicaltrials.gov (NCT03423550).

After receiving informed consent from each patient and prior to starting the treatment, two trained researchers (YC and YAK) performed oral swabs using the OMNIgene·ORAL OMR-110 kit (DNA Genotek, Ottawa, Canada) according to the manufacturer's instructions. The samples were immediately sent to the labs and kept at –80 until analysis. All other steps were performed according to the routine practice for clinically suspected TB. Smear and culture of acid fasting bacilli (AFB) were examined at least two times and the Xpert assay was performed according to the routine practice. QuantiFERON-TB Gold Plus (QFT-plus) was also performed according to the manufacturer's instruction [57, 58].

TB cases were defined as those treated with anti-TB chemotherapy for at least 6 months according to the ATS/IDSA and Korean guidelines at the discretion of respiratory and infectious specialists (SHK, YAK, and SWL) [59] and fulfillment of full-term treatment. A culture-positive TB case was defined as a patient with at least one positive culture result for MTB from their sputum. Culture-positive patients were considered smear-positive if they had at least one positive smear result (inclusive of scanty positive smears). A culture-negative TB was defined as patients with a high clinical likelihood of active TB and a negative mycobacterial culture finding in two or more sputum examinations, but with good clinical and radiographic responses to anti-TB treatment during follow-up. The specialists who decided the TB treatments were blinded to the results of the microfluidic platform.

3.2.3. Plasma and oral swab samples analysis

Plasma samples were used for cfDNA sampling, and Figure 3.1 depicts the overall workflow of the microfluidic platform. MTB cfDNA was isolated from plasma samples using a modified version of a previously described protocol [29]. Briefly, 3 mL of blood plasma was mixed with 1 mL of DTBP (100 mg/mL) without lysis buffer and injected into the microfluidic platform. DTBP can directly capture MTB cfDNA by covalent bonding and electrostatic interaction on the inner part of microfluidic surface of the microfluidic chip. The captured plasma cfDNA was washed with PBS and then extracted using 100 μL of elution buffer capable of breaking the binding affinity.

Oral swabs samples were used for pathogen enrichment/DNA extraction, and Figure 3.1 depicts the overall workflow of the microfluidic platform. The principle and the detailed structure of the microfluidic platform have been described previously [60-63]. The 1 mL of oral swab samples was liquefied with liquefaction solution (4% NALC, 1.45% sodium citrate, and 2.67% NaOH) at a 1:1 ratio as according to the method described by Ganoza et al [64]. The 2 mL of liquefied oral swab samples was mixed with 700 µL of DMP (100 mg/mL) without lysis buffer and injected into the microfluidic platform. DMP can be captured with the surface of MTB cells by electrostatic coupling. After incubation at RT for 20 min, the debris was removed and the cells were lysed by incubation with lysis buffer with proteinase K and DMP at 56 for 20 min. The captured DNA from oral swab samples was washed with PBS and then extracted using 100 µL of elution buffer capable of breaking the binding affinity. For the detection of MTB obtained from the plasma and oral swab samples, we used conventional MTB PCR to detect the IS*6110* transposase and catalase-peroxidase (*KatG*) gene of TB using the Taq PCR Core Kit. Further PCR-based confirmation was carried out by the amplification of the 308 bp DNA fragment specific for the IS*6110* gene and the 555 bp DNA fragment specific for *KatG* gene. All results were reported as “positive” or “negative”.

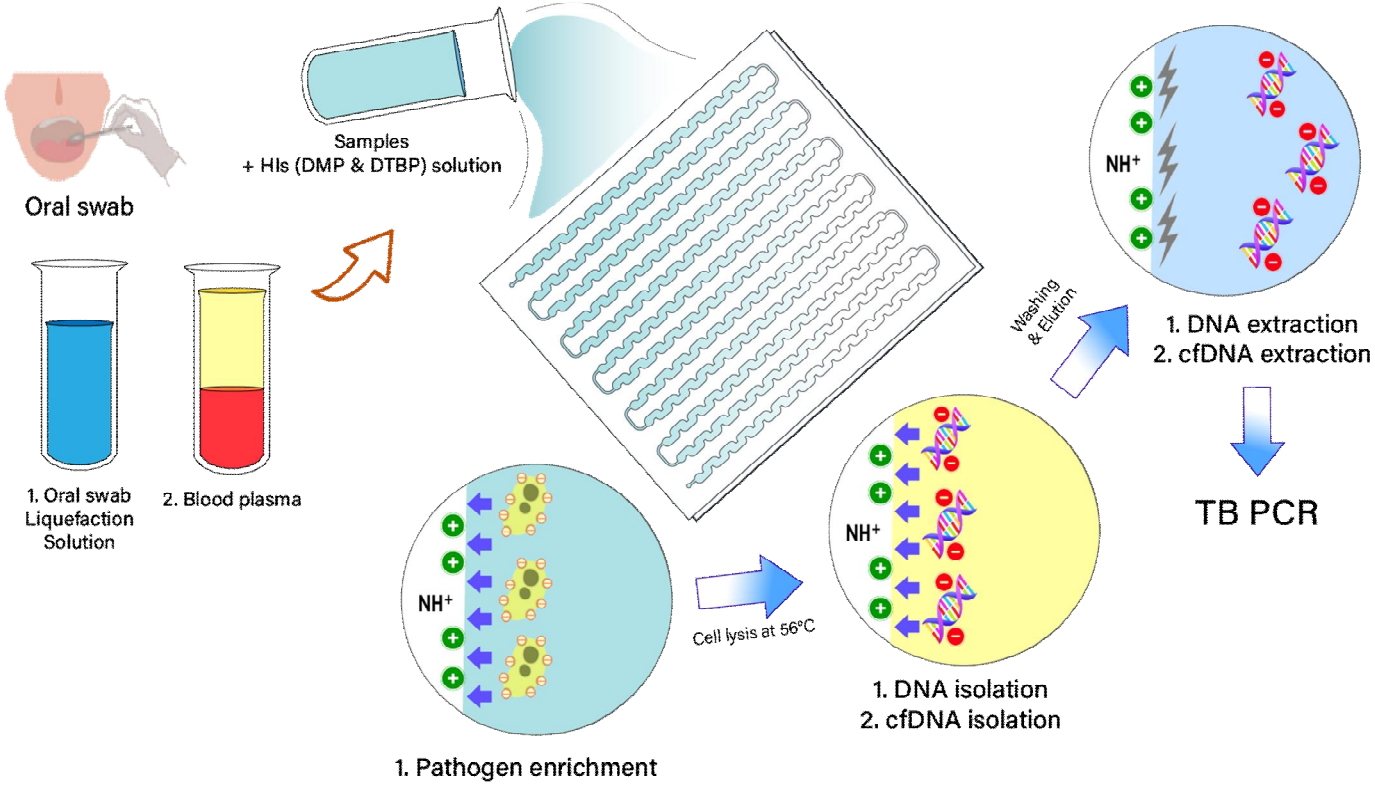
Oral swab
Samples
+ HIs (DMP & DTBP) solution
1. Oral swab
Liquefaction
Solution
2. Blood plasma
NH+
1. Pathogen enrichment
Cell lysis at 56°C
NH+
1. DNA isolation
2. cfDNA isolation
Washing
& Elution
NH+
1. DNA extraction
2. cfDNA extraction
TB PCR

Figure 3.1. Schematic representation of the pathogen enrichment/NAs extraction and cfNAs sampling using microfluidic platform for tuberculosis diagnosis. (1) A mixture of oral swab sample and liquefaction solution with DMP is added to the microfluidic platform to enrich the mycobacterium tuberculosis (MTB) and extract the DNA without the need for detergents or bulky instruments. After injecting 2 ml of liquefied oral swab samples into the microfluidic platform, the negative charged MTB binds to the positively charged DMP for enrichment. Then, DNA from the enriched MTB is isolated by the covalent bonding with DMP. (2) A blood plasma with DTBP is added to the microfluidic platform to enrich the cfDNA without the need for detergents or bulky instruments. After injecting 3 ml of blood plasma samples into the microfluidic platform, the negative charged cfDNA binds to the positively charged DTBP. (1, 2) After washing with PBS, the DNA is eluted for MTB detection with either PCR or real-time PCR.

3.2.4. Mycobacterial culture, Xpert, and IGRA

For culture identification of mycobacteria, clinical specimens from the suspected infection site were inoculated in liquid (Bactec MGIT 960) and solid (Ogawa media) culture media and cultured for at least 8 weeks. Xpert was performed following the manufacturer's protocol and previous reports [65, 66]. We also performed IGRA, including QuantiFERON-TB Gold In-Tube or Gold PLUS assay (Qiagen) and T-SPOT.*TB* assay (Oxford Immunotec) based on the manufacturer's protocols. The "indeterminate" or "borderline" IGRA results were considered negative.

3.2.5. Statistical analysis

Categorical variables were compared using the chi-square and Fisher's exact test, as appropriate, and continuous variables were analyzed using Student's *t* test or the Mann-Whitney U test, as appropriate, to compare the baseline clinical characteristics of patients with confirmed or probable TB and patients without TB. We evaluated the diagnostic performances (sensitivity, specificity, positive predictive value, negative predictive value, positive likelihood ratio, and negative likelihood ratio) of AFB microscopy, mycobacterial culture, Xpert, and microfluidic platform. We also compared the diagnostic performances with those of conventional diagnostic tests using McNemar's test. All tests of significance were two-tailed, and $p < 0.05$ were considered statistically significant. Calculations were performed using IBM SPSS Statistics for Windows, version 21.0 (IBM Corp).

3.3. Results

3.3.1. Study population for cfDNA sampling

A total of 96 patients suspected to have TB were prospectively enrolled. Among these patients, 55 patients were diagnosed with active TB: confirmed (n=34), probable (n=6), or possible (n=15) TB. The remaining 41 patients were not diagnosed with TB (not-TB) [56]. After excluding the 15 patients with possible TB, 81 patients were finally analyzed. The schematic flow chart of this study is shown in Figure 3.2. The baseline clinical characteristics of these patients are shown in Table 3.1. We compared the clinical characteristics of the TB group patients, including patients with confirmed (n=34) and probable (n=6) TB, and the not-TB group patients (n=41). There were no significant differences in demographics and underlying diseases and conditions between the two groups. Lung (22, 55.0%) was most common suspected site in the TB group followed by the lymph node (16, 40.0%), and central nervous 263 system (19, 46.3%) was the most common one in the not-TB group followed by the lung (12, 29.3%). There were 47 patients suspected to have EPTB without lung involvement. Patients with disseminated organ involvement (9, 22.5%) were only included in the TB group.

Figure 3.2. Schematic flow chart of the study in blood plasma

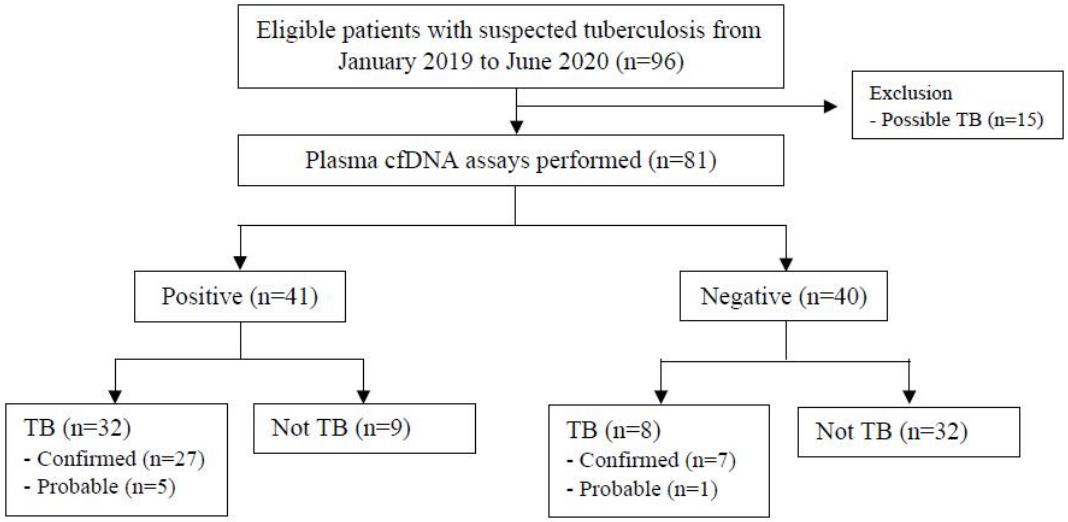

Table 3.1. Demographic characteristics, underlying disease and conditions, and suspected site of infection of patients with suspected tuberculosis.

	Confirmed or probable TB (n=40)	**Not TB (n=41)**	***P* value**
Demographics			
Age (median, IQR)	55.5 (41.5-62.3)	55.0 (29.0-65.0)	0.67
Male sex	19 (47.5)	19 (46.3)	0.92
Underlying diseases and conditions			
Diabetes mellitus	8 (20.0)	12 (29.3)	0.33
Liver cirrhosis	2 (5.0)	1 (2.4)	0.62
Hematologic malignancy	3 (7.5)	5 (12.2)	0.71
Solid cancer	4 (10.0)	2 (4.9)	0.43
Hematopoietic stem cell transplant	1 (2.5)	1 (2.4)	>0.99
Solid organ transplant	6 (15.0)	6 (14.6)	0.96
End stage renal disease	4 (10.0)	1 (2.4)	0.20
HIV infection	2/34 (5.9)	0/38	0.22
Immunocompromised status[a]	11 (27.5)	11 (26.8)	0.95
Neutropenia[b]	2 (5.0)	2 (4.9)	>0.99
Steroid use[c]	0	0	-
Receipt of immunosuppressants[d]	5 (12.5)	6 (14.6)	0.78
Receipt of chemotherapy[e]	1 (2.5)	2 (4.9)	>0.99
Receipt of anti-TNF-alpha agents[f]	0	0	-
History of treated TB	8 (20.0)	5 (12.2)	0.34
Suspected site of infection			
Pulmonary	22 (55.0)	12 (29.3)	0.19
Extrapulmonary			
Lymph node	16 (40.0)	4 (9.8)	0.002
Skeletal	7 (17.5)	5 (12.2)	0.50
Central nervous system	2 (5.0)	19 (46.3)	<0.001
Abdominal	6 (15.0)	2 (4.9)	0.16
Pleural	5 (12.5)	1 (2.4)	0.11
Genitourinary	2 (5.0)	0 (0)	0.24
Others	1 (2.5)	1 (2.4)	>0.99
Disseminated	9 (22.5)	0 (0)	0.001

TB, tuberculosis; IQR, interquartile range; HIV, human immnunodeficiency virus; TNF, tumor necrosis factor

[a] Defined as one of the following conditions: (i) daily receipt of immunosuppressants, including corticosteroids, (ii) human immunodeficiency virus infection, (iii) solid organ or hematopoietic stem cell transplant recipients, (iv) receipt of chemotherapy for underlying malignancy during the previous 6 months, and (v) underlying immune deficiency disorder.

[b] Absolute neutrophil count < 500/mm^3 for more than 7 days within previous 30 days

[c] At least 0.3 mg/kg/day of prednisolone for more than 3 weeks within previous 90 days

[d] Including immunosuppressants such as tacrolimus, cyclosporine, sirolimus, azathioprine, and mycophenolate mofetil within previous 90 days

[e] Within previous 30 days

[f] Withing previous 90 days

3.3.2. Diagnostic performances of AFB microscopy, mycobacterial culture, Xpert, IGRA, and plasma cfDNA

The diagnostic performances of the conventional tests (AFB microscopy, mycobacterial culture, Xpert, and IGRA) and plasma cfDNA assay are presented in Table 3.2. The sensitivity and specificity of plasma cfDNA assay were 80.0% [95% confidence interval (CI), 64.4–91.0] and 78.1% [62.4–89.4], respectively. The sensitivity of plasma cfDNA was higher than that of AFB microscopy (31.6% [17.5–48.7], p = 0.001). The sensitivity of plasma cfDNA was numerically higher than those of mycobacterial culture (65.8% [48.7–80.4], p = 0.33) and Xpert (61.1% [43.5–76.9], p = 0.14), although the differences were statistically insignificant. While the sensitivity and specificity of cfDNA assay were similar to those of IGRA (sensitivity 80.6% and specificity 71.4%), the combined sensitivity and specificity of the assays were 94.4% and 64.3%, respectively, which can be used to rule out TB. We also 279 performed subgroup analysis including 47 patients suspected to have EPTB (confirmed TB (n=13), probable TB (n=5), and not–TB (n=29)). In this subgroup analysis, the sensitivity of plasma cfDNA assay was 94.4% [72.7–99.9], which was significantly higher than that of AFB microscopy (12.5 [1.6–38.3], p = 0.002), mycobacterial culture (43.8% [19.8–70.1], p = 0.008), and Xpert (35.7% [12.8–64.9], p = 0.004) (Table 3.3). Nine patients with false positive plasma cfDNA assay results were diagnosed with alternative diseases: viral meningitis (n=3), bacterial meningitis (n=1), NMDA encephalitis (n=1), bacterial pneumonia (n=1), bacterial epidural abscess (n=1), nontuberculous mycobacteria lymphadenitis (n=1), and old TB sequalae (n=1). All patients recovered or at least did not deteriorate without anti-TB treatment. Among these patients, IGRA result was positive in four patients, negative in two patients, and not available in the remaining three patients. Two patients with positive IGRA results had past histories of TB.

Table 3.2. Diagnostic performances of AFB microscopy, mycobacterial culture, Xpert TB/RIF PCR, interferon-gamma releasing assay, and plasma cfDNA for diagnosing confirmed or probable tuberculosis.

	Sensitivity, % (n/N, 95% CI)	**Specificity, % (n/N, 95% CI)**	**Positive predictive value, % (95% CI)**	**Negative predictive value, % (95% CI)**	**Positive likelihood ratio**	**Negative likelihood ratio**
AFB microscopy	31.6 (12/38, 17.5-48.7)[a]	100.0 (37/37, 90.5-100.0)	100.0	58.7 (53.4-63.9)	-	0.7 (0.5-0.8)
Mycobacterial culture	65.8 (25/38, 48.7-80.4)[b]	100.0 (37/37, 90.5-100.0)	100.0	74.0 (64.7-81.6)	-	0.3 (0.2-0.5)
Xpert MTB/RIF PCR	61.1 (22/36, 43.5-76.9)[c]	100.0 (34/34, 89.7-100.0)	100.0	70.8 (61.7-78.5)	-	0.4 (0.3-0.6)
IGRA[*]	80.6 (29/36, 64.0-91.8)[d]	71.4 (20/28, 51.3-86.8)[e]	78.4 (66.3-87.0)	74.1 (58.5-85.3)	2.8 (1.5-5.2)	0.3 (0.1-0.6)
Plasma cfDNA	80.0 (32/40, 64.4-91.0)[a,b,c,d]	78.1 (32/41, 62.4-89.4)[e]	78.1 (66.2-86.6)	80.0 (67.8-88.4)	3.6 (2.0-6.6)	0.3 (0.1-0.5)
IGRA or cfDNA	94.4 (34/36, 81.3-99.3)	64.3 (18/28, 44.1-81.4)	77.3 (67.3-84.9)	90.0 (69.5-97.3)	2.6 (1.6-4.4)	0.1 (0.0-0.3)
IGRA and cfDNA	69.4 (25/36, 51.9-83.7)	85.7 (24/28, 97.3-96.0)	86.2 (71.1-94.1)	68.6 (56.6-78.5)	4.9 (1.9-12.4)	0.4 (0.2-0.6)

AFB, acid-fast bacilli; PCR, polymerase chain reaction; cfDNA, cell-free DNA; CI, confidence interval; IGRA, interferon-gamma releasing assay

[*] Including 54 QFT-TB and 17 T-SPOT.*TB* (7 patients underwent both QFT-TB and T-SPOT.*TB*)

[a] *P* value = 0.001 between plasma cfDNA and AFB miscroscopy

[b] *P* value = 0.33 between plasma cfDNA and mycobacterial culture

[c] *P* value = 0.14 between plasma cfDNA and Xpert TB/RIF PCR

[d] *P* value > 0.99 between plasma cfDNA and IGRA

[e] *P* value = 0.69 between plasma cfDNA and IGRA

Table 3.3. Diagnostic performances of AFB microscopy, mycobacterial culture, Xpert TB/RIF PCR, interferon-gamma releasing assay, and plasma cfDNA for diagnosing confirmed or probable tuberculosis in patients with suspected extrapulmonary tuberculosis.

	Sensitivity, % (n/N, 95% CI)	**Specificity, % (n/N, 95% CI)**	**Positive predictive value, % (95% CI)**	**Negative predictive value, % (95% CI)**	**Positive likelihood ratio (95% CI)**	**Negative likelihood ratio (95% CI)**
AFB microscopy	12.5 (2/16, 1.6-38.3)[a]	100.0 (25/25, 86.3-100.0)	100.0	64.1 (59.7-68.2)	-	0.9 (0.7-1.1)
Mycobacterial culture	43.8 (7/16, 19.8-70.1)[b]	100.0 (25/25, 86.3-100.0)	100.0	73.5 (64.3-81.1)	-	0.6 (0.4-0.9)
Xpert MTB/RIF PCR	35.7 (5/14, 12.8-64.9)[c]	76.5 (13/17, 50.1-93.2)	55.6 (29.2-79.1)	59.1 (47.4-69.8)	1.5 (0.5-4.6)	0.8 (0.5-1.3)
IGRA*	82.4 (14/17, 56.6-96.2)[d]	100.0 (22/22, 84.6-100.0)[e]	100.0	88.0 (72.4-95.3)	-	0.2 (0.1-0.5)
Plasma cfDNA	94.4 (17/18, 72.7-99.9)[a,b,c,d]	75.9 (22/29, 56.5-89.7)[e]	70.8 (55.8-82.4)	95.7 (76.4-99.3)	3.9 (2.0-7.5)	0.1 (0.0-0.50)
IGRA or cfDNA	100.0 (17/17, 80.5-100.0)	64.7 (11/17, 38.3-85.8)	73.9 (59.8-84.4)	100.0	2.8 (1.5-5.4)	0
IGRA and cfDNA	76.5 (13/17, 50.1-93.2)	88.2 (15/17, 63.6-98.5)	86.7 (63.3-96.1)	78.9 (61.0-90.0)	6.5 (1.7-24.5)	0.3(0.1-0.6)

AFB, acid-fast bacilli; PCR, polymerase chain reaction; cfDNA, cell-free DNA; CI, confidence interval; IGRA, interferon-gamma releasing assay

[*] Including 26 QFT-TB and 11 T-SPOT.*TB* (3 patients underwent both QFT-TB and T-SPOT.*TB*)

[a] *P* value = 0.002 between plasma cfDNA and AFB miscroscopy

[b] *P* value = 0.008 between plasma cfDNA and mycobacterial culture

[c] *P* value = 0.004 between plasma cfDNA and Xpert TB/RIF PCR

[d] *P* value > 0.99 between plasma cfDNA and IGRA

[e] *P* value = 0.63 between plasma cfDNA and IGRA

3.3.3. Study population for pathogen enrichment/DNA extraction

A total of 272 patients suspected of PTB were enrolled in this study. The patients' mean age was 59.8 ± 15.2 years and 174 (64.0%) patients were male. Malignant diseases (34.6%) and diabetes mellitus (19.9%) were the most common underlying diseases, followed by transplant status (4.8%) and liver cirrhosis (4.4%). Only one (0.4%) patient had an HIV infection (Table 3.4). Initially, 134 patients were diagnosed with TB and were started on anti-TB chemotherapy. Among them, six (4.4%) patients stopped receiving the chemotherapy because the clinical evidence for PTB was not considered enough to fulfill the treatment; the final diagnoses of these six patients were nontuberculous mycobacterium (NTM; n=2), pneumonia (n=1), and non-specific benign inflammatory lesion (n=3). A total of 128 patients were finally diagnosed with TB and underwent full-course chemotherapy, and were categorized into smear-positive culture-positive TB (n=35), smear-negative culture-positive TB (n=58), smear-negative culture-negative clinical TB (n=34); the remaining one could not produce a sputum sample. The remaining 144 patients did not meet the criteria of TB diagnosis according to the study definition (Fig. 3.3).

Table 3.4. Baseline characteristics in oral swab

	Total (n=272)	TB (n=128)	Not TB (n=144)	p value
Age, years ± SD	58·8 ± 15·2	56·4 ± 16·0	60·9 ± 14·1	0·014
Male sex, n (%)	174 (64·0)	85 (66·4)	89 (61·8)	0·43
Underlying disease, n (%)				
Malignant disease	94 (34·6)	31 (24·2)	63 (43·8)	0·001
Diabetes mellitus	54 (19·9)	24 (18·8)	30 (20·8)	0·67
Transplant recipient	13 (4·8)	8 (6·3)	5 (3·5)	0·28
Liver cirrhosis	12 (4·4)	5 (3·9)	7 (4·9)	0·70
Gastrectomy	7 (2·6)	1 (0·8)	6 (4·2)	0·13
Rheumatoid disease	3 (1·1)	0 (0·0)	3 (2·1)	0·25
HIV infection	1 (0·4)	1 (0·8)	0 (0·0)	0·47

SD, standard deviation; HIV, human immunodeficiency virus

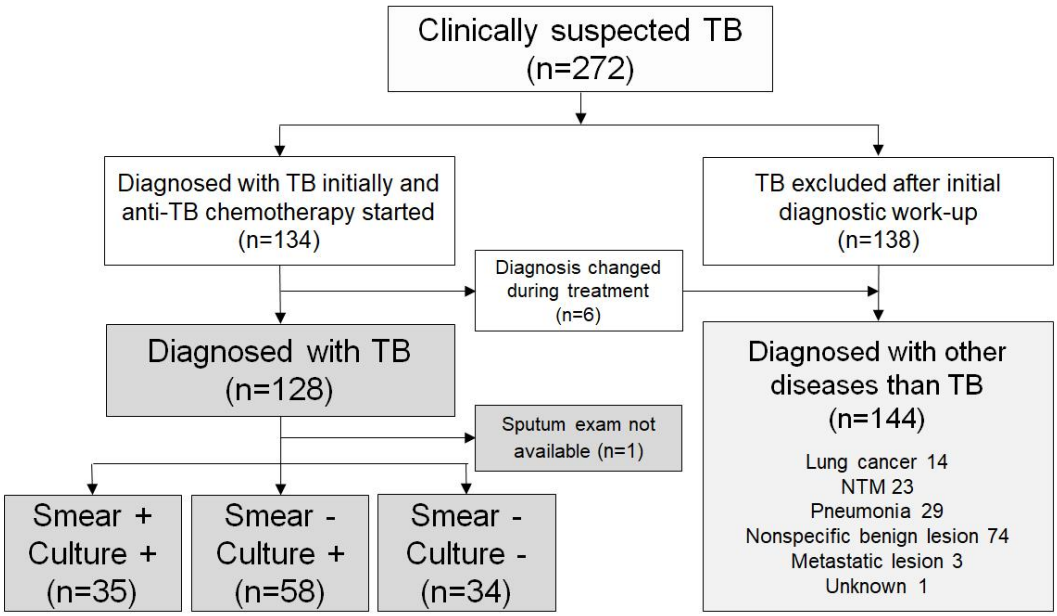

Figure 3.3. Diagnostic flow in oral swab. Among 272 patients with clinically suspected TB, 128 were finally diagnosed with TB by respiratory or infection specialists who were blinded to the results of pathogen enrichment/DNA extraction in oral swab samples.

3.3.4. Diagnostic performances of AFB microscopy, mycobacterial culture, Xpert, and oral swab DNA

Table 3.5 shows the results of the microfluidic platform and the Xpert assay according to clinical diagnosis stratified by AFB smear and MTB culture results, and their diagnostic performances compared with other tests are shown in Figure 3.4 and Table 3.6. In the overall patients, sensitivities of the microfluidic platform, Xpert, AFB smear, AFB culture, and QFT-plus assays for TB were 65.6%, 43.4%, 27.6%, 73.2%, and 68.2%, respectively. The sensitivity of the microfluidic platform was significantly higher than those of the Xpert assay ($p < 0.001$), but not significantly different from those of AFB culture ($p = 0.19$) and QFT-plus assay ($p = 0.72$). The specificities of the microfluidic platform, Xpert, AFB smear, AFB culture, and QFT-plus assays were 86.1%, 100%, 92.0%, 100%, and 61.7%, respectively. The specificity of the microfluidic platform was lower than those of Xpert and AFB culture, but significantly higher than that of QFT-plus (all $p < 0.001$). The sensitivities of the microfluidic platform and the Xpert assay were further analyzed according to the three categories of TB: smear-positive, smear-negative culture-positive, and culture-negative clinical TB (Fig. 3.4B).

The sensitivity of the microfluidic platform was not significantly different according to the TB categories and ranged from 63.8% to 68.6% ($p = 0.89$). In contrast, the sensitivity of the Xpert assay was the highest in smear-positive TB (79.4%) and was significantly lower in smear-negative culture-positive TB (41.1%, $p = 0.0004$) and culture-negative TB (9.4%, $p < 0.0001$). As such, whereas the two assays did not show significant differences in sensitivities in smear-positive TB ($p = 0.31$), the microfluidic platform had significantly higher sensitivities than did the Xpert assay in both smear-negative culture-positive TB ($p = 0.02$) and culture-negative TB ($p = 0.001$).

Table 3.5. Comparison of sputum exam results according to the categories of TB

		Microfluidic platform in oral swab (n=272)			**Xpert MTB/RIF** (n=252*)		
		Positive	Negative	Total	Positive	Negative	Total
	Total	84†	44	128	53	69	122
	Smear+ culture+	24	11	35	27	7	34
TB	Smear− culture+	37	21	58	23	33	56
	Smear− culture−	22	12	34	3	29	32
Not TB		20	124	144	0	130	130

*The results of Xpert MTB/RIF were not available in 20 patients.

†One patient without sputum exam was included. See Figure 2 for more details.

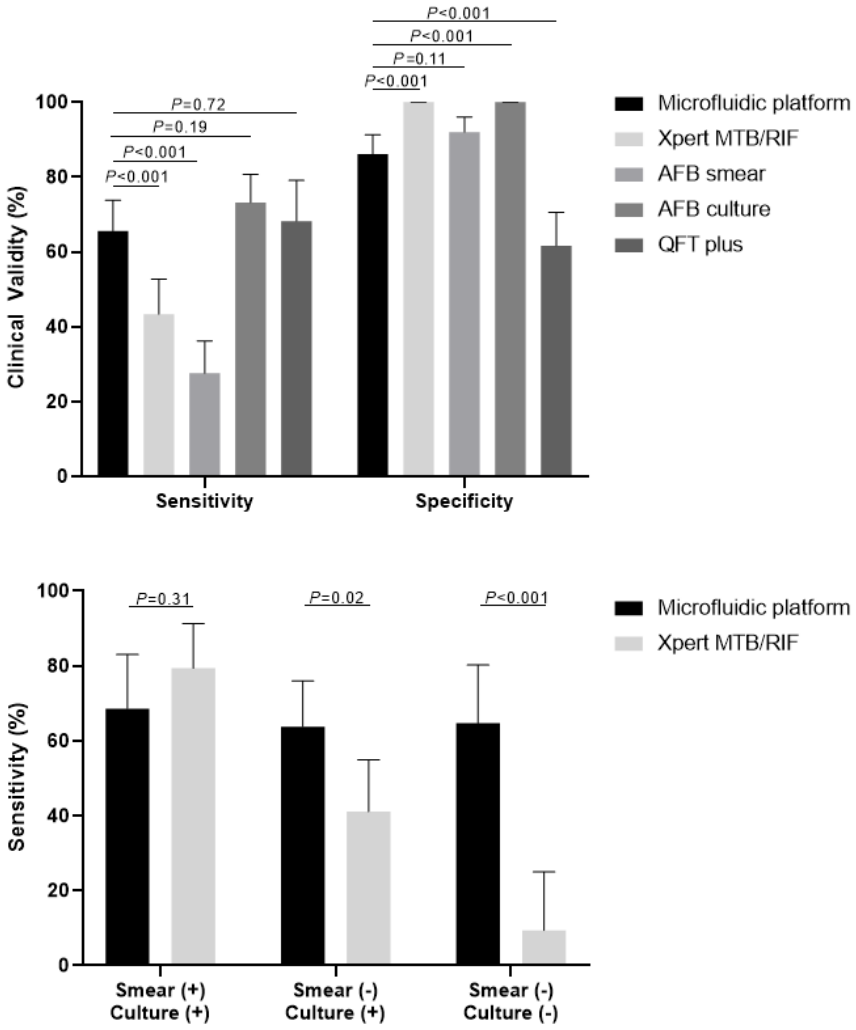

Figure 3.4. Clinical validity of the microfluidic platform in oral swab and the Xpert MTB/RIF assay for the diagnosis of TB. A) Sensitivities and specificities of the five different types of assays for the diagnosis of TB. (B) Sensitivities of microfluidic platform and Xpert MTB/RIF according to the categories of TB.

Table 3.6. Diagnostic performance of the TB assays according to the categories of TB

	Sensitivity % (n/N, 95% CI)	Specificity % (n/N, 95% CI)	PPV % (n/N, 95% CI)	NPV % (n/N, 95% CI)	Positive Likelihood Ratio (95% CI)	Negative Likelihood Ratio (95% CI)
TB (n=128) *vs* not TB (n=144)						
Microfluidic platform	66 (84/128, 57–74)	86 (124/144, 79–91)	81 (84/104, 73–87)	74 (124/168, 69–78)	4·73 (3·09–7·23)	0·40 (0·31–0·51)
Xpert MTB/RIF	43 (53/122, 34–53)	100 (130/130, 97–100)	100 (53/53)	65 (130/199, 62–69)	Not applicable	0·57 (0·48–0·66)
AFB smear	28 (35/127, 20–36)	92 (127/138, 86–96)	76 (35/46, 63–86)	58 (127/219, 55–61)	3·46 (1·84–6·51)	0·79 (0·70–0·89)
AFB culture	73 (93/127, 65–81)	100 (138/138, 97–100)	100 (93/93)	80 (138/172, 75–84)	Not applicable	0·27 (0·20–0·36)
IGRA	68 (45/66, 56–79)	62 (71/115, 52–71)	51 (45/89, 43–58)	77 (71/92, 70–83)	1·78 (1·34–2·37)	0·52 (0·35–0·76)
Culture-positive TB (n=99) *vs* not TB (n=144)						
Microfluidic platform	65 (64/99, 54–74)	86 (124/144, 79–91)	76 (64/84, 68–83)	78 (124/159, 73–82)	4·66 (3·02–7·17)	0·41 (0·31–0·54)
Xpert MTB/RIF	54 (51/95, 43–64)	100 (130/130, 97–100)	100 (51/51)	75 (130/174, 70–79)	Not applicable	0·46 (0·37–0·58)
AFB smear	35 (35/99, 26–46)	92 (127/138, 86–96)	76 (35/46, 63–86)	66 (127/191, 63–70)	4·44 (2·37–8·30)	0·70 (0·60–0·82)
AFB culture	94 (93/99, 87–98)	100 (138/138, 97–100)	100 (93/93)	96 (138/144, 91–98)	Not applicable	0·06 (0·03–0·13)
IGRA	73 (35/48, 58–85)	62 (71/115, 52–71)	44 (35/79, 37–52)	85 (71/84, 77–90)	1·91 (1·43–2·55)	0·44 (0·27–0·71)
Culture-negative TB (n=29) *vs* not TB (n=144)						
Microfluidic platform	69 (20/29, 49–85)	86 (124/144, 79–91)	50 (20/40, 38–62)	93 (124/133, 89–96)	4·978 (3·09–7·98)	0·36 (0·21–0·62)
Xpert MTB/RIF	7 (2/27, 1–24)	100 (130/130, 97–100)	100 (2/2)	84 (130/155, 82–85)	Not applicable	0·93 (0·83–1·03)
AFB smear	0 (0/28, 0–12)	92 (127/138, 86–96)	0 (0/11)	82 (127/155, 81–83)	0·00	1·09 (1·04–1·14)
AFB culture	0 (0/28, 0–12)	100 (138/138, 97–100)	Not applicable	83 (138/166, 83–83)	Not applicable	1·00 (1·00–1·00)
IGRA	56 (10/18, 31–78)	62 (71/115, 52–71)	19 (10/54, 12–27)	90 (71/79, 84–94)	1·45 (0·90–2·33)	0·72 (0·42–1·23)

PPV, positive predicted value; NPV, negative predicted value; CI, confidence interval; AFB, acid-fast bacilli; IGRA, interferon-gamma release assay.

3.4. Discussion and conclusion

3.4.1. Discussion and conclusion of cfDNA sampling

We evaluated the utility of plasma cfDNA for diagnosing active TB, enriched using our novel technique followed by conventional PCR. The sensitivity was significantly higher than that of AFB microscopy and comparable to or numerically higher than that of mycobacterial culture and Xpert. The diagnostic performances of plasma cfDNA assay were similar to those of IGRA, but the combined sensitivity of the two assays appeared to be complementary to rule out active TB. Interestingly, we showed that plasma cfDNA sensitivity was improved compared to those of AFB microscopy, mycobacterial culture, and Xpert in patients suspected to have EPTB, detecting which usually requires invasive diagnostic procedures. CfDNA detection in plasma has offered a promising and novel noninvasive modality in several medical fields [50, 51]. Pathogen-specific cfDNA has been also attractive in the field of infectious diseases. For example, Aspergillus PCR from plasma, serum, or whole blood has recently been applied to diagnose invasive aspergillosis [67, 68]. TB diagnosis is still challenging because of the poor performance of the diagnostic tools used currently [69]. Although WHO has endorsed Xpert and Xpert Ultra as sensitive and rapid diagnostic tools for TB recently, use of these assays is still limited in patients with PTB who have scarce sputum or difficulties to produce sufficient sputum and in patients with EPTB who need invasive targeted biopsy or surgery to obtain appropriate specimens for diagnosing TB. On the contrary, plasma cfDNA can be detected easily and conveniently in blood. Two recent studies have suggested that plasma cfDNA detection can be potentially used as an adjunctive and noninvasive TB diagnostic tool [54, 55]. These studies included patients with smear-positive PTB with high mycobacterial burden only. The C_T values for all positive cfDNA with targeting IS6110 were observed to be above 33 (median 38, IQR 37–39), which were high. Only one third of the patients with TB were detected positive using AFB microscopy and more than half patients had only EPTB in this study, indicating the inclusion of patients with relatively low mycobacterial burden in this study compared with those in previous studies; it is noteworthy that the sensitivity of plasma cfDNA was 80.0% in this study population. Particularly, the sensitivity of plasma cfDNA detection was substantially high (94.4%) in the patients with only EPTB. Although the present study

included few patients with only EPTB to draw a firm conclusion, our findings warrant further large clinical studies to evaluate the diagnostic utility in patients with pauci-bacillary TB or EPTB.

IGRA is also a blood-based diagnostic tool for TB. However, the sensitivity and specificity of IGRA are still suboptimal to confirm TB [70]. Since IGRA and cfDNA reflect host immune response to mycobacteria and mycobacteria itself, respectively, the two assays might theoretically be complementary to detect TB in suspected patients. Consistent with this hypothesis, the combined sensitivity of the assays in the blood of patients suspected to have TB was sufficient to rule out TB. Therefore, we suggest that these two complementary tests may be used as a rule–out test in patients suspected to have TB who could not tolerate invasive diagnostic procedures. It is noteworthy that we recently developed the dual IFN-gamma and TNF-alpha releasing assay using fluorospot with high specificity (94%) [71]. When the cellular component including peripheral blood mononuclear cells is used for fluorospot assay and the remaining supernatant plasma is used for cfDNA assay, both assays from a single blood sample might provide high sensitivity without compromising specificity. We are presently conducting this proof-of-concept study by using cfDNA and fluorospot assays in patients suspected to have TB.

In this study, the specificity of plasma cfDNA assay was lower than that in the previous studies [54, 55]. Nine patients without TB were detected to be positive by using plasma cfDNA assay. Some possible explanations about these results are listed below. First, we might have misdiagnosed these patients as without TB. However, since all of these patients were diagnosed with alternative diseases and recovered without anti-TB treatment, the possibility of misdiagnosis might be low. Second, the cross-contamination of *M. tuberculosis* DNA would be possible when using microfluidic platform. However, we think the risk of external contamination is extremely low based on our previous study [60]. Finally, these false positive findings may have resulted from past infection of TB or latent TB infection (LTBI). Among the six patients without active TB who tested positive by cfDNA assay and had available IGRA results, four were revealed to be positive by IGRA. Among these four patients, two patients had histories of anti-TB treatment and the remaining two patients were revealed to have LTBI based on IGRA. Therefore, further studies on cfDNA

detection in blood from patients with prior history of TB or LTBI are needed. Furthermore, the potential role of cfDNA in the diagnosis of subclinical or incipient TB that has recently been proposed as occuring between LTBI and TB in the disease spectrum [72] is worth determination. This study has some limitations. First, this study included a small number of patients at a single center. Therefore, large studies from multi-centers should be conducted. Second, only two patients with HIV infection was included in this study. Therefore, our data might not be applicable in the countries with high HIV prevalence. Third, we did not perform mycobacterial blood culture. Thus, we could not confirm whether the plasma cfDNA originated from actual cell-free *M. tuberculosis* DNA or mycobacteremia. However, the rate of mycobacteremia in patients with TB is low especially in HIV–uninfected patients based on previous studies [54, 73]; it was, thus, considered to be insignificant in our study population.

In conclusion, plasma cfDNA assay seems to be a useful adjunct to the current tests for diagnosing TB, especially when used in combination with IGRA for ruling out TB. In addition, the definite strengths of plasma cfDNA assay are less-invasiveness, simplicity, and ease of performance in patients who have difficulties to provide appropriate specimens for TB diagnosis. Therefore, we expect that this assay can be utilized to diagnose active TB complementarily with other conventional assays.

3.4.2. Discussion and conclusion of pathogen enrichment/DNA extraction

In this real-world practice setting study, we showed that the microfluidic platform, a non-sputum based diagnostic test, can detect PTB with high sensitivity, which was comparable or superior to those of sputum-based conventional tests such as AFB culture and Xpert. The superiority of the microfluidic platform was more prominent in smear-negative PTB, especially in culture-negative clinical PTB, which are cases with a low bacterial load. Due to the high sensitivity, the microfluidic platform produced some false-positive cases; nevertheless, the microfluidic platform had an acceptable specificity of 86.1%.

The development of a rapid, accessible, and highly sensitive diagnostic tool is a major challenge in the control and management of TB. Among a total of 10 million new TB cases worldwide in 2017, as many as 3.6 million cases were estimated to have been not diagnosed

or detected,1 which may be the main source of transmission and morbidity. As an effort to overcome this diagnostic gap, the WHO recommended the use of the Xpert assay as the initial test for TB. However, the sensitivity of the Xpert assay is not high enough for pauci-bacillary TB cases [45, 74], and is thus limited for use in smear-negative TB cases that require more sensitive diagnostic methods. To meet this unmet clinical need, we applied the microfluidic platform, a new generation pathogen enriching technique, and demonstrated its efficacy in PTB and other infectious diseases [60-62]. In most conventional assays, only a small volume of clinical samples is used for the detection of pathogens due to the capacity of the assays; in contrast, the microfluidic platform is able to use large volumes of samples by enabling simultaneous concentration and extraction of the pathogens in a single system. Due to this advantage, the sensitivity of the microfluidic platform for pathogen diagnosis is significantly higher than those of the conventional assays [60-62]. In addition, the microfluidic platform reduces the time, cost, instrument requirements, and additional receptors for sample processing.

Easier, safer, and effective sampling methods are also essential in TB diagnosis [75]. Many patients struggle to produce an adequate amount of sputum for testing. Non-sputum-based samples, saliva, urine, blood, and exhaled breath concentrate were thus tested, but these samples were typically less useful than sputum [76-78], Recent studies suggested the use of oral swab samples, which can be easily obtained through non-invasive, non-aerosol-producing methods. Previous studies have shown that MTB DNA can be detected in oral swabs from human and non-human primates [79-81]. Wood et al. reported 90% sensitivity of oral swab samples, although the number of participants was small and more than half of them (60%) were smear-positive [82]. Luabeya et al. reported that oral swab samples had 92.8% sensitivity and 91.5% specificity [83]. These two studies showed promising results, but both used samples from patients with positive Xpert results and used two swabs instead of one.

In our real-world setting study, the microfluidic platform was applied to detect PTB using single oral swab samples obtained from 272 patients suspected of TB. This new method overcame the main limitation of the currently available diagnostics. First, it shortened the time required for diagnosis, which can take several weeks when using AFB

culture. Second, it increased the sensitivity, which is relatively low in Xpert for use in cases of smear-negative PTB. Third, it showed the potential usefulness of non-sputum-based assays, whose efficacies were comparable or even superior to conventional sputum-based techniques. Non-sputum based assays will be especially helpful in mass-screening large groups of people (e.g., school, correctional facility, military base), in which obtaining sputum may be difficult in children or those without symptoms.

There is also an unmet clinical need for diagnosing extrapulmonary TB and PTB in patients who cannot produce an adequate amount of sputum. The sensitivities of Xpert in the diagnosis of PTB were shown to be very low when using samples other than sputum, such as exhaled breath condensates (0%) and saliva (38.5%) [76]. For TB pleurisy, the sensitivity was shown to be quite low at 30% [84]. The Xpert MTB/RIF Ultra assay showed improved sensitivities of 61% for TB pleurisy from pleural effusion and 44% for TB meningitis from cerebrospinal fluid (CSF) [85, 86]. Other techniques showed the possibility for the detection of MTB DNA from plasma [54]. The microfluidic platform can also be applied to various clinical specimens, including saliva, urine, blood, and CSF, while showing high pathogen detection sensitivity. Further study for the validation of microfluidic platform with various types of clinical samples and further development of the system with automation can widen its clinical utility. Indeed, our preliminary study using CSF in patients with suspected TB meningitis revealed that the microfluidic platform had a higher sensitivity than conventional assays including the Xpert MTB/RIF assay [62]. We expect that our on-going studies on the application of microfluidic platform in various specimens such as CSF, blood, and oral swab will be able to provide useful data on this issue.

In conclusion, the sensitivity of the oral swab-based microfluidic platform for the diagnosis of PTB was comparable or even superior to those of conventional sputum-based methods. The superiority of the microfluidic platform in sensitivity was more prominent in cases of smear-negative PTB, in which tests with a higher sensitivity are critically needed. Further studies on the application of automation will expand the role of the microfluidic platform in various clinical settings by using both sputum and non-sputum-based samples.

SECTION 2.

Advanced bio-optical sensing platform

Chapter 4. General information for bio-optical sensor

4.1. Significance and goal of study

An increasing number of pathogens that cause unexpected illnesses and epidemics among humans and animals have led to the loss of life and economic problems [87, 88]. Recently, emerging infectious diseases, such as Middle East respiratory syndrome-coronavirus (MERS-CoV) [89], Ebola virus (EBOV) [90], Zika virus (ZIKV) [91], outbreaks, have revealed that disease control systems require more e ective and coordinated responses, including vaccine development, diagnostic tools, and therapeutics [87]. According to the World Health Organization (WHO), an outbreak of MERS-CoV resulted in 1782 infections and 634 deaths in June 2016. In 2015, MERS-CoV infiltrated Republic of Korea, resulting in 186 infections and 39 deaths with high mortality rates of over 30% [92]. For more e ective prevention of emerging infectious disease threats, rapid diagnostics are needed to identify new pathogens for which vaccines and e ective therapeutics are not available.

Rapid diagnostic testing (RDT) based on antibody detection for infectious diseases produces results within an hour [93, 94]. However, the detection sensitivity of RDT is lower than that of sequence-based nucleic acid amplification methods. Hence, rapid diagnostics to identify and diagnose pathogens have been performed using nucleic acid-based detection techniques, such as end-point and real-time PCR, as gold standard methods [95]. While these methods are relatively sensitive and specific for pathogen detection, they have several limitations, including the long time to acquire results, high technicality, and costly equipment such as a thermal cycler [96-99].

Unlike DNA, RNA folds into specific base-paired conformations that contain single-stranded regions. Since single-strand structure of RNA is unstable, it is easily decomposed by high temperature and repetitive temperature changes. Meanwhile, isothermal

amplification technology has emerged as an alternative to RT-PCR to avoid such thermal constraints [100-104]. Many isothermal amplification methods have been developed to allow exponential amplification at both constant and low temperatures. Among the methods, recombinase polymerase amplification (RPA) does not require thermal cycling and operates at a single temperature [105-107]. RPA forms a complex of a primer and a recombinase enzyme to extend the DNA, which negates the need for a polymerase and cycle repetition. Despite the advantages of the isothermal methods, these methods still require improved sensitivity, additional steps including gel electrophoresis, and labeling with a fluorescent dye for detection. Together with this, biosensors that are label-free with real-time detection have been developed to overcome the limitations of isothermal methods, such as reduced reaction time and cost by eliminating the need for cycle completion, gel electrophoresis, and labeling [108-110].

Here, the advanced bio-optical sensing platform based on silicon microring resonator (SMR) was proposed. We reported an isothermal, label-free, one-step DNA/RNA amplification and detection system [31]. Moreover, we reported an improved bio-optical sensing platform by combining a RNA-guided clustered regularly interspaced short palindromic repeats/inactivated Cas9 protein (CRISPR/dCas9) [111] and novel arch-shaped multiple-target sensing [112]. To validate our advanced bio-optical sensing platform, optimization was performed using cell lines and bacteria, and clinical utility was confirmed using plasma samples of Q fever, scrub typhus (ST), severe fever with thrombocytopenia syndrome (SFTS) patients and nasopharyngeal samples of MERS-CoV and human coronavirus (HCoV) patients. These rapid, sensitive, and accurate diagnoses using advanced bio-optical sensing platform could be useful and potentially adaptable for better diagnosis across various clinical applications.

4.2. Components for bio-optical sensor

For use of bio-optical sensor, we were provided the SMR sensor device from One BioMed Pte. Ltd. Briefly, the SMR sensor device [2.5 cm × 1 cm × 0.3 cm] structures such as microring structures, waveguides, and gratings, were patterned on a commercially available 200 mm Silicon-On-Insulator (SOI) wafer with a 220 nm thick top silicon layer, and 2 μm thick buried oxide layer by 210 nm deep ultraviolet (UV) lithography. The structures were then etched into the buried oxide layer by a reactive ion-etching process, followed by the deposition of 1.5 mm high-density plasma (HDP) oxide as a top cladding layer [107]. An array of microrings was designed to consist of four rings that are connected to a common input waveguide (through). Each ring had a dedicated output waveguide (drop). One of the microrings, left under the SiO2 cladding, is used as a reference sensor to monitor temperature-induced drift. The output signals of the 3 remaining microrings are collected through a vertical grating coupler connected to a single-mode fiber optic probe. The tunable laser emits light from wavelength 1510–1612 nm, which corresponds to frequency from 1.861×10^5 GHz to 1.987×10^5 GHz. The ring resonance structure has multiple resonant wavelengths (frequencies) within the above wavelength range and the resonant peak we used for monitoring the wavelength shift is at −1550 nm (1.987×10^5 GHz). The insertion loss (IL) spectrum was measured using an EXFO IQS-2600B DWDM passive component test system [107]. All measured IL spectrums were analyzed with the Origin 7.0 data analysis and graphing software (OriginLab Corporation).

For modification of SMR sensor device, we used O2 plasma treatment system (CUTE, Femto Science Inc.), 3-aminopropyltriethoxysiane (APTES, 440140-100ML, Sigma-Aldrich), glutaraldehyde solution (GAD, 340855-25ML, Sigma-Aldrich), and target specific primers containing the 5′ amino-modifier C12 (Macrogen Inc.). The forward and reverse primers for bio-optical sensor were synthesized at the usual length of 35 bp (Table 4.1). For washing of SMR sensor device, we uesd ethyl alcohol 99.9% (Ducksan Co.), UltraPure™ DNase/RNase-Free Distilled Water (Invitrogen), 1x PBS pH 7.4 (Gibco), Sodium cyanoborohydride solution (296954-50ML, Sigma-Aldrich) and MES (M3674-250G, Sigma-Aldrich). In preparation for bio-optical sensing, we used an acryl well for surrounding of microring sensor area, vortex-mixer and mini-microcentrifuge for mixing and centrifugation

of samples. For nucleic acid isothermal amplification, we used TwistAmp Basic recombinase polymerase amplification (RPA) for DNA and TwistAmp Basic recombinase polymerase amplification-reverse transcription (RPA-RT) for RNA from TwistDx. To prevent evaporation of reaction buffer on SMR sensor device, we used mineral oil (M5904-500ML) from Sigma-Aldrich. The modified SMR sensor device, after the primers immobilized on the surface of the sensor area, can be used until 2 days later, but we prefer to use the sensor on the same day for removing any influence on the detection sensitivity by unknown inhibitors. Then, the SMR sensor device can be reused after the Piranha cleaning (70:30 H_2SO_4:H_2O_2) and repeated surface modification. The SMR sensor device and setup were shown Figure 4.1

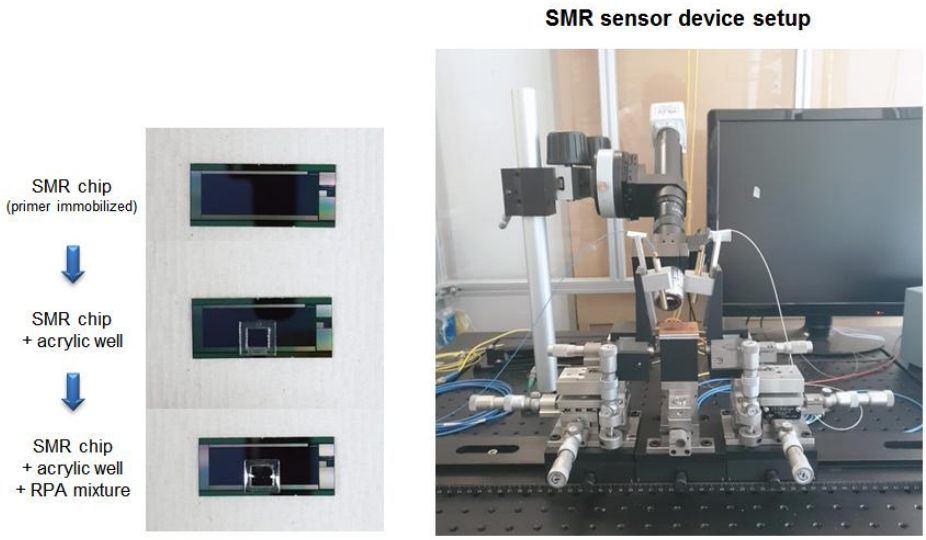

Figure 4.1. Image of the SMR sensor device and setup.

Table 4.1. Primer sequences for advanced bio-optical sensing platform in Section 2.

Assay		Primer	sequence (5'-3')	Modification
SMR biosensor	Q fever	Q fever - F	GAG CGA ACC ATT GGT ATC GGA CGT TTA TGG GGA TG	5' AmMC12
		Q fever - R	GTA TCT TTA ACA GCG CTT GAA CGT CTT GTT G	5' AmMC12
CRISPR/dCas9 -mediated biosensor	SFTS	SFTS - F	GGA GGC CTA CTC TCT GTG GCA AGA TGC CTT CA	5' AmMC12
		SFTS – R	GGC CTT CAG CCA CTT TAC CCG AAC ATC ATT GG	5' AmMC12
	ST	ST – F	GCA GCA GCA GCT GTT AGG CTT TTA AAT GGC AAT G	5' AmMC12
		ST - R	GCT GCT TGC AGT CAC CTT CAC CTT GAT TCT TTG	5' AmMC12
Arch-shaped multiple-target Sensing platform	MERS	MERS - F	CAA CGC GCG ATT CAG TTC CTC TTC ACA TAA TCG C	5' AmMC12
		MERS - R	CCT CTA CAC GG ACC CAT AGT AGC GCA GAG CTG C	5' AmMC12
		MERS - 10F	TTT TTT TTT TCA ACG CGC GAT TCA GTT CCT CTT CAC ATA ATC GC	5' AmMC12
		MERS - 10R	TTT TTT TTT TCC TCT ACA CGG GAC CCA TAG TAG CGC AGA GCT GC	5' AmMC12
		MERS - 20F	TTT TTT TTT TTT TTT TTT TTC AAC GCG CGA TTC AGT TCC TCT TCA CAT AAT CGC	5' AmMC12
		MERS - 20R	TTT TTT TTT TTT TTT TTT TTC CTC TAC ACG GGA CCC ATA GTA GCG CAG AGC TGC	5' AmMC12
		MERS - 30F	TTT TTT TTT TTT TTT TTT TTT TTT TTT TTT TTT TTT CAA CGC GCG ATT CAG TTC CTC TTC ACA TAA TCG C	5' AmMC12
		MERS - 30R	TTT TTT TTT TTT TTT TTT TTT TTT TTT TTT TTT TTT CCT CTA CAC GG ACC CAT AGT AGC GCA GAG CTG C	5' AmMC12
	ZIKV	ZIKV - 20F	TTT TTT TTT TTT TTT TTT TTT CAT ATT CCT TGT GCA CTG CGG CAT TCA CAT TCA C	5' AmMC12
		ZIKV - 20R	TTT TTT TTT TTT TTT TTT TTT TGG CGG TTA TCA GCC TTC CAA CTG GGG TCA GGG T	5' AmMC12
	EBOV	EBOV - 20F	TTT TTT TTT TTT TTT TTT TTA AGA TTA ATA ATT TTC CTC TCA TTG AAA TTT	5' AmMC12
		EBOV - 20R	TTT TTT TTT TTT TTT TTT TTT TCA ACT GAG CAC TGA TGC CCT TGC CCC CTC C	5' AmMC12
	HCoV	HCoV - 20F	TTT TTT TTT TTT TTT TTT TTG TCG ATC GGG ACC CAA GTA GCG ATG AGG CTA TTC	5' AmMC12
		HCoV - 20R	TTT TTT TTT TTT TTT TTT TTT GGA ATT AGG AGC AGA CCT TCC TGA GCC TTC A	5' AmMC12

4.3 Isothermal amplification strategy

As an isothermal amplification strategy used for nucleic acid amplification, RPA technology does not require the initial denaturation step of target nucleic acid and was optimized at a relatively low temperature of 37–43°C. In addition, it is also robust at off temperatures and low temperature setups, and generally operates at the typically ambient temperature of 25°C. If the reaction temperature changes slightly or drops to the RT level, the SMR sensor device takes a longer time for detection than the optimal temperature level, but it can detect target nucleic acid. Since the sensor area for the target detection is filled with the reaction mixture, the influence of humidity on the detection sensitivity is very small.

Briefly, the wavelength without any molecules on the SMR sensor device was not shifted at the initial wavelength value. However, when the desired molecule was attached to the sensor, the wavelength was shifted about 100–1000 pm depending on the target concentrations. Using this mechanism, the bio-optical sensor could quantitatively detect the target molecules.

4.4. Conventional RNA extraction

We used QIAamp viral RNA mini kit (52906, Qiagen) for extraction of viral RNA All viral RNA extraction processes were carried out according to the manufacturer's instructions. Approximately 60 µL of viral RNA was extracted. The extracted viral RNA was screened by real-time RT-PCR and stored at −80°C until use.

4.5. Conventional and real-time RT-PCR

Conventional assays, such as end-point and real-time RT-PCR, were used for comparison with the advanced bio-optical sensing platform to test its utility. The forward and reverse primers were synthesized at the usual length of 24 bp (Table 4.2). A OneStep RT-PCR Kit (210215, Qiagen) was used to produce cDNAs and amplified DNAs for further use. End-point RT-PCR consist of an initial reverse transcription step at 50°C for 30 min, followed by at 95°C for 15 min and 45 cycles at 95°C for 30 s, 60°C for 30 s, and 72°C for 30 s and final elongation step 72°C for 10 min. The reaction mixtures containing 25 µL of end-point RT-PCR reagent mixtures, 5x one-step RT-PCR bu er, 0.25 mM deoxynucleotide

triphosphate, 25 pmol of each primer, 1 μL of one-step RT-PCR Enzyme Mix, and 5 μL of RNA template. Gel electrophoresis was performed to separate RT-PCR products on a 2% agarose gel containing LoadingSTAR (A750, Dyne Bio Inc.). The gel was visualized using a ChemiDoc XRS + system (Bio-Rad).

The real-time RT-PCR procedure used was modified from the Bio-Rad CFX96 Instrument protocol and Brilliant III SYBR qRT-PCR Master Mix (600886, Agilent Technologies) was used. The real-time RT-PCR consisted of an initial reverse transcription step at 50°C for 20 min, followed by at 95°C for 15 min and 45 cycles at 95°C for 15 s, 60°C for 20 s, and 72°C for 20 s, followed by a cooling step at 40°C for 30 s. Additionally, reaction mixtures containing 20 μL of real-time RT-PCR reagent mixtures, 2x brilliant SYBR green qRT-PCR master mix, 25 pmol of each primer, and 5 μL of RNA template were prepared. The amplified products with SYBR Green signals were obtained using a CFX96 Real-time PCR System (Bio-Rad).

Table 4.2. Primer sequences for conventional and real-time PCR in Section 2.

Assay		Primer	sequence (5'–3')
Conventional & real-time PCR	Q fever	Q fever - F	GAGCGAACCATTGGTATCG
		Q fever - R	CTTTAACAGCGCTTGAACGT
	SFTS	SFTS - F	CGA GAG AGC TGG CCT ATG AA
		SFTS – R	TTC CCT GAT GCC TTG ACG AT
	ST	ST – F	GCA GCA GCT GTT AGG CTT TT
		ST - R	TTG CAG TCA CCT TCA CCT TG
	MERS	MERS - F	GCA ACG CGC GAT TCA GTT
		MERS - R	GCC TCT ACA CGG GAC CCA TA
	ZIKV	ZIKV - F	GGG CGT GTC ATA TTC CTT GTG C
		ZIKV - R	ACG GGG TTG GCG GTT ATC AGC
	EBOV	EBOV - F	GTG TGC GAA TAA CTA TGA GGA AG
		EBOV - R	CTA GAT GTT GAC AAG GGA TTT T
	HCoV	HCoV - F	CGA TGA GGC TAT TCC GAC TAG GT
		HCoV - R	CCT TCC TGA GCC TTC AAT ATA GTA ACC

4.6. T7 in vitro transcribed RNA preparation

We generate the T7 in vitro transcribed RNAs (T7 RNAs) to assess the detection ability of the advanced bio-optical sensing platform using the MEGAscript T7 Transcription kit (Invitrogen). For ZIKV, we used the QIAamp viral RNA mini kit to extract RNA from the medium of the NATtrol Zika Virus, External Run Control containing strain of MR766 (Zeptometrix Corporation), which was formulated with purified, intact virus particles chemically modified to render them non-infectious and refrigerator-stable. For EBOV, we used an EBOV Positive Control from the Ebola Virus (EBOV) Real-time RT-PCR kit containing EBOV NP gene RNA (Liferiver Bio-Tech Corp.). For others, we used clinical specimens for synthesis of T7 in vitro transcribed RNA. The amplified products generated in the end-point RT-PCR were used to create the T7 in vitro transcribed RNA. Synthetic RNA transcripts were purified with a MEGAclear Kit (Invitrogen) and quantified using a Nanodrop spectrophotometer (ThermoFisher). The purified T7 RNA were stored at −80°C until use.

Chapter 5. Bio-optical sensor for detection of Q fever

5.1. Introduction

Non- or less invasive methods for collecting human fluidic specimens, such as blood, urine, saliva, and swab, are cost-e ective, fast, and can be used repeatedly for a variety of infectious disease diagnoses reflecting the patient's current status [113-116]. In particular, because blood is a rich source of genetic material, disease marker, and infectious agent, diagnosis using biomolecules of the blood is a powerful approach for the detection of infectious diseases [117, 118]. Commonly, the four heme groups of hemoglobin present in red blood cells (RBCs) inhibit genetic analysis and diagnosis through their iron, so blood plasma is used to separate red blood cells from whole blood through centrifugation [119, 120]. Even in the e orts to eliminate the inhibitors, including hemoglobin, IgG fraction, leukocyte DNA, and anticoagulants such as EDTA, heparin, and, sodium citrate, which are present in the plasma, these inhibitors act as an impediment to the diagnosis of infectious diseases, leading to an increased false-negative rate and low detection sensitivity [121-124]. Therefore, diagnostic techniques are needed that can overcome low sensitivity and non-specific reactions as they are una ected by various inhibitors present in the blood plasma.

Conventional methods for diagnosing Q fever typically use antibodies or nucleic acids detection methods. Antibody-based methods include indirect immunofluorescence [125] and enzyme-linked immunosorbent assay (ELISA) [126]. These methods have several limitations, such as a low sensitivity and specificity. Nucleic acids-based methods use an end-point and real-time PCR for the direct detection of *Coxiella burnetii* [127, 128]. Although the PCR-based methods have a relatively high sensitivity and specificity compared to the antibody-based method, they require large equipment, such as a temperature control device and expensive dyes such as SYBR green and ethidium bromide (EtBr) dyes.

In this work, we present a highly sensitive SMR biosensor based on isothermal nucleic acid amplification for the label-free detection of infectious agents using blood plasma specimens. Their operation is based on the change of the refractive index to the measurable spectral shift of the optical transmission, and they enable a real-time, label-free detection by monitoring changes in resonant wavelengths generated by biomolecules such as pathogen,

proteins, and nucleic acids coupled with sensor ligands present on the sensor surface [29, 60, 106, 129-131]. The SMR sensor device using extracted DNA from the blood plasma of infectious disease patients shows that it is possible to diagnose patients who are di cult to clinically diagnose quickly and in a real-time manner. Acute Q fever may progress to a persistent, intensive infection such as endocarditis if not initially treated, but it is di cult to diagnose because there are no distinct features that distinguish it from other febrile diseases [132, 133]. In this study, we are developing a sensor based on SMR to detect the extracted DNA from 35 clinical samples (including 16 Q acute Q fever samples infected with *Coxiella burnetii* and 19 samples infected with other febrile diseases). Furthermore, we described several novelties regarding the SMR sensor device for diagnosing Q fever compared to the previous study. In our previous proof-of-concept study, the SMR sensor device was more sensitively developed for the detection of *C. burnetii* than conventional methods for Q fever diagnosis using frozen formaldehyde-fixed para n-embedded tissue and frozen blood plasma specimens from the Q fever patients [30, 134]. On the other hand, in this study, we first optimized the sensor for a rapid and accurate diagnosis of Q fever in prospectively collected fresh blood plasma specimens. Second, we validated that the sensor can distinguish Q fever from other febrile diseases, which are showing similar symptoms with Q fever patients. Third, the detection time of the SMR sensor device for diagnosing Q fever (10 min) was 20 min faster than that of the previous study (30 min). Fourth, we validated the clinical utility of the sensor in 35 patient samples. These results present that it can be applied to the diagnosis of diseases using clinical blood plasma in emergency patients with rapidity and specificity (Table 5.1).

Table 5.1. Comparison of the current and previous system of the SMR biosensor.

Content	Recent	Previous
Target diseases	Q fever	Q fever Tick-borne diseases Respiratory virus infection diseases
Clinical specimen	Fresh blood plasma	Frozen tissue Frozen blood plasma Nasopharyngeal
Amplification condition	38 °C (for DNA)	38°C (for DNA) 43°C (for RNA)
Limit of detection (copies/reaction)	10^1-10^2	NT
Reaction time	20 min	30 min
Detection time	10 min	20-30min

5.2. Materials and methods

5.2.1. SMR sensor device fabrication and surface functionalization

The SMR sensor device fabricated and described for the functionalization of the sensor using previous protocols [30, 130, 131]. Briefly, the functionalization of the SMR sensor devices consists of four steps, the first step being the hyrdoxyl group modification on the chip surface using the oxygen plasma treatment. The second step is silanization, using APTES. The O_2 plasma treated sensor was immersed in a solution of 2% APTES in a mixture of ethanol-H2O (95:5, v/v) for two hours and was then thoroughly rinsed with ethanol and DW. The third step is modified with GAD as an amine-amine crosslinking agent between amine functionalized modified sensors and a NH_2 terminated DNA primer, in order to form an amide bond by covalent bonding on the surface of the sensor. The sensors were cured by heating them to 120°C for 15 min. The sensors were then incubated with 2.5% GAD in DW containing 5 mM sodium cyanoborohydride for 1 h, then rinsed with DW and dried under a N_2 stream. The last step is the immobilization of a NH_2 terminated DNA probe. Pretreated sensors were prepared by incubation overnight (16 h) in 5 mM solutions of a DNA probe containing 5 mM sodium cyanoborohydride at RT. After incubation, unbound target specific primers were removed by washing them with 50 mM MES buffer, and the sensor was dried using an N_2 steam. An acrylic well was then pasted onto the chip in order to enclose the microring sensor area. At this time, the chips were considered ready for the optical measurement. The functionalized SMR sensor devices were sealed and stored at RT for later use.

5.2.2. Amplification and detection using SMR sensor device

We prepared RPA solution capable of nucleic acid amplification under isothermal (37–42°C) conditions in order to amplify and detect *C. burnetii* DNA. The primers and RPA solutions used in the SMR sensor device were prepared using the protocol described in a previous study [30, 130]. To optimize the sensor surface nucleic acid amplification using the RPA solution, 29.5 μL of rehydration buffer, 15 μL of DW, 2 μM dethiothreitol (DTT), and 2.5 μL of 10 mM reverse primer were mixed, and the solution was added to one dried enzyme pellet. Then, 2.5 μL of magnesium acetate (MgAc) solution was dispensed into the

cap of the tube. The unidirectional shake mode mixing protocol helps to homogeneously distribute the molecules required for the reactions present in the buffer. For use in the sensor reaction, only 10 μL of the 50 μL mixture solution is sampled and mixed with 5 μL of extracted DNA from the patient samples. 15 μL of the solution is filled into acrylic wells enclosing the microrings on the sensor, and the mineral oil is dispensed in order to prevent evaporation during amplification. To maintain the isothermal condition, a thermoelectric cooler (TEC) connected to a proportional integral differential controller (Alpha Omega Instruments) was used, and the resonance spectrum of the device was used immediately as a reference for obtaining the baseline. SMR allows the target DNA to selectively bind and amplify to the immobilized primer in the evanescent field of the resonator waveguide and then to increase the proportion of each wavelength. The wavelength shift was collected every 5 min for up to 20 min to monitor the amplification of the target DNA in a label-free and real-time manner.

5.2.3. Blood plasma from Q-fever patients

The 35 blood plasma samples from 16 acute Q fever patients infected with *C. burnetii* and 19 other febrile diseases were obtained using protocols approved by the Institutional Review Board of Asan Medical Center (2018–9023), Republic of Korea [133]. We also obtained the institutional approval and written consent of the patient. *C. burnetii*, DNA was extracted from blood plasma samples at a starting volume of 200 μL each and eluted approximately 100 μL using elution buffer. The extracted DNA was stored at −20°C until use.

5.3. Results and discussion

5.3.1. Principle of SMR biosensor

Figure 5.1 shows a schematic of the detection principle using the SMR biosensor for DNA extracted from the blood plasma of the acute Q fever patients. The extracted DNA is amplified by the isothermal-based, RPA reagent. The primer immobilized in the SMR sensor device is complementary to the target sequence, and was designed for RPA isothermal amplification. The amine terminated, forward primer was grafted on the surface of sensor device, and the reverse primer was mixed with the extracted DNA and the RPA reagent in the acrylic well. The immobilized primer was hybridized with the target DNA on the SMR surface, and the target was amplified by the RPA reagent at 38°C. The resonant wavelength is shifted over time by the amplified target product and measured in a label-free, real-time manner. Figure 5.2 shows the representative resonant wavelength shift for the detection of *C. burnetii* up to 20 min between the target from acute Q fever and other febrile diseased patients. The resonant wavelength shifts in 20 min using the SMR sensor device were 429.41 pm ± 16.27 in the acute Q fever plasma sample (positive) and 170.33 pm ± 13.30 in other febrile disease samples (negative). The resonant wavelength shift in the presence of *C. burnetii* DNA can be higher than the detection criterion, which was established by the resonant wavelength obtained from the negative samples. As a result, the targets were detected in plasma samples by measuring the resonant wavelength shift within 10 min.

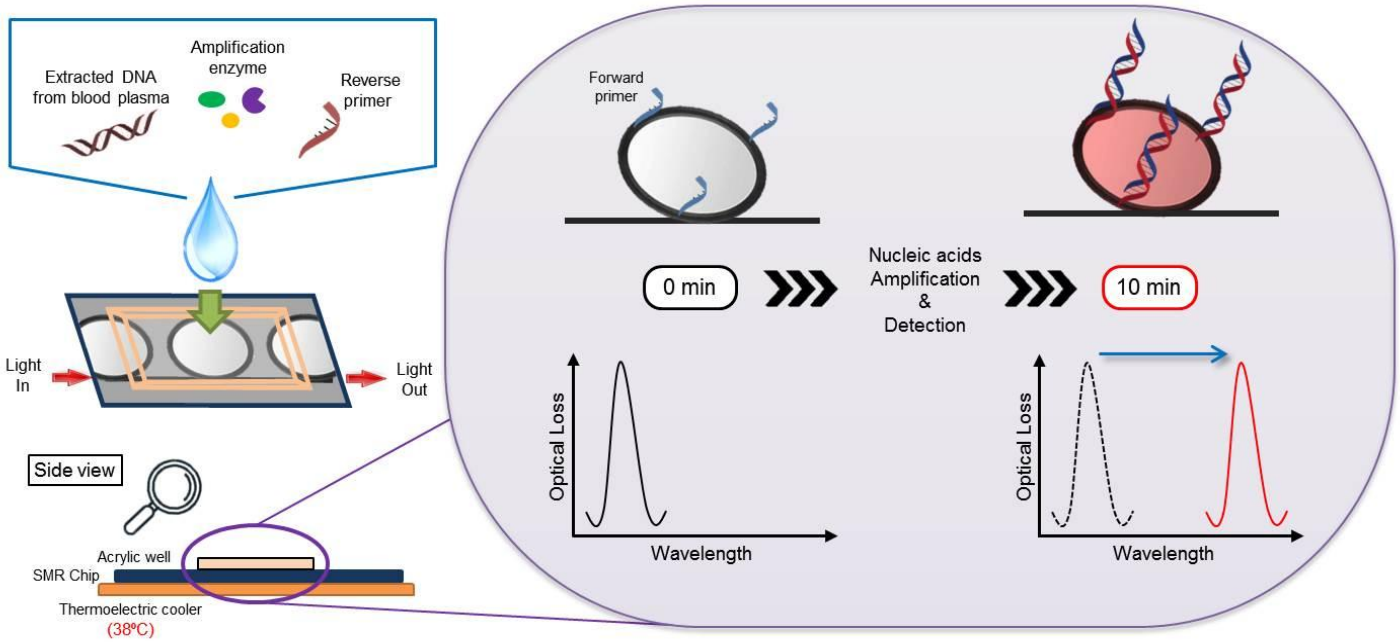
Extracted DNA from blood plasma
Amplification enzyme
Reverse primer
Light In
Light Out
Side view
Acrylic well
SMR Chip
Thermoelectric cooler
(38ºC)
Forward primer
0 min
Nucleic acids Amplification & Detection
10 min
Optical Loss
Wavelength
Optical Loss
Wavelength

Figure 5.1. Schematic representation of the principle of isothermal nucleic acid amplification and detection using SMR biosensor in clinical blood plasma specimens. In the isothermal condition (38 °C), the DNA is hybridized with immobilized DNA primer and the target sequence is amplified by the RPA reagent. The resonant wavelength is shifted over time by nucleic acid amplification on the sensor microring and measured in a real-time manner.

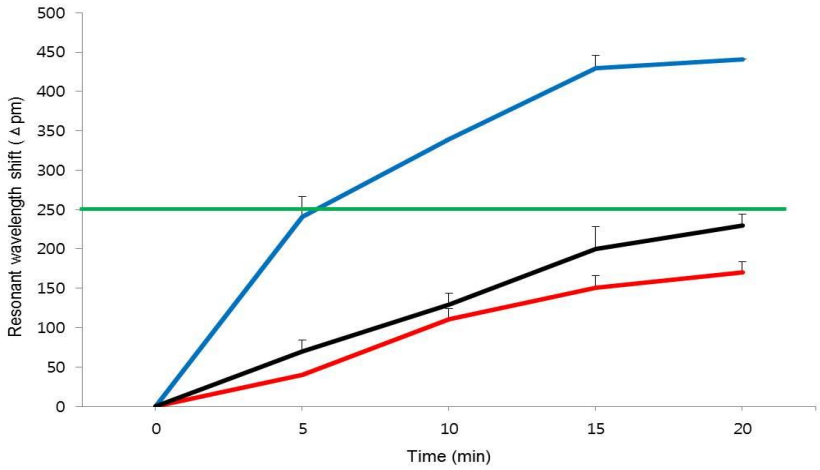

Figure 5.2. Identification resonant wavelength shift for *C. burnetii* detection using a SMR biosensor. The blue line shows an acute Q fever specimen (*C. burnetii* DNA) as a positive, and the red and dark line indicate the other febrile disease specimen and healthy control (no infection) as negatives, respectively. The resonant wavelength shift for detection of *C. burnetii* was shown within 20 min. The green line indicates a criterion for positive and negative determination in 10 min. The error bars indicate the standard deviation of the mean, based on at least three, independent experiments.

5.3.2. Sensitivity of SMR biosensor in clinical plasma specimens

To verify the clinical sensitivity of the SMR biosensor, the clinical plasma samples obtained from 16 confirmed Q fever patients, and 19 other febrile diseases were used (Fig. 5.3). Since Q fever does not differ significantly from other febrile diseases, the detection of acute Q fever through a rapid and accurate diagnosis is important [133]. We used the primers of the IS1111a gene of *C. burnetii* (NCBI Nr. M8806) in previous study [30] and measured the resonant wavelength shift assay every 5 min up to 20 min. The SMR biosensor detected 14 of 16 patients infected with 16 confirmed Q fever samples, and showed a high sensitivity of over 87.5% (14/16) in 10 min (Table 5.2). Notably, the SMR sensor device is capable of Q fever rapid detection within 10 min, except the extraction step of DNA from the plasma samples. Nevertheless, the sensor is faster than the conventional end-point PCR method for pathogen detection (> 2 h) [133]. Therefore, we have shown that this SMR biosensor can be useful for pathogen detection in blood plasma samples.

5.3.3. Specificity of SMR sensor device in clinical plasma specimens

To identify the clinical specificity of the SMR biosensor, we used a clinical plasma sample from each of 19 patients with other febrile diseases (Fig. 5.3). We also measured the resonant wavelength shift every 5 min for as long as 20 min using clinical specimens of other febrile diseases. The SMR biosensor confirmed that *C. burnetii* was not detected in 17 of 19 other febrile samples and showed a high specificity of 89.5% (17/19) at 10 min (Table 5.2). Therefore, the SMR biosensors have a higher specificity when using plasma samples from other febrile diseases. Our SMR biosensor showed a superior ability to detect pathogens in actual plasma samples and with a clinical utility.

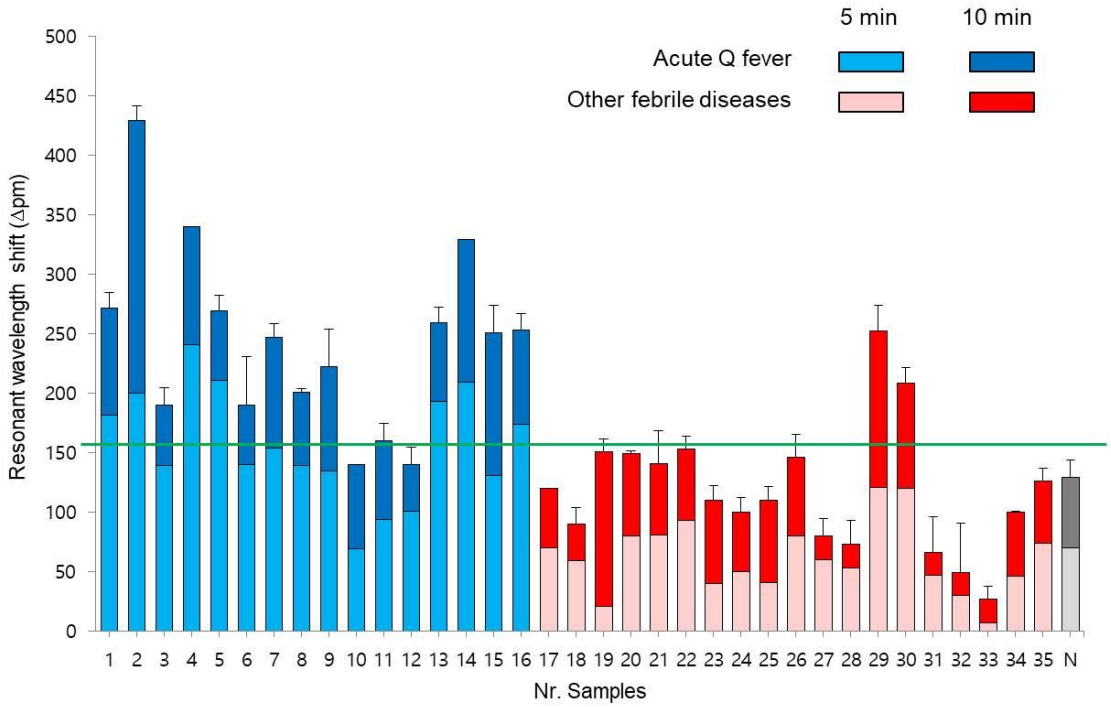
5 min
10 min
Acute Q fever
Other febrile diseases
Resonant wavelength shift (Δpm)
500
450
400
350
300
250
200
150
100
50
0
1 2 3 4 5 6 7 8 9 10 11 12 13 14 15 16 17 18 19 20 21 22 23 24 25 26 27 28 29 30 31 32 33 34 35 N
Nr. Samples

Figure 5.3. Clinical utility of the SMR biosensor with 35 patient blood plasma specimens for *C. burnetii* detection. The bar graph shows the resonant wavelength shift in 5 and 10 min. The blue bars indicate the result of 5 min (light blue) and 10 min (blue) of 16 samples of acute Q fever patients, and the red bars indicate the result of 5 min (light red) and 10 min (red) of 19 samples of other febrile diseases patients and gray bar indicates the result of 5 min (light gray) and 10 min (gray) of healthy control. The green line indicates a criterion for positive and negative determination in 10 min. The error bars indicate the standard deviation of the mean, based on at least three, independent experiments.

Table 5.2. Clinical sensitivity and specificity of the SMR biosensor for Q fever diagnosis using 35 clinical specimens at 10 min.

	SMR biosensor				**End-point PCR [28]**		
	Clinical Positive	Clinical Negative			Clinical Positive	Clinical Negative	
Test Positive	14	2	16	Test Positive	13	2	15
Test Negative	2	17	19	Test Negative	3	17	20
	16	19			16	19	
	Sensitivity 87.5%	Specificity 89.5%			Sensitivity 81.3%	Specificity 89.5%	

5.4. Conclusion

In this study, we proposed a rapid and accurate diagnosis technique for infectious disease in plasma samples using the SMR biosensor. Our system showed the real-time and label-free detection of DNA from *Coxiella burnetii* using plasma samples from Q fever patients In addition, a small amount of reaction volume (a total of 15 μL volume contained RPA reaction buffer and 5 μL of extracted DNA) was compared to that of the conventional PCR assay (a total of 25 μL volume contained PCR reaction buffer and 5 μL of extracted DNA), no thermoregulator was required and it was possible to determine positive or negative within 10 min. Our system has several advantages in plasma-based diagnostic. First of all, it is suitable for diagnosis using clinical samples, such as plasma, obtained from the patients. Previously reported plasma-based infectious disease diagnoses using the conventional PCR method showed a low sensitivity and specificity due to the various inhibitors contained in plasma, thus requiring an additional purification step after the DNA extraction because it was diffcult to accurately diagnose the infected patients [96]. This study confirms the clinical utility of 35 clinical plasma samples without additional purification steps after the DNA extraction using the SMR sensor device. The sensitivity of our SMR biosensor (87.5%) with blood plasma samples was higher than the PCR assay (81.3%), and it was confirmed that the SMR sensor device showed a similar specificity (89.5%) compared to the PCR assay. The immobilization of the DNA probe and amplification of the DNA product on the surface can reduce the non-specific reactions caused by primers present in the liquid phase, thereby increasing the detection specificity [112]. These results show that the SMR biosensor can be used as a substitute for the existing plasma-based diagnostic method because it can be detected more quickly (< 10 min) than the PCR assay (> 2 h) and also has a high sensitivity. Despite the enhancement of the current SMR sensor device, the validation of the sensor must be verified by using plasma samples from patients with various infectious diseases and various symptoms. Therefore, further development is required in order to process a large number of plasma samples through the scaling-up of the SMR biosensor or in order to be able to process a variety of biomarkers at the same time.

Chapter 6. CRISPR/dCas9-mediated bio-optical sensor

6.1. Introduction

In vivo genome editing technologies have great clinical application potentials [135, 136]. Zinc-finger nucleases (ZFNs) or transcription activator-like e ectors (TALEs)-based editing tools have been introduced for DNA targeting and regulation, however, these proteins need to be individually designed for DNA binding, which remains a hurdle for regulating multiple loci [135, 137]. In contrast, RNA-guided clustered regularly interspaced short palindromic repeats (CRISPR) associated Cas9 targets specific genomic loci via a single guide RNA (sgRNA), which contains a 20 bp guide sequence followed by a 3 bp protospacer adjacent motif (PAM) and recognizes target DNA through Watson-Crick base pairing [138]. The system uses an endonuclease Cas9 for nucleotide sequence based DNA targeting. Cas9 is guided by the sgRNA that specifically bind to and cleave double-stranded DNA in a site-specific manner [139-142]. Recently, Cas9 nuclease can be used to enrich and detect the small amounts of tumor fragments in the ctDNA or Zika virus [143, 144]. Also, other types of Cas proteins such as Cas12a or Cas13 are used for rapid detection of nucleic acids [145-148]. In addition to wild-type Cas9 or Cas9 orthologue proteins, catalytically inactivated Cas9 protein (dCas9) has great potential for various biological studies [149, 150]. In contrast to the wild type Cas9, the nuclease-deficient dCas9 have the ability to bind to DNA using sgRNA without cutting. Hence, dCas9 technology is a widely useful tool for in vivo and in vitro diagnostics [138, 149-151].

In this study, we developed an improved diagnostic tool by combining a CRISPR/dCas9 and an isothermal diagnostic approach based on SMR biosensor for simultaneous nucleic acid (RNA and DNA) amplification and detection with speed as well as high sensitivity and specificity. In the case of combination of dCas9 and isothermal based biosensor, dCas9 can recognize the target DNA or cDNA but not cut the sequences of target. Because of the binding property of dCas9, the refractive index is changed based on the binding with target and dCas9 that could be more enhanced the sensitivity than SMR biosensor alone. On the other hand, Cas9 can recognize the target DNA or cDNA and cut the target sequences. Thus, the binding-induced changes are not a ected. We demonstrated the

clinical usefulness of this technology by using 3 *Orientia tsutsugamushi*, the causative agent of ST, and 3 bunyavirus, the causative agent of SFTS. ST and SFTS are tick-borne infectious diseases that are common in Eastern Asia, especially in Korea, China, and Japan [149, 150]. Moreover, the clinical presentations of these diseases substantially overlap; therefore, a rapid and highly sensitive detection method is greatly needed. Our method clearly distinguished between ST and SFTS within 20 min from serum samples.

6.2. Materials and methods

6.2.1. Protein purification

For purification of recombinant dCas9 protein, T7 Express BL21 (DE3) *E.coli* were transformed with pET28a-His6-dCas9 plasmid. After culturing *E.coli* in Luria-Bertani (LB) broth at 30°C, protein expression was induced with 0.2 mM isopropyl β-d-1-thiogalactopyranoside (IPTG) for 16 h at 16°C. Cell pellet was collected by centrifugation at 5000g, and then lysed by sonication in lysis bu er (NaH2PO4 50 mM, NaCl 300 mM, imidazole 10 mM pH 8.0, 1 mM PMSF, 1 mM DTT, 1 mg/mL lysozyme). Soluble lysate was obtained by centrifugation at 8000g and incubated with Ni-NTA agarose beads for 1–2 h (Qiagen). Protein bound Ni-nitrilotriacetic acid (NTA) agarose beads were washed (NaH2PO4 50 mM, NaCl 300 mM, imidazole 20 mM pH 8.0) and dCas9 protein was eluted with imidazole containing bu er (NaH2PO4 50 mM, NaCl 300 mM, imidazole 250 mM pH 8.0). With 100 K Amicon centrifugal filter (Millipore), the bu er of eluted protein was exchanged, concentrated, and analyzed with 4–12% Bis-Tris gels (ThermoFisher).

6.2.2. In vitro cleavage assay

The PCR products (400 ng), which contained each *Orientia Tsutsugamushi* and bunyavirus DNA sequence, were mixed with 5.9 μL of rehydration bu er and 0.5 μL of 280 mM MgAc solution supplied in RPA-RT. In 10 μL reactions, bu er mixed PCR products were incubated with 1 μg Cas9 protein and 750 ng sgRNA for 1 h at 37°C as previous study [152]. For the positive control of the cleavage assay, same PCR products were cleaved in 1x NEBu er 3.1 (100 mM NaCl, 50 mM Tris-HCl, 10 mM MgCl2, 100 μg/mL BSA, New England BioLabs) condition. The RNase A (4 μg) was added to samples to remove sgRNA and the final samples were analyzed with agarose gel electrophoresis.

6.2.3. In vitro binding assay

dsDNA templates were prepared by annealing the 5′ biotinylated target DNA strands and the non-biotinylated non-target DNA strands at a 1:1.5 molar ratio. (OT_1_F_biotin: TATAAAGATCTTGTTAAATTGCAGCGTCATGCAGGAATTAGGAAAGC,
OT_1_R:GCTTTCCTAATTCCTGCATGACGCTGCAATTTAACAAGATCTTTATA,

SFTS_F_biotin:AAAAATTAGCTGCCCAACAAGAAGAAGATGCAAAGAATCAAGGT GAA, SFTS_R: TTCACCTTGATTCTTTGCATCTTCTTCTTGTTGGGCAGCTAATTTTT) 10 nM dsDNA was incubated with 300 nM dCas9 and 1 μM sgRNA in cleavage bu er condition. After 20 min incubation at 37°C, samples were resolved with 10% TBE gels using 0.5x TBE bu er supplemented with 5 mM MgCl2. Then, in vitro binding status was analyzed by using Chemiluminescent Nucleic Acid Detection Module Kit (ThermoFisher) and Biodyne B Nylon Membrane (ThermoFisher) according to the manufacturer's protocol.

6.2.4. Operation of CRISPR/dCas9-mediated biosensor and SMR biosensor alone

For simultaneous amplification and detection of target DNA or RNA using SMR biosensor alone, we used the RPA and RPA-RT solution for DNA and RNA, respectively. To prepare RPA or RPA-RT solution, 29.5 μL rehydration bu er, 15 μL of RNase inhibitor and H2O, 2.5 μL of 10 μM another primer were mixed. Then, reaction mix was added to freeze-dried enzyme. After that, 2.5 μL of 280 mM MgAc was dissolved into the tube. After mixing, 50 μL of reaction bu er was split into five 10 μL aliquots. To begin the reactions, 5 μL of DNA or RNA extracted from blood serum of the patients and 3 μL of dCas9 RNPs (300 ng of dCas9 and 225 ng of gRNA) were added to 10 μL reaction aliquot. The volume of 18 μL mixture was added into a SMR sensor device with an acrylic well placed surround the microring sensor area and 10 μL mineral oil added to prevent evaporation the mixture during amplification. The chip was then placed on a thermal pad to keep a specific temperature (38°C for DNA and 43°C for RNA). The wavelength shift was measured every 5 min to monitor the amplification of target DNA or RNA. Relative resonant wavelength shift was calculated by the equation; ΔΔpm = (target wavelength value, pm) − (non–target wavelength value, pm).

6.2.5. Blood plasma from tick-borne diseases patients

ST and SFTS serum samples were collected from the patients in Asan Medical Center. The study protocol was approved by the Institutional Review Board of Asan Medical Center, and informed consent was obtained from all participants. SFTS was confirmed by detecting viral ribonucleic acid (RNA) by real-time RT-PCR in serum, using a DiaStar 2x OneStep

RT-PCR Pre Mix kit (SolGent). A diagnosis of ST was established when we observed either a single positive result of an immunofluorescence assay (IFA; SD Bioline Tsutsugamushi Assay; Standard Diagnostics), or a ≥1:640 or fourfold rise of IFA titer in successive samples.

6.3. Results and discussion

6.3.1. CRISPR/dCas9-mediated biosensor as a molecular diagnostic tool

Figure 6.1A shows the design of CRISPR/dCas9-mediated biosensor that couples SMR-based isothermal nucleic acid amplification and dCas9 RNP. For simultaneous amplification and detection of nucleic acid, sequence specific primer of target was immobilized to the surface of the SMR biosensor and dCas9 RNP was in reaction chamber with single temperature for isothermal reaction with RPA. For DNA, a primer binds a recombinase enzyme to extend the DNA. For RNA, RPA-RT was used for the formation of complex of a primer and a recombinase enzyme to transcribe cDNA from RNA. The amplified nucleic acid targets were simultaneously detected by monitoring the wavelength shift. During the nucleic acid amplification process with dCas9 RNP on the SMR biosensor, the immobilized primer was hybridized with the target templates; dCas9 RNP, which allows sequence specific binding to the target nucleic acids (nearby the waveguide surface at immobilized forward primer, Fig. 6.2), subsequently caused a dramatic increase as a signal enhancer in the proportion of each resonant wavelength. The SMR biosensors transduce the presence of target molecules based on binding-induced changes in the refractive index proximal to the waveguide surface. dCas9 binds to the amplified product on the surface of the sensor and increases the molecular weight of the sensor surface, thereby increasing the detection sensitivity by increasing the refractive index change. Therefore, the CRISPR/dCas9-mediated biosensor detected the pathogenic nucleic acids with high sensitivity within 20 min compared to the SMR alone (Fig. 6.1A).

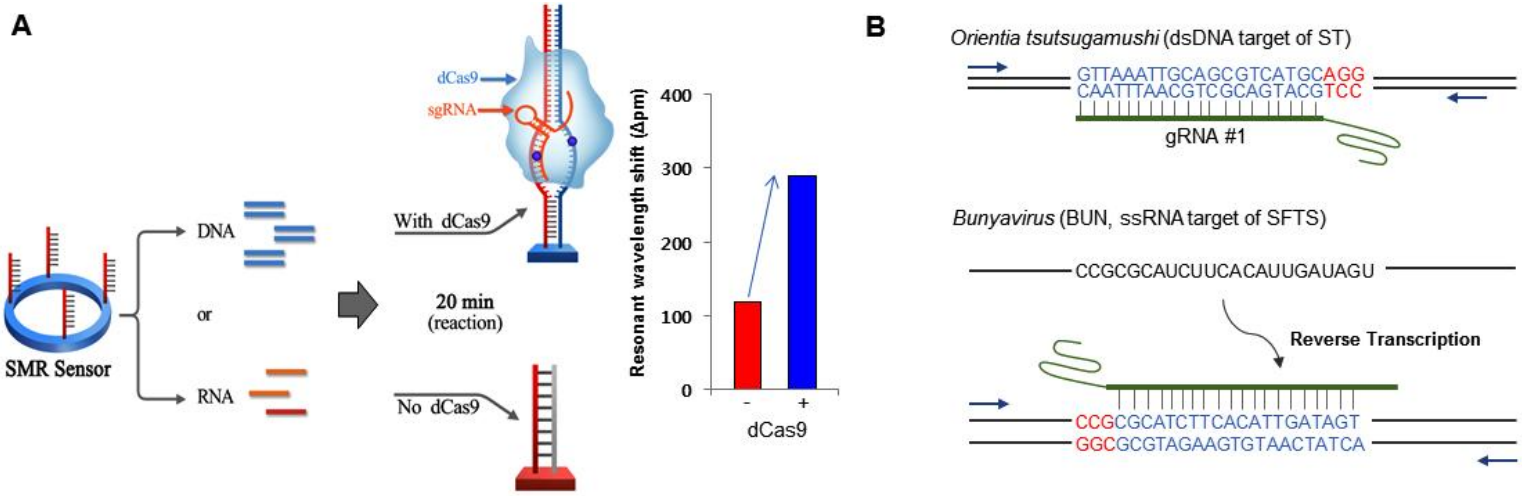
A
SMR Sensor
DNA
or
RNA
dCas9
sgRNA
With dCas9
No dCas9
20 min
(reaction)
Resonant wavelength shift (Δpm)
400
300
200
100
0
-
+
dCas9
B
Orientia tsutsugamushi (dsDNA target of ST)
GTTAAATTGCAGCGTCATGCAGG
CAATTTAACGTCGCAGTACGTCC
gRNA #1
Bunyavirus (BUN, ssRNA target of SFTS)
CCGCGCAUCUUCACAUUGAUAGU
Reverse Transcription
CCGCGCATCTTCACATTGATAGT
GGCGCGTAGAAGTGTAACTATCA

Figure 6.1. Schematic of CRISPR/dCas9-mediated biosensor. (A) Principle of CRISPR/dCas9-mediated biosensor. (B) The schematics of gRNA design targeting ST (*Orientia tsutsugamushi*) and SFTS (Bunyavirus). The target site is highlighted in blue and the PAM sequence is shown in red. (For interpretation of the references to color in this figure legend, the reader is referred to the web version of this article).

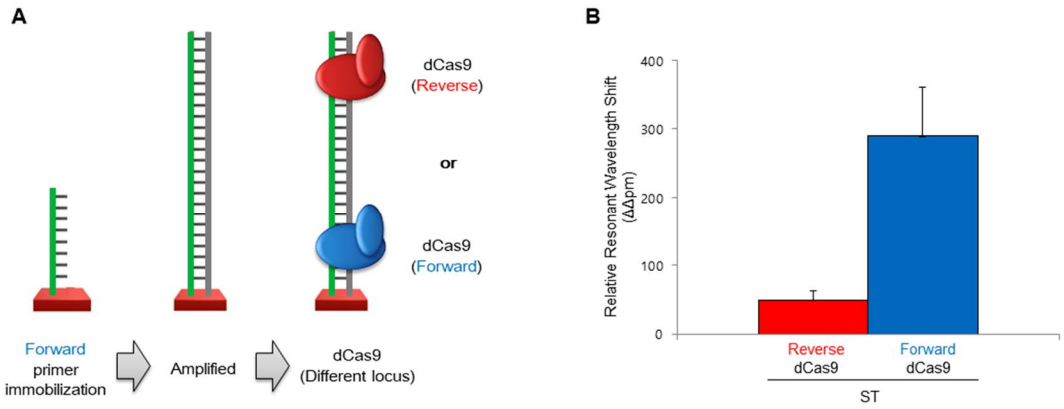

Figure 6.2. Optimization of binding locus of dCas9 RNP on the target primer sequence. (A) Schematic of CRISPR/dCas9-mediated biosensor with dCas9 recognizing targets in different locus (either forward or reverse). (B) Relative resonant wavelength shift of CRISPR/dCas9-mediated biosensor with dCas9 recognizing targets in different locus for detection of ST at 15 min

6.3.2. Assay optimization

To achieve sensitive detection with dCas9 RNP on SMR biosensor, we constructed guide RNAs (gRNAs) targeting two tick-borne pathogens that have substantially overlapping clinical presentations: *Orientia tsutsugamushi*, the causative agent of ST, and bunyavirus, the causative agent of SFTS (Fig. 6.1B). We observed that Cas9 RNPs induced targeted DNA cleavage and dCas9 RNPs bound target DNA in RPA bu er conditions using an in vitro cleavage assay and an electrophoretic mobility shift assay (EMSA), respectively (Fig. 6.3). To determine whether dCas9 RNP could enhance the detection sensitivity of the SMR biosensor, we amplified DNA fragments from ST clinical samples; as a result, we observed that the signal was higher with ST + dCas9 RNPs than with ST alone or ST + Cas9 RNPs at all time points (5–30 min)(Fig. 6.4A). The relative resonant wavelength shift results of the ST with dCas9 RNPs showed that it is possible to clearly separate the positive and negative than ST alone and ST with Cas9 RNPs. In the case of ST with Cas9 RNPs, because of the cutting property of Cas9 RNPs, the result of relative resonant wavelength shift was reduced and looked like a negative. This improvement is due to the specific binding of dCas9 RNPs with the target fragment on the biosensor, and not a non-specific binding e ect (Fig. 6.4B). Remarkably, dCas9 RNPs improved both detection sensitivity and specificity. We also optimized the concentration of dCas9 RNPs for sensitive and specific detection of pathogenic nucleic acids (Fig. 6.4C).

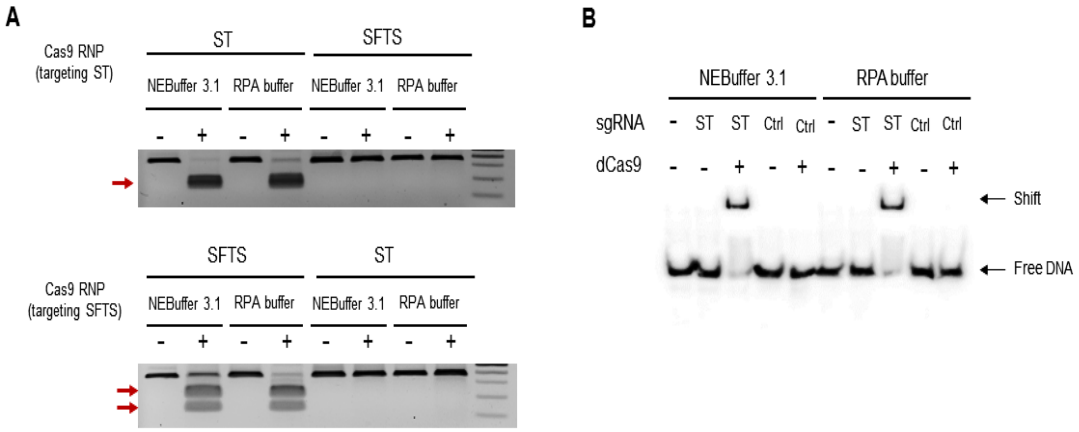

Figure 6.3. Ability of dCas9 RNP in reaction buffer. (A) in vitro cleavage assay to investigate the activity of gRNAs in the RPA buffer condition. Cas9 RNP could cleave the PCR products in both the RPA buffer and the NEBuffer 3.1 condition only when gRNAs were matched to the target PCR products. (B) Electrophoretic mobility shift assay (EMSA) using dCas9 RNP and the 5′ biotinylated DNA duplexes. The target DNA duplexes were only shifted with the matched gRNAs in both the RPA buffer and the NEBuffer 3.1 condition.

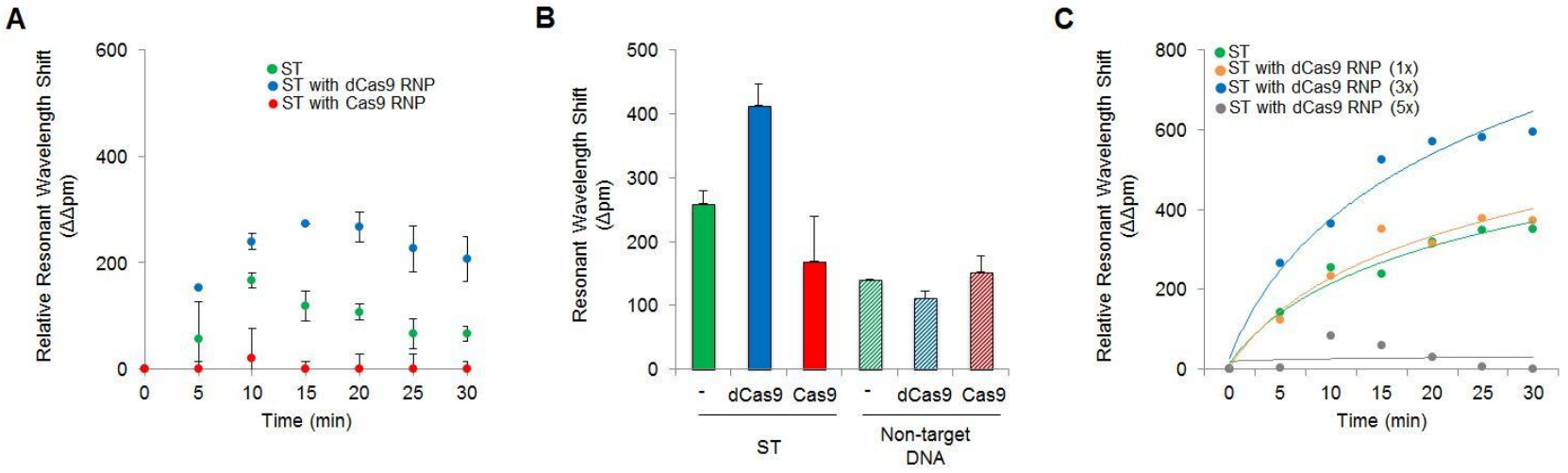
A
Relative Resonant Wavelength Shift (ΔΔpm)
600
400
200
0
0
5
10
15
20
25
30
Time (min)
ST
ST with dCas9 RNP
ST with Cas9 RNP
B
Resonant Wavelength Shift (Δpm)
500
400
300
200
100
0
-
dCas9
Cas9
-
dCas9
Cas9
ST
Non-target DNA
C
Relative Resonant Wavelength Shift (ΔΔpm)
800
600
400
200
0
0
5
10
15
20
25
30
Time (min)
ST
ST with dCas9 RNP (1x)
ST with dCas9 RNP (3x)
ST with dCas9 RNP (5x)

Figure 6.4. Characterization of CRISPR/dCas9-mediated biosensor. (A) CRISPR/dCas9-mediated biosensor detection of ST-DNA within 30 min. ST (SMR biosensor only, green), ST with dCas9 ribonucleoprotein (RNP) (dCas9 with biosensor, blue), ST with Cas9 RNP (Cas9 with biosensor, red), and negative control (black-X). (B) Resonant wavelength shift of CRISPR/dCas9-mediated biosensor for detection of ST in 15 min. SMR biosensor alone (green), with dCas9 RNP (blue) and with Cas9 RNP (red). (C) Relative resonant wavelength shift of CRISPR/dCas9-mediated biosensor in 30 min. The colors represent the amount of the dCas9 RNP; green (ST without dCas9 RNP), orange (ST with 1× of dCas9 RNP, $p > 0.1$), blue (ST with 3× of dCas9 RNP, $p < 0.001$), and grey (ST with 5× of dCas9 RNP, $p > 0.1$). Error bars indicate standard deviation from the mean, based on at least 3 independent experiments. (For interpretation of the references to color in this figure legend, the reader is referred to the web version of this article).

6.3.3. Single molecule detection using CRISPR/dCas9-mediated biosensor

Next, we determined the detection sensitivity of CRISPR/dCas9-mediated biosensor for detection of pathogenic DNA (for ST) or RNA (for SFTS) fragments from *Orientia tsutsugamushi* and bunyavirus. We used a RPA or RPA-RT based CRISPR/dCa9 mediated biosensor for double-stranded DNA and single-stranded RNA amplification, respectively. To test the detection sensitivity of ST and SFTS alone, and with dCas9 RNPs, we used serially diluted samples containing 1×10^0 to 5×10^9 copies of the ST PCR product and T7 transcribed SFTS RNA. As a result, by using dCas9 RNPs, we achieved single-molecule sensitivity for the detection of ST (0.54 aM) and SFTS (0.63 aM) within 30 min (Fig. 6.5A and B). The detection sensitivity of this CRISPR/dCas9-mediated biosensor (1 copy) was superior to that of the SMR biosensor alone (up to 10 copies) (Fig. 6.5A and B) and real-time PCRs (up to 100 copies) (Fig. 6.5C and D).

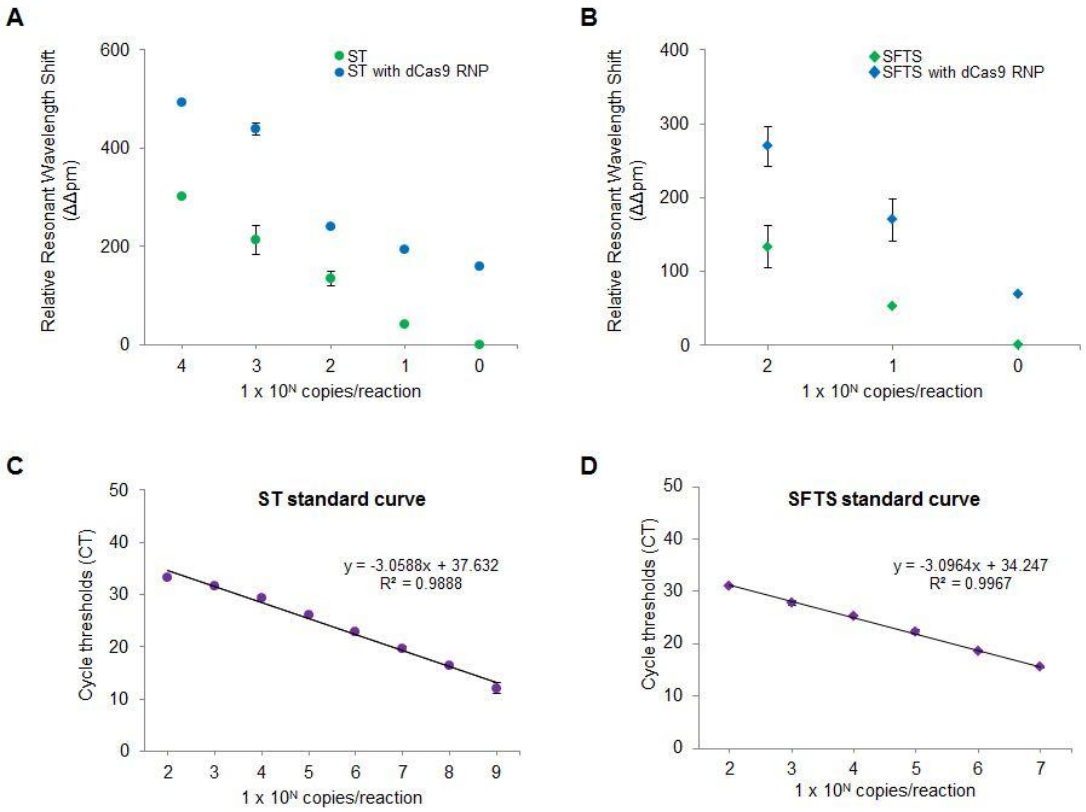

Figure 6.5. Comparison of detection limit of CRISPR/dCas9-mediated biosensor and real-time PCRs for DNA and RNA. (A) CRISPR/dCas9-mediated biosensor can detect dsDNA of ST at concentration down to 0.54 aM (blue circle), more sensitive than biosensor alone (green circle). (B) CRISPR/dCas9-mediated biosensor detected RNA fragment of SFTS at a concentration of 0.63 aM (blue triangle), which was more sensitive than biosensor alone (green triangle). (C) Linear relationship between the concentration of target DNA and Ct value of fluorescence signal by real-time PCR. The target DNA at low concentration (< 100 copies/ml) was not detected (over 40 Ct value). (D) Linear relationship between the concentration of target RNA and Ct value of fluorescence signal by real-time RT-PCR. The RNA target at low concentration (< 100 copies/ml) was not detected (over 40 Ct value). Error bars indicate standard deviation from the mean, based on at least 3 independent experiments. (For interpretation of the references to color in this figure legend, the reader is referred to the web version of this article).

6.3.4. Utility of CRISPR/dCas9-mediated biosensor in clinical samples

Finally, we investigated the clinical utility of this CRISPR/dCas9-mediated biosensor for clinical applications that require speed, high sensitivity, and specificity, such as the diagnosis of incipient tick-borne illnesses. We used the CRISPR/dCas9-mediated biosensor to analyze six clinical samples of three from ST patients and three from SFTS patients (Fig. 6.6). When we employed the CRISPR/dCas9-mediated biosensor with ST primers, we observed elevated signals only in ST samples and not in SFTS samples (Fig. 6.6A). When we employed the CRISPR/dCas9-mediated biosensor with SFTS primers, we detected elevated signals only in SFTS samples. Remarkably, the SFTS samples were more clearly detected by the CRISPR/dCas9-mediated biosensor than by the SMR biosensor alone (Fig. 6.6B). Thus, we demonstrated that the CRISPR/dCas9-mediated biosensor can clearly distinguish the two pathogens from clinical samples.

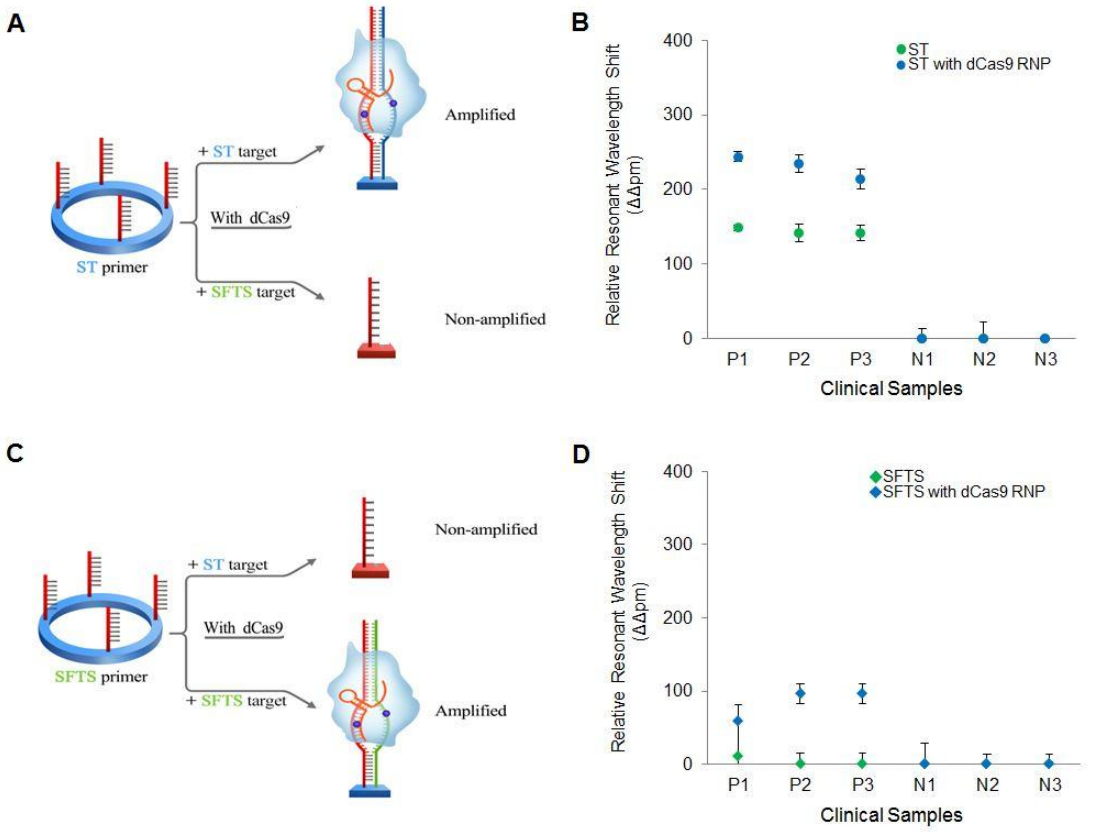

Figure 6.6. Clinical utility of CRISPR/dCas9-mediated biosensor. (A) Schematic of CRISPR/dCas9-mediated biosensor for ST diagnosis in ST and SFTS samples. (B) Highly sensitive and specific detection of ST-DNA with CRISPR/dCas9-mediated biosensor (blue circle) in six clinical samples compared to that of SMR biosensor alone (green circle). P1-3, human sera from ST patients as positives; N1-3, human sera from severe fever with thrombocytopenia syndrome (SFTS) patients as negatives. (C) Schematic of CRISPR/dCas9-mediated biosensor for SFTS diagnosis in ST and SFTS samples. (D) Highly sensitive and specific detection of SFTS-RNA with CRISPR/dCas9-mediated biosensor (blue triangle) in six clinical samples compared to that of biosensor alone (green triangle). P1-3, human sera from SFTS patients as positives; N1-3, human sera from ST patients as negatives. Error bars indicate standard deviation from the mean, based on at least three independent experiments. (For interpretation of the references to color in this figure legend, the reader is referred to the web version of this article)

6.4. Conclusion

We developed a CRISPR/dCas9-mediated biosensor that combines a catalytically inactive dCas9 and SMR biosensor based isothermal nucleic acid amplification for rapid and high sensitive detection of pathogens in clinical settings. Using CRISPR/dCas9-mediated biosensor, we achieved single molecule sensitivity for the detection of ST (0.54 aM) and SFTS (0.63 aM). Also, our method clearly distinguished between ST and SFTS within 20 min from serum samples.

We addressed several features for clinical use of this assay. First, CRISPR/dCas9-mediated biosensor enhances detection sensitivity through triple-targeting (primer, target strand, and dCas9). dCas9 shows higher sensitivity and specificity than the conventional method because it requires accurate target recognition of 20 nt of gRNA (Table 6.1). Importantly, the triple-targeting method provides a significant advancement in terms of detection sensitivity from our previous SMR biosensor approach that utilized primer to target strand only [106, 131]. By using triple-targeting, we were able to detect a single copy target, which translates into 10 times higher sensitivity than that of SMR biosensor alone (10 copies) and 100 times more sensitive than that of real-time RT-PCR methods (100 copies). Second, the readout system of CRISPR/dCas9-mediated biosensor differs from other CRISPR based diagnostic assays (i.e., fluorescence dye) in fundamental ways [145-148]. SMR biosensor based isothermal nucleic acid amplification assay can be simultaneously amplified and detect the target without labeling. In addition, CRISPR/dCas9 enhanced the refractive index change on the sensor surface. Therefore, the readout of sample using our assay can be carried out within 20 min. Third, the results of false-positive or false-negative are minimized by the use of sgRNA, primer, and dCas9. We have also shown that this assay is able to clearly distinguish the two pathogens in clinical samples. Our data on the clinical sensitivity and specificity highlights the utility and practicality of CRISPR/dCas9-mediated biosensor. Fourth, Gootenberg et al. developed a CRISPR/Cas13a (previously known as C2c2)-based diagnostic assay [145, 146]. Because Cas13a is a programmable RNA-guided ribonuclease, Cas13a-based diagnosis is an RNA-based detection method that exploits the collateral e ect of Cas13a. Our complementary approach using CRISPR/dCas9 is a DNA-

based detection method that is able to detect nucleic acids during isothermal nucleic acid amplification without in vitro RNA transcription.

Finally, our CRISPR/dCas9-mediated biosensor method is being further improved for convenient operation based on the ASSURED criteria (A ordable, Sensitivity, Specificity, User friendly, Rapid, Equipment-free, Deliverable) in clinical settings [151]. A microfluidic platform is being developed for sample processing that uses non-chaotropic reagent-based thin film techniques. The platform is devised to allow simple, low-cost, rapid, and high-throughput nucleic acids (DNA, RNA) extraction from human body fluids [153, 154]. We believe that the final integration of sample preparation and CRISPR/dCas9-mediated biosensors into a single cartridge will significantly facilitate emerging pathogen diagnosis for making timely treatment decision for emerging infectious diseases.

Table 6.1. Comparison of the gold nanoparticle-DNA complex and CRISPR/dCas9 sensor

	Gold nanoparticle-DNA complex	**CRISPR/dCas9 sensor**
Signal Amplification factor	Gold nanoparticle	CRISPR/dCas9 RNP
Target recognition	DNA probe	guide RNA
Advantage	Adjustable AuNP size	RNA & protein complex High sensitivity and specificity
Disadvantage	Complex-complex Non-specific interaction	X
Muliplex	Decrease sensitivity due to non-specific interaction	Possible

Chapter 7. Arch-shaped multiple-target bio-optical sensor

7.1. Introduction

Multiplex detection techniques are critical for rapid diagnostics; however, self-inhibition and false-positive results caused by primer dimerization (from a primer-target template mismatch or primer itself) can reduce detection sensitivity and specificity in clinical applications. To overcome the limitations of multiplex detection, a solid-phase DNA amplification technique was developed by grafting both forward and reverse primers. However, the amplification e ciency of the grafting primer assay was approximately 90% lower than that of conventional PCR in solution. Thus, the solid-phase DNA amplification technique has not been widely explored for applications in pathogen diagnostics. These limitations have made it di cult to apply diagnostic methods in hospitals. Resolving these limitations will require the development of diagnostic methods that are easy-to-use, accurate, and rapid for use in hospitals.

Here, we reported a novel arch-shaped multiple-target sensing platform for rapid diagnosis and identification of emerging infectious pathogens. An isothermal amplification enzyme and oligonucleotide primers were immobilized on a SMR sensor device for specific detection of target nucleic acids from emerging infectious pathogens, such as MERS-CoV, Zika, and Ebola. In this study, rather than applying the amplified target and probe hybridization assay, we established long (> 50 base pair, bp) oligonucleotide primers at a high concentration (5 μM) to create an arch-shape on the sensor surface for solid-phase amplification, thus overcoming primer dimerization. The SMR biosensor allows for sensitive, label-free, and real-time sensing [130, 131], and the long primers at a high concentration greatly increased the rate and detection sensitivity of this method. For nucleic acid amplification, we used a RPA, which requires a small instrument for isothermal amplification [155]. Using the arch-shaped sensing platform, we detected RNA from HCoV, MERS-CoV, ZIKA, and EBOV with high sensitivity and specificity. The detection limit was 10 fold more sensitive than that of real-time RT-PCR. Furthermore, this multiple-target sensing platform rapidly (< 20 min) detected MERS-CoV in 20 clinical specimens, including

MERS-CoV and HCoV infections. Therefore, the arch-shaped multiple-target sensing platform can be used to rapidly identify pathogens in various clinical applications.

7.2. Materials and methods

7.2.1. Development and operation of the arch-shaped multiple-target sensor

To use the arch-shaped multiple-target sensing platform as a multiple detection system, we structured the SMR sensor device as previously described [130, 131]. For arch-shaped amplification and detection with specific primers immobilized on the sensor, a three-step primer modification was required on the surface of the sensing chip. First, amine group modification using APTES was performed on the sensing surface. Subsequently, the sensors were treated with oxygenated plasma and soaked in a solution of 2% APTES in a mixture of ethanol–H2O (95:5, v/v) for 2 h, followed by thorough rinsing with ethanol and DW. Second, carboxyl group modification was conducted using GAD as a linker. The sensors were cured by heating to 120°C for 15 min. Next, the sensors were incubated with 2.5% GAD in DW containing 5 mM sodium cyanoborohydride for 1 h, rinsed with DW, and dried under a nitrogen stream. Third, both forward and reverse primers were immobilized to target specific primers containing the 5′ amino-modifier C12. The pretreated sensor was prepared by overnight incubation at RT in a 5 or 10 μM mixture of forward and reverse primers containing 5 mM sodium cyanoborohydride. After incubation, unbound target specific primers were removed by washing with MES buffer and the sensors were dried using N_2. The prepared SMR sensor device was stored at RT until further use. To test the target amplification and detection in the primer immobilized SMR sensor device, RPA-RT containing 29.5 μL of rehydration bu er, 15 μL of RNase inhibitor and water, 2 μM of DTT, recombinase, polymerase enzyme, and 2.5 μLof MgAc solution. To start the reaction, 10 μL of RPA-RT solution and 5 μL of target RNA were mixed. Next, 15 μL of this mixture was added to the SMR sensor device with an acrylic well surrounding the microring sensor area. Additionally, mineral oil was added to prevent evaporation of the mixture during amplification. The arch-shaped multiple-target sensor assay was operated at a constant temperature (43°C). The sensor consists of four rings connected to a common input and separate dedicated output waveguides. One of the four microrings was used as a reference sensor to monitor temperature-induced drift. The 3 remaining microrings were used for sensing three targets (MERS, EBOV, and ZIKV) with a vertical grating coupler. For multiple-target monitoring, each dedicated output waveguide corresponding to the microring

immobilized di erent target specific primer was measured sequentially by moving the optical fiber. To obtain a baseline as a reference, the resonance wavelength was immediately measured. The resonance wavelength shift for multiple target detection was then measured every 5 min for up to 30 min to monitor the arch-shaped amplification of MERS, ZIKV, EBOV, and HCoV RNAs in a label-free and real-time manner.

7.2.2. Primer length and concentration for arch-shaped multiple-target sensing

We designed the Arch-RPA-RT primer based on genome sequence information for MERS, ZIKV, EBOV, and HCoV. The non-specific poly dT spacer sequence at the 5′ end of the primer allowed for the amplification product to warp to an arch shape in solid-phase amplification [156]. As such, primers were designed that were 10, 20, and 30 bp longer than the conventional primers. Di erent lengths of MERS primers for detecting MERS and HCoV were immobilized to the microring on the SMR sensor device. Subsequently, primers of suitable length for detecting MERS, ZIKV, EBOV, and HCoV were immobilized on the microring resonance sensors. For multiplexing experiments, we used an ultra-small dosage dispensing system with sciFLEXARRAYER SX (SCIENION AG) to avoid cross-contamination. Subsequently, droplets of other target specific primers solutions were dispensed to the microring at desired locations. Because a smaller amount of primer volume was used than in the previous method, a higher concentration of primer solution was used. Finally, the resonance wavelength shift by products of arch-shaped amplification was measured on the microring.

7.2.3. Nasopharyngeal swab from Middle East respiratory syndrome coronavirus and human coronavirus patients

To determine the utility of the arch-shaped multiple-target sensor, we used the QIAamp viral RNA mini kit to extract RNA from 20 nasopharyngeal samples of MERS and HCoV patients. The nasopharyngeal samples were collected from patients at the Asan Medical Center. The Institutional Review Board of Asan Medical Center approved the study protocol, and informed consent was obtained from all participants. We used samples at a starting volume of 200 μL each which were eluted to approximately 60 μL using viral

elution bu er. The extracted RNA was screened using the real-time RT-PCR assay for confirmation and stored at −80°C until further use.

7.3. Results and discussion

7.3.1. Design of arch-shaped multiple-target sensing platform

Figure 7.1 shows the design of the arch-shaped multiple-target sensing platform for rapid diagnosis of emerging infectious pathogens, such as MERS-CoV, HCoV, ZIKV, and EBOV, using a SMR sensor device. We established a series of primers for target amplification and simultaneous detection of specific multiple-targets rather than asymmetric amplification on a SMR sensor device lacking multiple target detection. For multiple-target sensing, the sensor surface was first amine-modified with APTES and linked to the NH_2-modified 5′-end of both primers. Second, both primers (forward and reverse) of a target were immobilized on the SMR sensor device surface. Immobilization of both primers reduces non-specific target binding and false-positives due to primer-dimerization, which leads to the production of non-specific PCR products in the solution. To form an arch-shaped template on the surface, we used longer primers containing non-specific poly dT spacers. The pair of primers for a single target was immobilized on an individual sensor using a spotting system (Fig. 7.2). Third, either RPA or RPA-RT was added for isothermal nucleic acid amplification. During the amplification reaction, both primers were covalently bound to the SMR sensor device and target templates were hybridized to both primers. To produce a copy of the hybridized template, RPA enzyme was activated to amplify the target template on the sensor surface. The attached forward primer bound the template, which could also bind to the attached reverse primer and form additional arch-shaped copies near the initial copies. Finally, we used an SMR sensor device, which is a rapid and highly sensitive system for evaluation in a real-time and label-free manner, for the signal readout from multiple sensors. We monitored the resonance wavelength shift changes for up to 30 min. The resonance wavelength shift was obtained by individual sensors using the immobilized specific primers (Fig. 7.1).

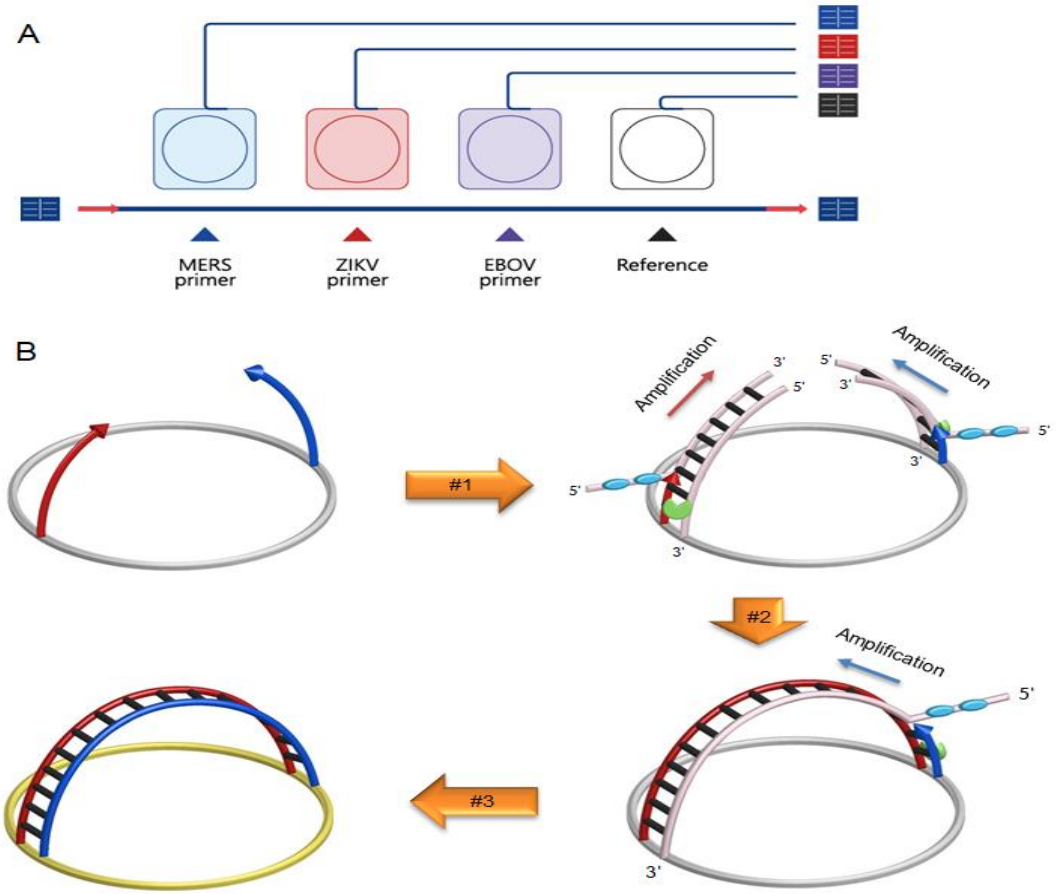
A
MERS primer
ZIKV primer
EBOV primer
Reference
B
#1
Amplification
Amplification
3'
5'
#2
Amplification
#3

Figure 7.1. Scheme of arch-shaped multiple-target sensing platform for diagnosis and identification of emerging infectious pathogens. (A) Array of silicon microring resonator (SMR) sensors for multiple-target detection. Each microring was modified with specific primers (forward and reverse) of MERS-CoV (blue), ZIKV (red), and EBOV (purple) recognizable target sequences. (B) Scheme representation of the principle of arch-shaped amplification and detection assay. First, SMR biosensors with specific primers immobilized to detect target RNA were prepared. Next, a mixture containing recombinase polymerase amplification-reverse transcription (RPA-RT) reagent and target extracted RNA was added to the platform (#1). During the reaction, RNA was synthesized by the RPA-RT enzyme mixture in an isothermal state (43 °C) as cDNA and either recombinase/forward (red arrow) primer or recombinase/reverse (blue arrow) primer complexes bound to double-stranded target cDNA and facilitated strand exchange at a constant temperature. After the displaced strand formed a D-loop by gp32 (sky blue), the immobilized primers were extended by polymerase (green) on the sensor surface (#2). The extended primers formed an arch-shaped amplification complex in the same microring and continued amplification (#3). Target detection was monitored in real-time by measuring the resonant wavelength shift by arch-shaped amplified products on the solid surface.

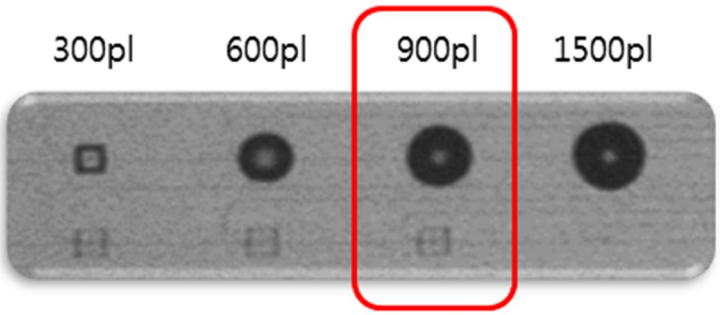

Figure 7.2. Image of spotting volume using the microspotting machine.

7.3.2. Optimization of arch-shaped multiple-target sensing platform

We first determined the optimized protocol for arch-shaped multiple-target sensing. Asymmetric amplification (one primer immobilized on a solid surface) generated one of the strands from the target template, and thus the detection sensitivity was less than that of symmetric amplification [157]. Therefore, to overcome the limitations of solid surface amplification methods, the size and concentration of the attached primers should exceed the critical value for e cient amplification on the solid surface. To optimize the primer protocol for multiple-targets, T7 RNA transcripts from a MERS-CoV sample were prepared for the model pathogen. We examined di erent primer lengths, including a non-specific oligo dT sequence, to determine the optimal primer length. The resonance wavelength of 54 bp primers was found to have shifted significantly compared to other primer sizes (Fig. 7.3A). Moreover, we determined the concentration of the attached primers (5 μM) (Fig. 7.3B). A primer concentration of 1 pM resulted in asymmetric amplification, indicating that this concentration was not suitable for the arch-shaped multiple-target sensing platform. Even high concentrations (10 μM) of attached primers could not discriminate between target and non-target templates (Fig. 7.3B). Therefore, the size and concentration of the attached primers were determined to establish arch-shaped surface amplification on the sensing surface.

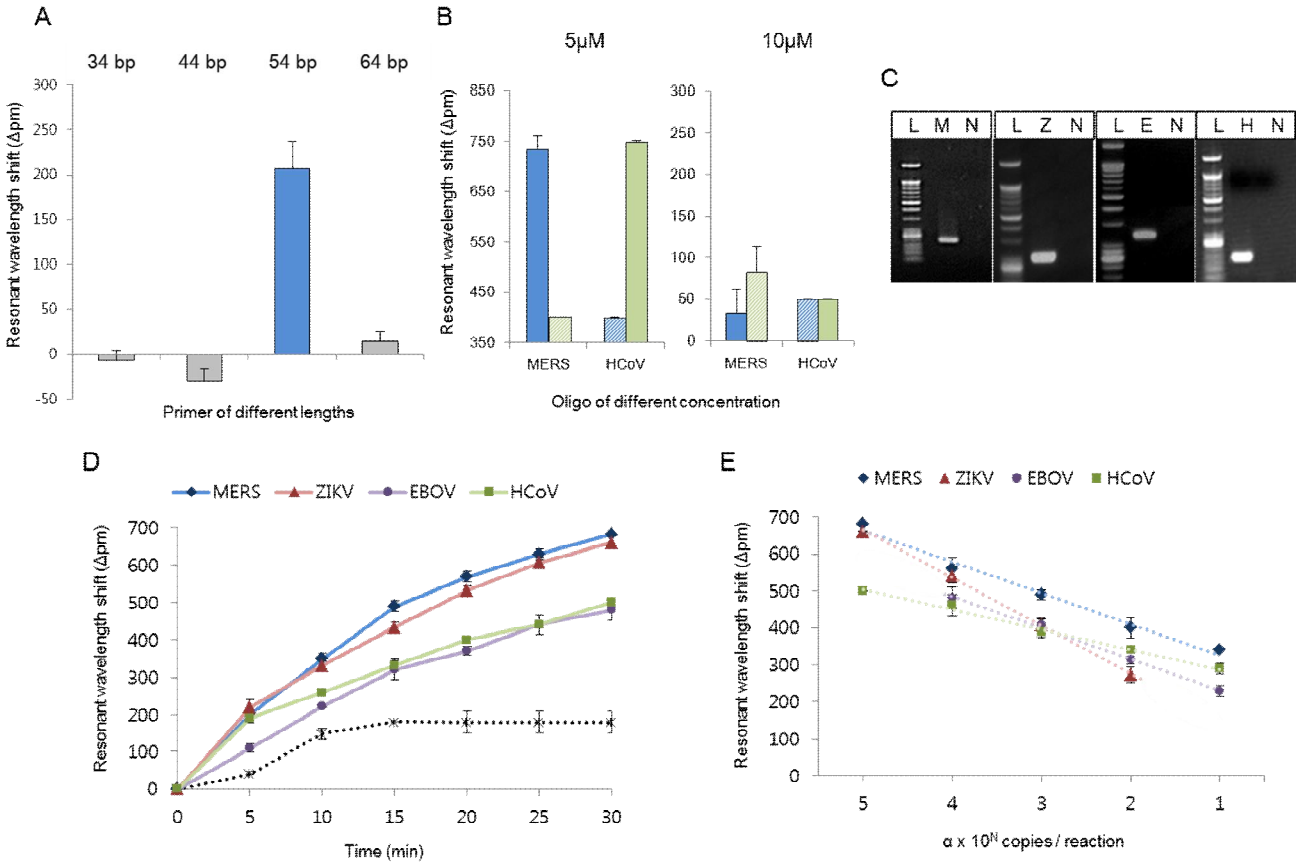
A
34 bp
44 bp
54 bp
64 bp
Resonant wavelength shift (Δpm)
Primer of different lengths
B
5μM
10μM
Resonant wavelength shift (Δpm)
MERS
HCoV
MERS
HCoV
Oligo of different concentration
C
L M N
L Z N
L E N
L H N
D
MERS
ZIKV
EBOV
HCoV
Resonant wavelength shift (Δpm)
Time (min)
E
MERS
ZIKV
EBOV
HCoV
Resonant wavelength shift (Δpm)
α x 10^N copies / reaction

Figure 7.3. Detection sensitivity of the arch-shaped multiple-target sensing. (A) Primer length testing for formation of the arch-shape. Monitoring of resonance wavelength shift by different oligonucleotide lengths of the MERS-specific primer immobilized on the sensor. (B) Primer concentration testing. Monitoring of resonance wavelength shift by different concentrations (5 and 10 μM) of the MERS (blue) and HCoV (green)-specific primer immobilized on the sensor for multiple-target detection. (C) Gel electrophoresis data for end-point RT-PCR products from MERS, ZIKV, EBOV, and HCoV (L: 50-bp DNA marker, M: MERS RNA template, Z: ZIKV RNA template, E: EBOV RNA template, H: HCoV RNA template, N: Negative control). (D) Resonance wavelength shift using the arch-shaped multiple-target sensing platform showing results of amplification and detection of MERS (blue diamond), ZIKV (red triangle), EBOV (purple circle), HCoV (green square), and negative control (non-target RNA, black asterisk) in a label-free and real-time manner. (E) Linear relationship between resonance wavelength shift by arch-shaped sensing platform and the concentration of targets in 30 min. Error bars indicate standard deviation of the mean based on at least 3 independent experiments.

7.3.3. Detection sensitivity and specificity of the arch-shaped multiple-target sensing platform

We next determined the detection sensitivity of the arch-shaped multiple-target sensing platform using MERS-CoV, HCoV, ZIKV, and EBOV as emerging infectious pathogens. T7 RNA transcripts of these pathogens, RNA of MERS-CoV or HCoV from clinical samples, or RNA of ZIKV and EBOV from commercialized kits (positive controls, 10^5 copies/reaction) were prepared at varying concentrations of 10^0–10^5 copies/reaction (Fig. 7.3C and E). Using the platform, the target RNA (10^5 copies/reaction) from the pathogens was clearly identified compared to non-targets within 30 min. The resonance wavelengths were shifted up to 681.48 ± 30.43, 500.75 ± 14.35, 660.55 ± 21.22, and 480.45 ± 28.55 pm for MERS-CoV, HCoV, ZIKV, and EBOV, respectively (Fig. 7.3D). Interestingly, the resonance wavelength results clearly revealed the target RNA in 5–10 min. Furthermore, we detected as few as 10–100 copies of RNA when serial dilutions of pathogen RNA were used with the platform (Fig. 7.3E). The wavelength change results showed good linearity with di erent concentrations (R2 = 0.9863, 0.9943, 0.9992, and 0.9971 for MERS-CoV, HCoV, ZIKV, and EBOV, respectively) in 30 min. We compared the RPA and SMR assay using this multiple-target sensor assay (Fig. 7.4). After confirming the detection of the amplified EBOV target in the RPA assay, the target band was clearly distinguished down to 5×10^3 copies/reaction (Fig. 7.4A). Additionally, after con–firming the detection of the amplified MERS target in the SMR assay, the target was clearly distinguished down to 2.5×10^2 copies/reaction (Fig. 7.4B). Notably, the sensitivity of the multiple-target sensing platform was 10–100 fold higher than that (10^3 copies/reaction) of the quantitative real-time reverse transcription PCR, RPA, and SMR assays (Table 7.1, Fig. 7.4 and 7.5).

Subsequently, we used the multiple-target sensing platform to identify di erent targets. A series of target primers from three pathogens, specifically MERS-CoV, ZIKV, and EBOV, was immobilized to the individual sensor with the spotting machine, which can immobilize the primer in a specific area (Fig. 7.6A). Using the specific attached primers for MERS-CoV, the amplified MERS-CoV RNA was detected with low background signals from other pathogens (Fig. 7.6B). Similarly, primers for other pathogens showed high specificity with low non–target binding (Fig. 7.6B). Additionally, when mixed virus (MERS

and HCoV) samples were used, the resonance wavelength shift of the MERS–specific primer immobilized on the platform was 560.71 ± 28.51 pm when only MERS (2.5×10^4 copies/reaction) virus was present and was 572.98 ± 11.05 pm when both MERS (2.5×10^4 copies/reaction) and HCoV (1.5×10^4 copies/reaction) viruses were present. The resonance wavelength analysis clearly detected the target RNA in the mixed virus samples, which showed similar results to the use of the single virus sample (Fig. 7.7). Indeed, a rapid, high sensitivity, and high specificity platform for multiple-target detection is needed for emerging pathogen diagnosis. The arch-shaped multiple-target sensing platform enables rapid and accurate pathogen genotyping.

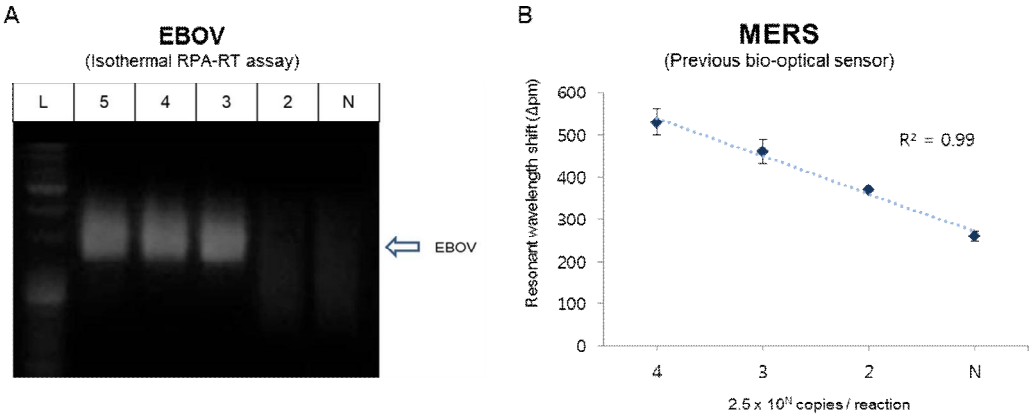

Figure 7.4. Limit of detection of conventional isothermal RPA-RT and previous single-target sensor assay. (A) Gel electrophoresis data for RPA-RT products from T7 *in vitro*-transcribed EBOV RNA. L: 25/100-bp ladder, 5: 5×10^5 copies/reaction, 4: 5×10^4 copies/reaction, 3: 5×10^3 copies/reaction, 2: 5×10^2 copies/reaction, N: negative control (HCT116 gRNA). (B) Linear relationship between the T7 *in vitro*-transcribed MERS RNA concentration and the resonance wavelength shift by previous single-target sensor assay. Error bars indicate standard deviation of the mean based on at least 3 independent experiments.

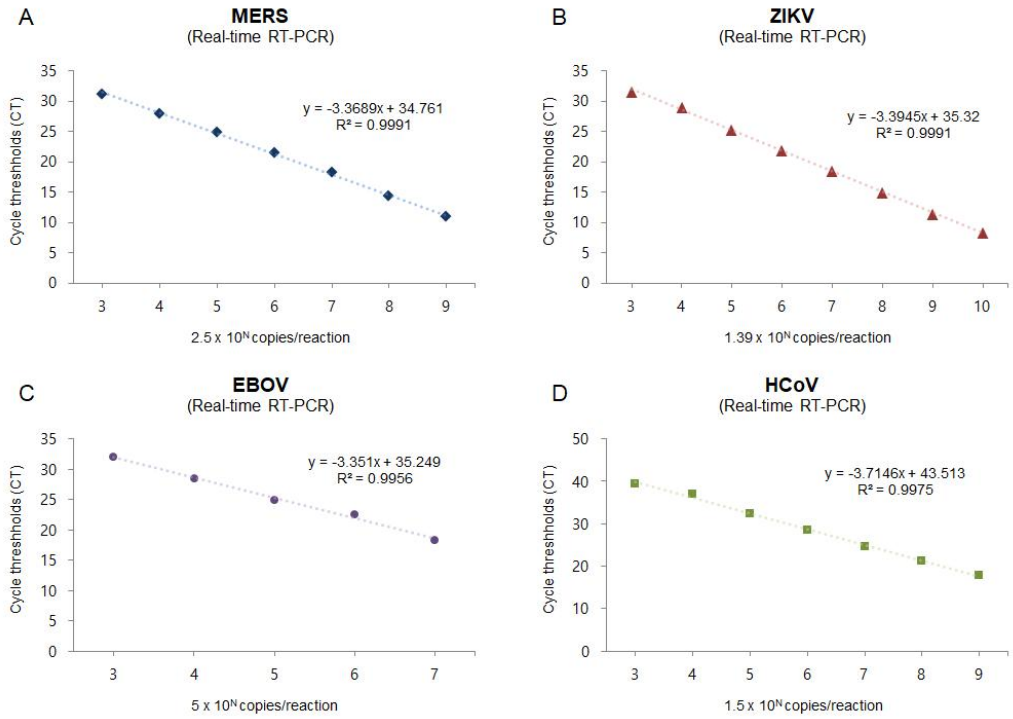

Figure 7.5. Linear relationship of the MERS, ZIKV, EBOV, and HCoV using real-time PCR. (A) MERS (blue diamond), (B) ZIKV (red triangle), (C) EBOV (purple circle), and (D) HCoV (green square). Error bars indicate standard deviation of the mean based on at least 3 independent experiments.

Table 7.1. Results of arch shaped multiple-target sensing and concentration conversion of clinical specimens

Clinical specimens		Arch shaped Wavelength shift (Δpm)	Concentration conversion (Copies/reaction)
MERS CoV	M1	290.2850	18.54
	M2	260.0750	8.78
	M3	349.4950	80.15
	M4	250.3550	6.91
	M5	269.8850	11.20
	M6	220.8333	3.33
	M7	230.6250	4.24
	M8	270.9750	11.50
	M9	370.4750	134.64
	M10	338.2850	60.75
	M11	299.9700	23.56
HCoV OC43	H1	490.3800	6.67 x 104
	H2	250.3900	5.79
	H3	500.1245	9.75 x 104
	H4	410.8400	3.01 x 103
	H5	220.2900	1.79
	H6	627.3533	1.39 x 107
	H7	240.1750	3.89
	H8	359.6900	4.10 x 102
	H9	330.2550	1.30 x 102

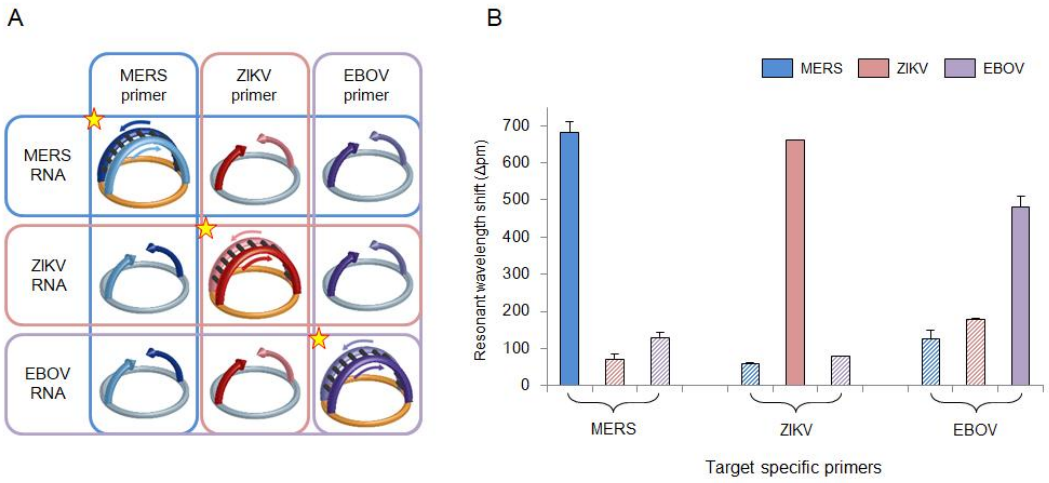

Figure 7.6. Cross-reactivity testing of the arch-shaped multiple-target sensing. (A) Scheme of the arch-shaped amplification and detection using different target RNAs and different target specific primers of MERS, ZIKV, and EBOV on the individual sensing platform. (B) Resonance wavelength shift by target RNA and target specific primers for MERS, ZIKV, and EBOV detection on the sensor. Error bars indicate standard deviation of the mean based on at least 3 independent experiments.

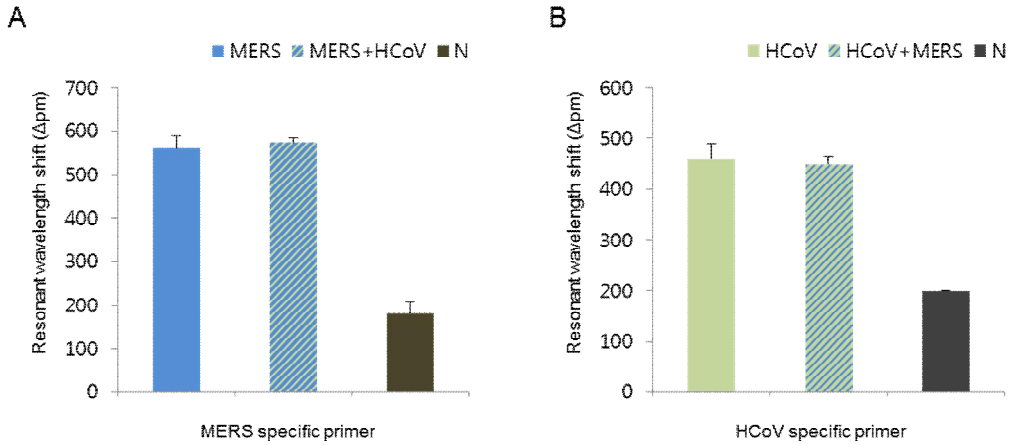

Figure 7.7. Comparison of resonance wavelength shift with single virus and both viruses in multiple-target sensor. (A) Resonance wavelength shift of multiple-target sensor immobilized with MERS specific primers using MERS only (2.5×10^4 copies/reaction, blue), MERS (2.5×10^4 copies/reaction), and HCoV (1.5×10^4 copies/reaction) mixed (blue with green oblique line) and negative control (HCT116 gRNA, dark gray). (B) Resonance wavelength shift of multiple-target sensor immobilized with HCoV specific primers using HCoV only (1.5×10^4 copies/reaction, green), HCoV (1.5×10^4 copies/reaction), and MERS (2.5×10^4 copies/reaction) mixed (green with blue oblique line) and negative control (HCT116 gRNA, dark gray). Error bars indicate standard deviation of the mean based on at least 3 independent experiments.

7.3.4. Clinical testing of arch-shaped multiple-target sensing platform in clinical specimens

We evaluated the clinical utility of the arch-shaped multiple-target sensing platform using clinical specimens (Fig. 7.8). Particularly, methods for di erentiating emerging infectious pathogens from similar pathogens are needed. In 2015, there was a MERS-CoV outbreak in Republic of Korea. During this outbreak, diagnostic platforms were urgently needed to di erentiate between MERS-CoV and HCoV to ensure specific treatment. To optimize the multiple-target sensing for MERS-CoV prior to use in clinical samples, T7 of in vitro-transcribed MERS-CoV and HCoV-OC43 RNA was prepared. Two sensing microrings for the MERS-CoV and HCoV primers were in the same waveguide. Subsequently, the RNA template of either MERS-CoV or HCoV was added onto the platform (Fig. 7.9A and B). To eliminate the background signal from non-target binding, we used the following equation: Using the MERS-CoV primers with the equation, amplified RNA from MERS-CoV was detected with no signal from HCoV from 5 to 30 min. Additionally, when using the HCoV primers, amplified RNA from HCoV was detected, while MERS-CoV was not (Fig. 7.9A and B). Further, the relative resonance wavelength shifts clearly distinguished positive and negative results when detecting multiple targets.

Finally, we analyzed RNAs from 20 clinical nasopharyngeal samples, including those of 11 MERS-CoV infected patients collected from July 2015 in Republic of Korea and 9 HCoV-OC43 infected patients (Fig. 7.9C and D). Patient samples were analyzed by quantitative real-time reverse transcription PCR (procedural time, 2–3 h) and the arch-shaped multiple-target sensing platform (procedural time, 20 min). For clinical testing (sensitivity and specificity) of the multiple-target sensing platform, we added RNA from MERS-CoV patients into the platform, which included immobilized primers with either MERS-CoV or HCoV on an individual sensing ring. The wavelength shifted to higher than 220.83 pm in the MERS-CoV sensing ring; however, the wavelength shifted to lower than 146.24 pm in the HCoV-OC43 sensing ring. In contrast, when the RNA of HCoV-OC43 patients was added, the wavelength shifted to higher than 220.29 pm in the HCoV-OC43 sensing ring and shifted to lower than 143.55 pm in the MERS-CoV sensing ring. These results confirm that the arch-shaped multiple-target sensing platform can accurately identify MERS-CoV or HCoV in clinical samples (Fig. 7.8 and 7.9, Table 7.2).

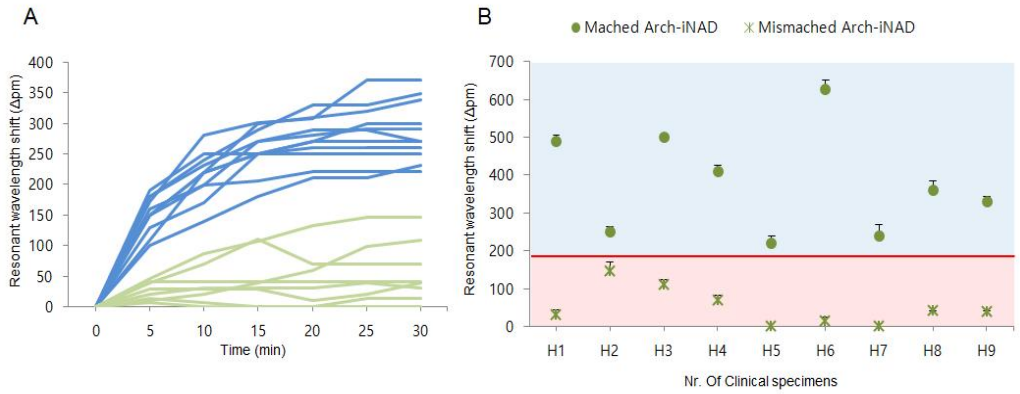

Figure 7.8. Arch-shaped multiple-target sensing in clinical samples. (A) Line graph showing resonant wavelength shift results of 11 MERS patient samples and 9 HCoV patient samples using the arch-shaped multiple-target sensing platform for MERS-CoV detection. (B) Dot graph showing the resonant wavelength shifts of 11 HCoV patient samples. Green circles represent results of HCoV target sensor with HCoV RNA (matched) and green asterisk represent results of MERS target sensor with HCoV RNA (mismatched). Colors represent positive (blue) and negative (red). Error bars indicate standard deviation of the mean based on at least 3 independent experiments.

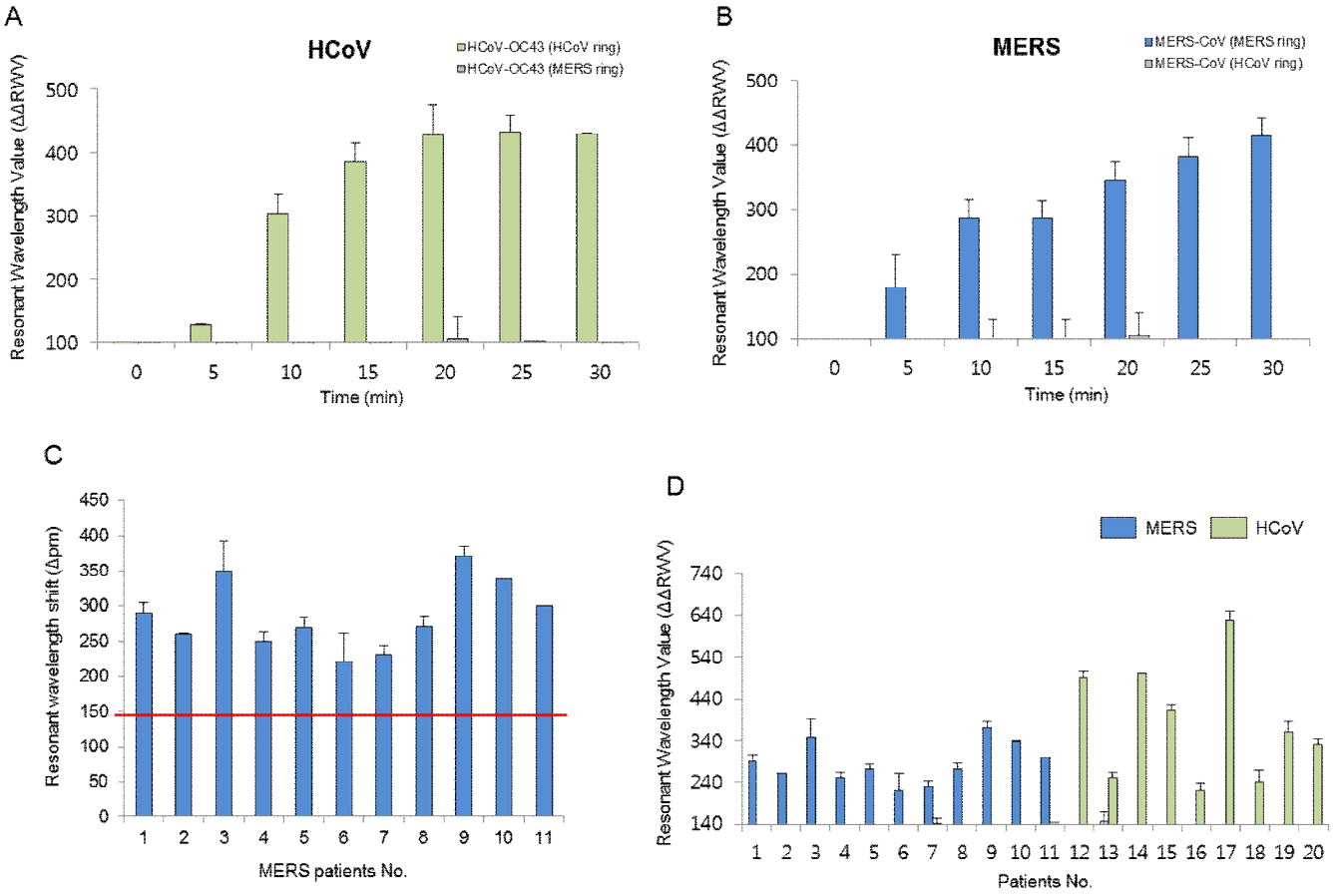
A
HCoV
HCoV-OC43 (HCoV ring)
HCoV-OC43 (MERS ring)
Resonant Wavelength Value (ΔΔRWV)
500
400
300
200
100
0
5
10
15
20
25
30
Time (min)
B
MERS
MERS-CoV (MERS ring)
MERS-CoV (HCoV ring)
Resonant Wavelength Value (ΔΔRWV)
500
400
300
200
100
0
5
10
15
20
25
30
Time (min)
C
Resonant wavelength shift (Δpm)
450
400
350
300
250
200
150
100
50
0
1
2
3
4
5
6
7
8
9
10
11
MERS patients No.
D
MERS
HCoV
Resonant Wavelength Value (ΔΔRWV)
740
640
540
440
340
240
140
1
2
3
4
5
6
7
8
9
10
11
12
13
14
15
16
17
18
19
20
Patients No.

Figure 7.9. Clinical utility of the arch-shaped multiple-target sensing platform in clinical specimens. (A–B) Multiple-target testing for detection of MERS-CoV and HCoV on different target specific primers immobilized on individual sensor microrings on an array. (A) Resonance wavelength value of HCoV into the platform. (B) Resonance wavelength value of MERS-CoV into the platform. (C) Analysis of 11 RNAs from clinical samples of MERS patients in 30 min. The red line represents the cut-off (criterion) for reporting a sample as virus (positive/negative). (D) Clinical diagnostic testing using 20 clinical samples, including 11 MERS patients (No. 1–11) and 9 HCoV patients (No. 12–20). Error bars indicate standard deviation of the mean based on at least 3 independent experiments.

Table 7.2. Comparison of the arch-shaped multiple-target sensor, previous single-target sensor and real-time RT-PCR assay

Contents		Arch-shaped Multiple targets	SMR Single target	Conventional Real-time PCR
Primer state	**Forward**	Immobilized	Immobilized	Soluble
	Reverse	Immobilized	Soluble	Soluble
Primer-Dimerization		X	△	○
Amplification method		Isothermal (38 - 43°C)	Isothermal (38 - 43°C)	Thermocycler (95°C ➔ 60°C ➔ 72°C)
Reaction time		20 min	20 min	2h
Detection		Label-free Real-time	Label-free Real-time	Fluorescence signal (Labeled)
Detection Limit (copies/reaction)	**MERS**	10^1	10^2	10^3
	ZIKV	10^2	NT	10^3
	EBOV	10^1	NT	10^3
	HCoV	10^1	10^2	10^3
Principle of Detection		Arch-shaped amplification (Label-free)	NT	Probe-based detection (Labeled)

NT: Not tested

7.4. Conclusion

Since the advent of solid-phase amplification technologies, asymmetric and bridge-based amplification approaches have been established. However, the amplification e ciency of these methods is too low for clinical use [157-159]. In this study, we developed a method for enhancing the sensitivity of solid-phase amplification approaches by using an optimal length (about 50 bp) and concentration (5 μM) of oligonucleotide primers within the SMR sensor device. Using this platform, inhibition due to primer-dimerization can be prevented during multiple-target detection. Further, we performed diagnostic and identification testing on the platform using several emerging infectious pathogens, such as MERS-CoV, HCoV, ZIKV, and EBOV. We compared the arch-shaped multiple-target sensing platform results to those obtained by PCR (Table 2). Based on the results, the platform showed high accuracy for detecting all pathogen types identified by PCR. Additionally, the detection limit of the platform was superior to that of the conventional method. Therefore, this method can be used for early diagnosis and identification of pathogens in low-level pathogen samples. This platform has advantages over the isothermal, PCR, and bio-optical sensing systems, particularly in terms of time (< 20 min) and label-free detection. Furthermore, the clinical utility of the platform for identifying multiple pathogens in clinical samples is useful for overcoming the limitations of conventional approaches. Further in–depth studies to maximize the clinical ability of the platform in larger prospective clinical trials are needed. Therefore, the arch-shaped multiple-target sensing platform can be used for rapid diagnosis and identification of pathogens in various clinical applications.

CONCLUSION

The POCT platform is emerging as a promising platform to provide timely, high-quality, and optimal clinical results for cancer and infectious diseases. The POCT platform should be prepared to meet the WHO guidelines (ASSURED: affordable, sensitive, specific, user friendly, rapid and robust, equipment-free, and deliverable) and is aimed at rapidly and accurately diagnosing diseases through qualitative and quantitative analysis of biomarkers such as nucleic acids, exosomes, proteins, and cells. In this study, we proposed the advanced disease diagnostic platform based on molecular diagnosis using bio-composite, microfluidic chip, and SMR biosensor.

The bio-composite and microfluidic platforms were used for sample preparation using small and large volume of clinical specimens. These platforms enable rapid and simple pathogen enrichment and nucleic acid extraction by electrostatic bonding with the negative charge of pathogen and nucleic acid and covalent bonding with amine group of nucleic acid. We showed that the bio-composite platform has high nucleic acid capture efficiency, and it is possible to extract high purity and quality of cell-free nucleic acid from plasma samples of colorectal and pancreatic cancer patients without a cell lysis step and special equipment. In addition, we showed that the microfluidic platform enables cell-free nucleic acid and pathogen enrichment and nucleic acid extraction based on high pathogen and nucleic acid capture efficiency from plasma and oral swab samples of tuberculosis patients. It was shown to have higher sensitivity than existing methods such as AFB smear, culture and Xpert for diagnosing active tuberculosis. Especially, when used in combination with IGRA, It seems to be a useful adjunct to current tests to diagnose active tuberculosis.

The bio-optical sensing platforms were used for detection using extracted nucleic acid from clinical specimens. These platforms enable rapid, label-free and real-time nucleic acid amplification/detection by using SMR sensor and isothermal amplification strategy. We showed that the SMR biosensor can detect Q fever from plasma samples of Q fever and other febrile diseases patients with high sensitivity within 10 min. In addition, we showed that improved bio-optical sensing platforms, CRISPR/dCas9-mediated biosensor and arch-

shaped multiple-target biosensor, have higher sensitivity and specificity by targeting the amplified nucleic acid using CRISPR/dCas9, enabling multiplex detection through arch-shaped nucleic acid amplification. The CRISPR/dCas9-mediated biosensor can clearly distinguish ST and SFTS from plasma samples within 20 min. The arch-shaped multiple-target biosensor can detect MERS-CoV in nasopharyngeal samples, including MERS-CoV and HCoV infections.

The advanced disease diagnostic platform proposed in this study has various advantages over conventional diagnostic methods as POCT and improved diagnostics. However, there are several issues that need to be solved in order to be used in clinical trial. First, it is necessary to further establish the clinical utility of the advanced disease diagnostic platform using various diseases specimens. Second, in vitro diagnostic medical device approval from the Ministry of Food and Drug Safety is required. Third, there is a need for miniaturization of the bio-optical sensor devices for use POCT. Fourth, diagnostic devices must work well even in poor environmental conditions and establish diagnostic criteria that can be clearly identified. Despite these issues, the advanced disease diagnostic platform has been shown by using various samples as an in vitro diagnostic platform that integrates sample preparation and nucleic acid amplification/detection and can replace existing techniques. We believe that the advanced disease diagnostic platform will play an important role in protecting our world from various diseases as POCT and more advanced diagnostic methods.

REFERENCES

[1] E. Crowley, F. Di Nicolantonio, F. Loupakis, A. Bardelli, Liquid biopsy: monitoring cancer-genetics in the blood, Nat Rev Clin Oncol, 10(2013) 472-84.

[2] H. Schwarzenbach, D.S. Hoon, K. Pantel, Cell-free nucleic acids as biomarkers in cancer patients, Nat Rev Cancer, 11(2011) 426-37.

[3] J.C.M. Wan, C. Massie, J. Garcia-Corbacho, F. Mouliere, J.D. Brenton, C. Caldas, et al., Liquid biopsies come of age: towards implementation of circulating tumour DNA, Nat Rev Cancer, 17(2017) 223-38.

[4] D. Han, R. Li, J. Shi, P. Tan, R. Zhang, J. Li, Liquid biopsy for infectious diseases: a focus on microbial cell-free DNA sequencing, Theranostics, 10(2020) 5501-13.

[5] P. Mandel, P. Metais, Nuclear Acids In Human Blood Plasma, C R Seances Soc Biol Fil, 142(1948) 241-3.

[6] S. El Messaoudi, F. Rolet, F. Mouliere, A.R. Thierry, Circulating cell free DNA: Preanalytical considerations, Clin Chim Acta, 424(2013) 222-30.

[7] S. Jahr, H. Hentze, S. Englisch, D. Hardt, F.O. Fackelmayer, R.D. Hesch, et al., DNA fragments in the blood plasma of cancer patients: quantitations and evidence for their origin from apoptotic and necrotic cells, Cancer Res, 61(2001) 1659-65.

[8] L.A. Diaz, Jr., A. Bardelli, Liquid biopsies: genotyping circulating tumor DNA, J Clin Oncol, 32(2014) 579-86.

[9] C. Alix-Panabieres, K. Pantel, Clinical Applications of Circulating Tumor Cells and Circulating Tumor DNA as Liquid Biopsy, Cancer Discov, 6(2016) 479-91.

[10] F. Diehl, K. Schmidt, M.A. Choti, K. Romans, S. Goodman, M. Li, et al., Circulating mutant DNA to assess tumor dynamics, Nat Med, 14(2008) 985-90.

[11] C. Bettegowda, M. Sausen, R.J. Leary, I. Kinde, Y. Wang, N. Agrawal, et al., Detection of circulating tumor DNA in early- and late-stage human malignancies, Sci Transl Med, 6(2014) 224ra24.

[12] M. Fleischhacker, B. Schmidt, Circulating nucleic acids (CNAs) and cancer--a survey, Biochim Biophys Acta, 1775(2007) 181-232.

[13] J.L. Park, H.J. Kim, B.Y. Choi, H.C. Lee, H.R. Jang, K.S. Song, et al., Quantitative analysis of cell-free DNA in the plasma of gastric cancer patients, Oncol Lett, 3(2012) 921-6.

[14] Z.H. Huang, L.H. Li, D. Hua, Quantitative analysis of plasma circulating DNA at diagnosis and during follow-up of breast cancer patients, Cancer Lett, 243(2006) 64-70.

[15] K.A. Yoon, S. Park, S.H. Lee, J.H. Kim, J.S. Lee, Comparison of circulating plasma DNA levels between lung cancer patients and healthy controls, J Mol Diagn, 11(2009) 182-5.

[16] O.A. Zill, C. Greene, D. Sebisanovic, L.M. Siew, J. Leng, M. Vu, et al., Cell-Free DNA Next-Generation Sequencing in Pancreatobiliary Carcinomas, Cancer Discov, 5(2015) 1040-8.

[17] G.R. Oxnard, C.P. Paweletz, Y. Kuang, S.L. Mach, A. O'Connell, M.M. Messineo, et al., Noninvasive detection of response and resistance in EGFR-mutant lung cancer using quantitative next-generation genotyping of cell-free plasma DNA, Clin Cancer Res, 20(2014) 1698-705.

[18] C. Perez-Barrios, I. Nieto-Alcolado, M. Torrente, C. Jimenez-Sanchez, V. Calvo, L. Gutierrez-Sanz, et al., Comparison of methods for circulating cell-free DNA isolation using blood from cancer patients: impact on biomarker testing, Transl Lung Cancer Res, 5(2016) 665-72.

[19] B. Koo, E. Jun, H. Liu, E.J. Kim, Y.Y. Park, S.B. Lim, et al., A biocomposite-based rapid sampling assay for circulating cell-free DNA in liquid biopsy samples from human cancers, Sci Rep, 10(2020) 14932.

[20] E. Takai, Y. Totoki, H. Nakamura, C. Morizane, S. Nara, N. Hama, et al., Clinical utility of circulating tumor DNA for molecular assessment in pancreatic cancer, Sci Rep, 5(2015) 18425.

[21] P. Rawla, T. Sunkara, A. Barsouk, Epidemiology of colorectal cancer: incidence, mortality, survival, and risk factors, Prz Gastroenterol, 14(2019) 89-103.

[22] J.D. Cohen, A.A. Javed, C. Thoburn, F. Wong, J. Tie, P. Gibbs, et al., Combined circulating tumor DNA and protein biomarker-based liquid biopsy for the earlier detection of pancreatic cancers, Proc Natl Acad Sci U S A, 114(2017) 10202-7.

[23] C.J. Punt, M. Koopman, L. Vermeulen, From tumour heterogeneity to advances in precision treatment of colorectal cancer, Nat Rev Clin Oncol, 14(2017) 235-46.

[24] J. Earl, S. Garcia-Nieto, J.C. Martinez-Avila, J. Montans, A. Sanjuanbenito, M. Rodriguez-Garrote, et al., Circulating tumor cells (Ctc) and kras mutant circulating free Dna (cfdna) detection in peripheral blood as biomarkers in patients diagnosed with exocrine pancreatic cancer, BMC Cancer, 15(2015) 797.

[25] F. Zhao, B. Koo, H. Liu, C. Eun Jin, Y. Shin, A single-tube approach for in vitro diagnostics using diatomaceous earth and optical sensor, Biosens Bioelectron, 99(2018) 443-9.

[26] H. Ehrlich, K.D. Demadis, O.S. Pokrovsky, P.G. Koutsoukos, Modern views on desilicification: biosilica and abiotic silica dissolution in natural and artificial environments, Chem Rev, 110(2010) 4656-89.

[27] S.J. Barrow, S. Kasera, M.J. Rowland, J. del Barrio, O.A. Scherman, Cucurbituril-Based Molecular Recognition, Chem Rev, 115(2015) 12320-406.

[28] Y. Luan, H. Liu, Z. Qiao, B. Koo, J. Shin, Y.O. Jang, et al., An enhanced recyclable 3D adsorbent for diverse bio-applications using biocompatible magnetic nanomulberry and cucurbituril composites, Sci Rep, 10(2020) 443.

[29] C.E. Jin, B. Koo, T.Y. Lee, K. Han, S.B. Lim, I.J. Park, et al., Simple and Low-Cost Sampling of Cell-Free Nucleic Acids from Blood Plasma for Rapid and Sensitive Detection of Circulating Tumor DNA, Adv Sci (Weinh), 5(2018) 1800614.

[30] B. Koo, C.E. Jin, S.Y. Park, T.Y. Lee, J. Nam, Y.R. Jang, et al., A rapid bio-optical sensor for diagnosing Q fever in clinical specimens, J Biophotonics, 11(2018) e201700167.

[31] B. Koo, C.E. Jin, M. Bae, Y.O. Jang, J.Y. Kim, S.H. Kim, et al., Detection of Coxiella burnetii Using Silicon Microring Resonator in Patient Blood Plasma, Micromachines (Basel), 10(2019).

[32] C.E. Jin, S.S. Yeom, B. Koo, T.Y. Lee, J.H. Lee, Y. Shin, et al., Rapid and accurate detection of KRAS mutations in colorectal cancers using the isothermal-based optical sensor for companion diagnostics, Oncotarget, 8(2017) 83860-71.

[33] H. Liu, F. Zhao, C.E. Jin, B. Koo, E.Y. Lee, L. Zhong, et al., Large Instrument- and Detergent-Free Assay for Ultrasensitive Nucleic Acids Isolation via Binary Nanomaterial, Anal Chem, 90(2018) 5108-15.

[34] M. Lapin, S. Oltedal, K. Tjensvoll, T. Buhl, R. Smaaland, H. Garresori, et al., Fragment size and level of cell-free DNA provide prognostic information in patients with advanced pancreatic cancer, J Transl Med, 16(2018) 300.

[35] N.A. Hussein, S.N. Mohamed, M.A. Ahmed, Plasma ALU-247, ALU-115, and cfDNA Integrity as Diagnostic and Prognostic Biomarkers for Breast Cancer, Appl Biochem Biotechnol, 187(2019) 1028-45.

[36] J. Marrugo-Ramirez, M. Mir, J. Samitier, Blood-Based Cancer Biomarkers in Liquid Biopsy: A Promising Non-Invasive Alternative to Tissue Biopsy, Int J Mol Sci, 19(2018).

[37] S. Volik, M. Alcaide, R.D. Morin, C. Collins, Cell-free DNA (cfDNA): Clinical Significance and Utility in Cancer Shaped By Emerging Technologies, Mol Cancer Res, 14(2016) 898-908.

[38] L. Mazutis, A.F. Araghi, O.J. Miller, J.C. Baret, L. Frenz, A. Janoshazi, et al., Droplet-based microfluidic systems for high-throughput single DNA molecule isothermal amplification and analysis, Anal Chem, 81(2009) 4813-21.

[39] M.M. Kiss, L. Ortoleva-Donnelly, N.R. Beer, J. Warner, C.G. Bailey, B.W. Colston, et al., High-throughput quantitative polymerase chain reaction in picoliter droplets, Anal Chem, 80(2008) 8975-81.

[40] D. Dressman, H. Yan, G. Traverso, K.W. Kinzler, B. Vogelstein, Transforming single DNA molecules into fluorescent magnetic particles for detection and enumeration of genetic variations, Proc Natl Acad Sci U S A, 100(2003) 8817-22.

[41] R. Lampignano, M.H.D. Neumann, S. Weber, V. Kloten, A. Herdean, T. Voss, et al., Multicenter Evaluation of Circulating Cell-Free DNA Extraction and Downstream Analyses for the Development of Standardized (Pre)analytical Work Flows, Clin Chem, 66(2020) 149-60.

[42] J. Virenfeldt, F. Rudolf, C. Camara, A. Furtado, V. Gomes, P. Aaby, et al., Treatment delay affects clinical severity of tuberculosis: a longitudinal cohort study, BMJ Open, 4(2014) e004818.

[43] Policy Statement: Automated Real-Time Nucleic Acid Amplification Technology for Rapid and Simultaneous Detection of Tuberculosis and Rifampicin Resistance: Xpert MTB/RIF System, Geneva, 2011.

[44] D. Falzon, H.J. Schunemann, E. Harausz, L. Gonzalez-Angulo, C. Lienhardt, E. Jaramillo, et al., World Health Organization treatment guidelines for drug-resistant tuberculosis, 2016 update, Eur Respir J, 49(2017).

[45] C.C. Boehme, P. Nabeta, D. Hillemann, M.P. Nicol, S. Shenai, F. Krapp, et al., Rapid molecular detection of tuberculosis and rifampin resistance, N Engl J Med, 363(2010) 1005-15.

[46] H.S. Lee, S.J. Kee, J.H. Shin, Y.S. Kwon, S. Chun, J.H. Lee, et al., Xpert MTB/RIF Assay as a Substitute for Smear Microscopy in an Intermediate-Burden Setting, Am J Respir Crit Care Med, 199(2019) 784-94.

[47] K.R. Steingart, I. Schiller, D.J. Horne, M. Pai, C.C. Boehme, N. Dendukuri, Xpert(R) MTB/RIF assay for pulmonary tuberculosis and rifampicin resistance in adults, Cochrane Database Syst Rev, (2014) CD009593.

[48] S.E. Dorman, S.G. Schumacher, D. Alland, P. Nabeta, D.T. Armstrong, B. King, et al., Xpert MTB/RIF Ultra for detection of Mycobacterium tuberculosis and rifampicin resistance: a prospective multicentre diagnostic accuracy study, Lancet Infect Dis, 18(2018) 76-84.

[49] C.H. Collins, J.M. Grange, Tuberculosis acquired in laboratories and necropsy rooms, Commun Dis Public Health, 2(1999) 161-7.

[50] A.R. Gregg, I.B. Van den Veyver, S.J. Gross, R. Madankumar, B.D. Rink, M.E. Norton, Noninvasive prenatal screening by next-generation sequencing, Annu Rev Genomics Hum Genet, 15(2014) 327-47.

[51] H.A. Parsons, J.A. Beaver, B.H. Park, Circulating Plasma Tumor DNA, Adv Exp Med Biol, 882(2016) 259-76.

[52] S. Holdenrieder, P. Stieber, Therapy control in oncology by circulating nucleosomes, Ann N Y Acad Sci, 1022(2004) 211-6.

[53] R. Placido, G. Mancino, A. Amendola, F. Mariani, S. Vendetti, M. Piacentini, et al., Apoptosis of human monocytes/macrophages in Mycobacterium tuberculosis infection, J Pathol, 181(1997) 31-8.

[54] E.S. Click, W. Murithi, G.S. Ouma, K. McCarthy, M. Willby, S. Musau, et al., Detection of Apparent Cell-free M. tuberculosis DNA from Plasma, Sci Rep, 8(2018) 645.

[55] R. Ushio, M. Yamamoto, K. Nakashima, H. Watanabe, K. Nagai, Y. Shibata, et al., Digital PCR assay detection of circulating Mycobacterium tuberculosis DNA in pulmonary tuberculosis patient plasma, Tuberculosis (Edinb), 99(2016) 47-53.

[56] Y.M. Lee, S.O. Lee, S.H. Choi, Y.S. Kim, J.H. Woo, D.Y. Kim, et al., A prospective longitudinal study evaluating the usefulness of the interferon-gamma releasing assay for predicting active tuberculosis in allogeneic hematopoietic stem cell transplant recipients, J Infect, 69(2014) 165-73.

[57] J.B. Selkon, S. Devadatta, K.G. Kulkarni, D.A. Mitchison, A.S. Narayana, C.N. Nair, et al., The Emergence of Isoniazid-Resistant Cultures in Patients with Pulmonary Tuberculosis during Treatment with Isoniazid Alone or Isoniazid Plus Pas, Bull World Health Organ, 31(1964) 273-94.

[58] A. Shafeque, J. Bigio, C.A. Hogan, M. Pai, N. Banaei, Fourth-Generation QuantiFERON-TB Gold Plus: What Is the Evidence?, J Clin Microbiol, 58(2020).

[59] D.M. Lewinsohn, M.K. Leonard, P.A. LoBue, D.L. Cohn, C.L. Daley, E. Desmond, et al., Official American Thoracic Society/Infectious Diseases Society of America/Centers for Disease Control and Prevention Clinical Practice Guidelines: Diagnosis of Tuberculosis in Adults and Children, Clin Infect Dis, 64(2017) e1-e33.

[60] C.E. Jin, B. Koo, E.Y. Lee, J.Y. Kim, S.H. Kim, Y. Shin, Simple and label-free pathogen enrichment via homobifunctional imidoesters using a microfluidic (SLIM) system for ultrasensitive pathogen detection in various clinical specimens, Biosens Bioelectron, 111(2018) 66-73.

[61] S.W. Lee, Y.A. Kang, C.E. Jin, H.C. Kim, G.S. Noh, H.J. Lee, et al., Gene-based diagnosis of tuberculosis with a new-generation pathogen enrichment technique, Eur Respir J, 55(2020).

[62] J.H. Park, C.E. Jin, B. Koo, J.S. Kwon, H.H. Cha, J.Y. Kim, et al., A Simple Microfluidic Assay for Diagnosing Tuberculous Meningitis in HIV-Uninfected Patients, J Clin Microbiol, 57(2019).

[63] C.E. Jin, B. Koo, H.J. Lee, I.J. Park, S.H. Kim, Y. Shin, Bis(sulfosuccinimidyl)suberate-Based Helix-Shaped Microchannels as Enhancers of Biomolecule Isolation from Liquid Biopsies, Anal Chem, 92(2020) 11994-2001.

[64] C.A. Ganoza, J.N. Ricaldi, J. Chauca, G. Rojas, C. Munayco, J. Agapito, et al., Novel hypertonic saline-sodium hydroxide (HS-SH) method for decontamination and concentration of sputum samples for Mycobacterium tuberculosis microscopy and culture, J Med Microbiol, 57(2008) 1094-8.

[65] Xpert MTB/RIF Implementation Manual: Technical and Operational 'How-To'; Practical Considerations, Geneva, 2014.

[66] C.M. Denkinger, S.G. Schumacher, C.C. Boehme, N. Dendukuri, M. Pai, K.R. Steingart, Xpert MTB/RIF assay for the diagnosis of extrapulmonary tuberculosis: a systematic review and meta-analysis, Eur Respir J, 44(2014) 435-46.

[67] J.P. Donnelly, S.C. Chen, C.A. Kauffman, W.J. Steinbach, J.W. Baddley, P.E. Verweij, et al., Revision and Update of the Consensus Definitions of Invasive Fungal Disease From the European Organization for Research and Treatment of Cancer and the Mycoses Study Group Education and Research Consortium, Clin Infect Dis, 71(2020) 1367-76.

[68] P.L. White, R.A. Barnes, J. Springer, L. Klingspor, M. Cuenca-Estrella, C.O. Morton, et al., Clinical Performance of Aspergillus PCR for Testing Serum and Plasma: a Study by the European Aspergillus PCR Initiative, J Clin Microbiol, 53(2015) 2832-7.

[69] Diagnostic Standards and Classification of Tuberculosis in Adults and Children. This official statement of the American Thoracic Society and the Centers for Disease Control and Prevention was adopted by the ATS Board of Directors, July 1999. This statement was

endorsed by the Council of the Infectious Disease Society of America, September 1999, Am J Respir Crit Care Med, 161(2000) 1376-95.

[70] O.H. Cho, K.H. Park, S.M. Kim, S.J. Park, S.M. Moon, Y.P. Chong, et al., Diagnostic performance of T-SPOT.TB for extrapulmonary tuberculosis according to the site of infection, J Infect, 63(2011) 362-9.

[71] J.Y. Kim, Y.A. Kang, J.H. Park, H.H. Cha, N.Y. Jeon, S.W. Lee, et al., An IFN-gamma and TNF-alpha dual release fluorospot assay for diagnosing active tuberculosis, Clin Microbiol Infect, 26(2020) 928-34.

[72] P.K. Drain, K.L. Bajema, D. Dowdy, K. Dheda, K. Naidoo, S.G. Schumacher, et al., Incipient and Subclinical Tuberculosis: a Clinical Review of Early Stages and Progression of Infection, Clin Microbiol Rev, 31(2018).

[73] E. Bouza, M.D. Diaz-Lopez, S. Moreno, J.C. Bernaldo de Quiros, T. Vicente, J. Berenguer, Mycobacterium tuberculosis bacteremia in patients with and without human immunodeficiency virus infection, Arch Intern Med, 153(1993) 496-500.

[74] C.C. Boehme, M.P. Nicol, P. Nabeta, J.S. Michael, E. Gotuzzo, R. Tahirli, et al., Feasibility, diagnostic accuracy, and effectiveness of decentralised use of the Xpert MTB/RIF test for diagnosis of tuberculosis and multidrug resistance: a multicentre implementation study, Lancet, 377(2011) 1495-505.

[75] A.S. Fauci, R.W. Eisinger, Reimagining the Research Approach to Tuberculosis(dagger), Am J Trop Med Hyg, 98(2018) 650-2.

[76] S. Shenai, D. Amisano, K. Ronacher, M. Kriel, P.P. Banada, T. Song, et al., Exploring alternative biomaterials for diagnosis of pulmonary tuberculosis in HIV-negative patients by use of the GeneXpert MTB/RIF assay, J Clin Microbiol, 51(2013) 4161-6.

[77] M.P. Nicol, K. Spiers, L. Workman, W. Isaacs, J. Munro, F. Black, et al., Xpert MTB/RIF testing of stool samples for the diagnosis of pulmonary tuberculosis in children, Clin Infect Dis, 57(2013) e18-21.

[78] M. Shah, C. Hanrahan, Z.Y. Wang, N. Dendukuri, S.D. Lawn, C.M. Denkinger, et al., Lateral flow urine lipoarabinomannan assay for detecting active tuberculosis in HIV-positive adults, Cochrane Database Syst Rev, (2016) CD011420.

[79] G.A. Engel, A.K. Wilbur, A. Westmark, D. Horn, J. Johnson, L. Jones-Engel, Naturally acquired Mycobacterium tuberculosis complex in laboratory pig-tailed macaques, Emerg Microbes Infect, 1(2012) e30.

[80] A.K. Wilbur, L.S. Kubatko, A.M. Hurtado, K.R. Hill, A.C. Stone, Vitamin D receptor gene polymorphisms and susceptibility M. tuberculosis in native Paraguayans, Tuberculosis (Edinb), 87(2007) 329-37.

[81] A.K. Wilbur, G.A. Engel, A. Rompis, A.P. IG, B.P. Lee, N. Aggimarangsee, et al., From the mouths of monkeys: detection of Mycobacterium tuberculosis complex DNA from buccal swabs of synanthropic macaques, Am J Primatol, 74(2012) 676-86.

[82] R.C. Wood, A.K. Luabeya, K.M. Weigel, A.K. Wilbur, L. Jones-Engel, M. Hatherill, et al., Detection of Mycobacterium tuberculosis DNA on the oral mucosa of tuberculosis patients, Sci Rep, 5(2015) 8668.

[83] A.K. Luabeya, R.C. Wood, J. Shenje, E. Filander, C. Ontong, S. Mabwe, et al., Noninvasive Detection of Tuberculosis by Oral Swab Analysis, J Clin Microbiol, 57(2019).

[84] Z.Y. Huo, L. Peng, Is Xpert MTB/RIF appropriate for diagnosing tuberculous pleurisy with pleural fluid samples? A systematic review, BMC Infect Dis, 18(2018) 284.

[85] N.C. Bahr, E. Nuwagira, E.E. Evans, F.V. Cresswell, P.V. Bystrom, A. Byamukama, et al., Diagnostic accuracy of Xpert MTB/RIF Ultra for tuberculous meningitis in HIV-infected adults: a prospective cohort study, Lancet Infect Dis, 18(2018) 68-75.

[86] G. Wang, S. Wang, G. Jiang, X. Yang, M. Huang, F. Huo, et al., Xpert MTB/RIF Ultra improved the diagnosis of paucibacillary tuberculosis: A prospective cohort study, J Infect, 78(2019) 311-6.

[87] P. Sands, C. Mundaca-Shah, V.J. Dzau, The Neglected Dimension of Global Security--A Framework for Countering Infectious-Disease Crises, N Engl J Med, 374(2016) 1281-7.

[88] B. Allegranzi, S. Bagheri Nejad, C. Combescure, W. Graafmans, H. Attar, L. Donaldson, et al., Burden of endemic health-care-associated infection in developing countries: systematic review and meta-analysis, Lancet, 377(2011) 228-41.

[89] A.M. Zaki, S. van Boheemen, T.M. Bestebroer, A.D. Osterhaus, R.A. Fouchier, Isolation of a novel coronavirus from a man with pneumonia in Saudi Arabia, N Engl J Med, 367(2012) 1814-20.

[90] M. Biava, F. Colavita, A. Marzorati, D. Russo, D. Pirola, A. Cocci, et al., Evaluation of a rapid and sensitive RT-qPCR assay for the detection of Ebola Virus, J Virol Methods, 252(2018) 70-4.

[91] J.L. Munoz-Jordan, Diagnosis of Zika Virus Infections: Challenges and Opportunities, J Infect Dis, 216(2017) S951-S6.

[92] S. Rao, A.C. Nyquist, Respiratory viruses and their impact in healthcare, Curr Opin Infect Dis, 27(2014) 342-7.

[93] M.L. Wilson, Malaria rapid diagnostic tests, Clin Infect Dis, 54(2012) 1637-41.

[94] F. Chappuis, S. Sundar, A. Hailu, H. Ghalib, S. Rijal, R.W. Peeling, et al., Visceral leishmaniasis: what are the needs for diagnosis, treatment and control?, Nat Rev Microbiol, 5(2007) 873-82.

[95] A. Zumla, D.S. Hui, S. Perlman, Middle East respiratory syndrome, Lancet, 386(2015) 995-1007.

[96] S. Yang, R.E. Rothman, PCR-based diagnostics for infectious diseases: uses, limitations, and future applications in acute-care settings, Lancet Infect Dis, 4(2004) 337-48.

[97] K.B. Barken, J.A. Haagensen, T. Tolker-Nielsen, Advances in nucleic acid-based diagnostics of bacterial infections, Clin Chim Acta, 384(2007) 1-11.

[98] Y. Mori, T. Notomi, Loop-mediated isothermal amplification (LAMP): a rapid, accurate, and cost-effective diagnostic method for infectious diseases, J Infect Chemother, 15(2009) 62-9.

[99] F.C. Huang, C.S. Liao, G.B. Lee, An integrated microfluidic chip for DNA/RNA amplification, electrophoresis separation and on-line optical detection, Electrophoresis, 27(2006) 3297-305.

[100] N. Agrawal, Y.A. Hassan, V.M. Ugaz, A pocket-sized convective PCR thermocycler, Angew Chem Int Ed Engl, 46(2007) 4316-9.

[101] J. Compton, Nucleic acid sequence-based amplification, Nature, 350(1991) 91-2.

[102] T. Notomi, H. Okayama, H. Masubuchi, T. Yonekawa, K. Watanabe, N. Amino, et al., Loop-mediated isothermal amplification of DNA, Nucleic Acids Res, 28(2000) E63.

[103] P.M. Lizardi, X. Huang, Z. Zhu, P. Bray-Ward, D.C. Thomas, D.C. Ward, Mutation detection and single-molecule counting using isothermal rolling-circle amplification, Nat Genet, 19(1998) 225-32.

[104] M. Vincent, Y. Xu, H. Kong, Helicase-dependent isothermal DNA amplification, EMBO Rep, 5(2004) 795-800.

[105] L. Lillis, D. Lehman, M.C. Singhal, J. Cantera, J. Singleton, P. Labarre, et al., Non-instrumented incubation of a recombinase polymerase amplification assay for the rapid and sensitive detection of proviral HIV-1 DNA, PLoS One, 9(2014) e108189.

[106] Y. Shin, A.P. Perera, K.W. Kim, M.K. Park, Real-time, label-free isothermal solid-phase amplification/detection (ISAD) device for rapid detection of genetic alteration in cancers, Lab Chip, 13(2013) 2106-14.

[107] Y. Shin, A.P. Perera, W.Y. Tang, D.L. Fu, Q. Liu, J.K. Sheng, et al., A rapid amplification/detection assay for analysis of Mycobacterium tuberculosis using an isothermal and silicon bio-photonic sensor complex, Biosens Bioelectron, 68(2015) 390-6.

[108] Q. Liu, J. Nam, S. Kim, C.T. Lim, M.K. Park, Y. Shin, Two-stage sample-to-answer system based on nucleic acid amplification approach for detection of malaria parasites, Biosens Bioelectron, 82(2016) 1-8.

[109] A.J. Baeumner, R.N. Cohen, V. Miksic, J. Min, RNA biosensor for the rapid detection of viable Escherichia coli in drinking water, Biosens Bioelectron, 18(2003) 405-13.

[110] Y. Yan, S. Ding, D. Zhao, R. Yuan, Y. Zhang, W. Cheng, Direct ultrasensitive electrochemical biosensing of pathogenic DNA using homogeneous target-initiated transcription amplification, Sci Rep, 6(2016) 18810.

[111] B. Koo, D.E. Kim, J. Kweon, C.E. Jin, S.H. Kim, Y. Kim, et al., CRISPR/dCas9-mediated biosensor for detection of tick-borne diseases, Sens Actuators B Chem, 273(2018) 316-21.

[112] B. Koo, K.H. Hong, C.E. Jin, J.Y. Kim, S.H. Kim, Y. Shin, Arch-shaped multiple-target sensing for rapid diagnosis and identification of emerging infectious pathogens, Biosens Bioelectron, 119(2018) 79-85.

[113] F. Banki, R.J. Mason, D. Oh, J.A. Hagen, S.R. DeMeester, J.C. Lipham, et al., Plasma DNA as a molecular marker for completeness of resection and recurrent disease in patients with esophageal cancer, Arch Surg, 142(2007) 533-8; discussion 8-9.

[114] D. Hessels, J.M. Klein Gunnewiek, I. van Oort, H.F. Karthaus, G.J. van Leenders, B. van Balken, et al., DD3(PCA3)-based molecular urine analysis for the diagnosis of prostate cancer, Eur Urol, 44(2003) 8-15; discussion -6.

[115] D. Malamud, Saliva as a diagnostic fluid, Dent Clin North Am, 55(2011) 159-78.

[116] G. Madico, T.C. Quinn, A. Rompalo, K.T. McKee, Jr., C.A. Gaydos, Diagnosis of Trichomonas vaginalis infection by PCR using vaginal swab samples, J Clin Microbiol, 36(1998) 3205-10.

[117] T.D. Kane, J.W. Alexander, J.A. Johannigman, The detection of microbial DNA in the blood: a sensitive method for diagnosing bacteremia and/or bacterial translocation in surgical patients, Ann Surg, 227(1998) 1-9.

[118] A. Lau, C. Halliday, S.C. Chen, E.G. Playford, K. Stanley, T.C. Sorrell, Comparison of whole blood, serum, and plasma for early detection of candidemia by multiplex-tandem PCR, J Clin Microbiol, 48(2010) 811-6.

[119] M. Sidstedt, J. Hedman, E.L. Romsos, L. Waitara, L. Wadso, C.R. Steffen, et al., Inhibition mechanisms of hemoglobin, immunoglobulin G, and whole blood in digital and real-time PCR, Anal Bioanal Chem, 410(2018) 2569-83.

[120] Y.T. Yeh, M. Nisic, X. Yu, Y. Xia, S.Y. Zheng, Point-of-care microdevices for blood plasma analysis in viral infectious diseases, Ann Biomed Eng, 42(2014) 2333-43.

[121] A. Akane, K. Matsubara, H. Nakamura, S. Takahashi, K. Kimura, Identification of the heme compound copurified with deoxyribonucleic acid (DNA) from bloodstains, a major inhibitor of polymerase chain reaction (PCR) amplification, J Forensic Sci, 39(1994) 362-72.

[122] P. Morata, M.I. Queipo-Ortuno, J. de Dios Colmenero, Strategy for optimizing DNA amplification in a peripheral blood PCR assay used for diagnosis of human brucellosis, J Clin Microbiol, 36(1998) 2443-6.

[123] W.A. Al-Soud, P. Radstrom, Purification and characterization of PCR-inhibitory components in blood cells, J Clin Microbiol, 39(2001) 485-93.

[124] J. Satsangi, D.P. Jewell, K. Welsh, M. Bunce, J.I. Bell, Effect of heparin on polymerase chain reaction, Lancet, 343(1994) 1509-10.

[125] A. Setiyono, M. Ogawa, Y. Cai, S. Shiga, T. Kishimoto, I. Kurane, New criteria for immunofluorescence assay for Q fever diagnosis in Japan, J Clin Microbiol, 43(2005) 5555-9.

[126] P.E. Fournier, T.J. Marrie, D. Raoult, Diagnosis of Q fever, J Clin Microbiol, 36(1998) 1823-34.

[127] M.M. de Rooij, F. Borlee, L.A. Smit, A. de Bruin, I. Janse, D.J. Heederik, et al., Detection of Coxiella burnetii in Ambient Air after a Large Q Fever Outbreak, PLoS One, 11(2016) e0151281.

[128] J. Elsa, O. Duron, B. Severine, D. Gonzalez-Acuna, K. Sidi-Boumedine, Molecular methods routinely used to detect Coxiella burnetii in ticks cross-react with Coxiella-like bacteria, Infect Ecol Epidemiol, 5(2015) 29230.

[129] T. Claes, W. Bogaerts, P. Bienstman, Vernier-cascade label-free biosensor with integrated arrayed waveguide grating for wavelength interrogation with low-cost broadband source, Opt Lett, 36(2011) 3320-2.

[130] J.Y. Kim, B. Koo, C.E. Jin, M.C. Kim, Y.P. Chong, S.O. Lee, et al., Rapid Diagnosis of Tick-Borne Illnesses by Use of One-Step Isothermal Nucleic Acid Amplification and Bio-Optical Sensor Detection, Clin Chem, 64(2018) 556-65.

[131] B. Koo, C.E. Jin, T.Y. Lee, J.H. Lee, M.K. Park, H. Sung, et al., An isothermal, label-free, and rapid one-step RNA amplification/detection assay for diagnosis of respiratory viral infections, Biosens Bioelectron, 90(2017) 187-94.

[132] M. Million, F. Thuny, H. Richet, D. Raoult, Long-term outcome of Q fever endocarditis: a 26-year personal survey, Lancet Infect Dis, 10(2010) 527-35.

[133] M. Bae, C.E. Jin, J.H. Park, M.J. Kim, Y.P. Chong, S.O. Lee, et al., Diagnostic usefulness of molecular detection of Coxiella burnetii from blood of patients with suspected acute Q fever, Medicine (Baltimore), 98(2019) e15724.

[134] Y.R. Jang, Y. Shin, C.E. Jin, B. Koo, S.Y. Park, M.C. Kim, et al., Molecular detection of Coxiella burnetii from the formalin-fixed tissues of Q fever patients with acute hepatitis, PLoS One, 12(2017) e0180237.

[135] H. Kim, J.S. Kim, A guide to genome engineering with programmable nucleases, Nat Rev Genet, 15(2014) 321-34.

[136] P.D. Hsu, E.S. Lander, F. Zhang, Development and applications of CRISPR-Cas9 for genome engineering, Cell, 157(2014) 1262-78.

[137] T. Gaj, C.A. Gersbach, C.F. Barbas, 3rd, ZFN, TALEN, and CRISPR/Cas-based methods for genome engineering, Trends Biotechnol, 31(2013) 397-405.

[138] A.A. Dominguez, W.A. Lim, L.S. Qi, Beyond editing: repurposing CRISPR-Cas9 for precision genome regulation and interrogation, Nat Rev Mol Cell Biol, 17(2016) 5-15.

[139] O. Shalem, N.E. Sanjana, F. Zhang, High-throughput functional genomics using CRISPR-Cas9, Nat Rev Genet, 16(2015) 299-311.

[140] R. Barrangou, C. Fremaux, H. Deveau, M. Richards, P. Boyaval, S. Moineau, et al., CRISPR provides acquired resistance against viruses in prokaryotes, Science, 315(2007) 1709-12.

[141] L.S. Qi, M.H. Larson, L.A. Gilbert, J.A. Doudna, J.S. Weissman, A.P. Arkin, et al., Repurposing CRISPR as an RNA-guided platform for sequence-specific control of gene expression, Cell, 152(2013) 1173-83.

[142] L.A. Gilbert, M.H. Larson, L. Morsut, Z. Liu, G.A. Brar, S.E. Torres, et al., CRISPR-mediated modular RNA-guided regulation of transcription in eukaryotes, Cell, 154(2013) 442-51.

[143] S.H. Lee, J. Yu, G.H. Hwang, S. Kim, H.S. Kim, S. Ye, et al., CUT-PCR: CRISPR-mediated, ultrasensitive detection of target DNA using PCR, Oncogene, 36(2017) 6823-9.

[144] K. Pardee, A.A. Green, M.K. Takahashi, D. Braff, G. Lambert, J.W. Lee, et al., Rapid, Low-Cost Detection of Zika Virus Using Programmable Biomolecular Components, Cell, 165(2016) 1255-66.

[145] J.S. Gootenberg, O.O. Abudayyeh, J.W. Lee, P. Essletzbichler, A.J. Dy, J. Joung, et al., Nucleic acid detection with CRISPR-Cas13a/C2c2, Science, 356(2017) 438-42.

[146] A. East-Seletsky, M.R. O'Connell, S.C. Knight, D. Burstein, J.H. Cate, R. Tjian, et al., Two distinct RNase activities of CRISPR-C2c2 enable guide-RNA processing and RNA detection, Nature, 538(2016) 270-3.

[147] J.S. Chen, E. Ma, L.B. Harrington, M. Da Costa, X. Tian, J.M. Palefsky, et al., CRISPR-Cas12a target binding unleashes indiscriminate single-stranded DNase activity, Science, 360(2018) 436-9.

[148] J.S. Gootenberg, O.O. Abudayyeh, M.J. Kellner, J. Joung, J.J. Collins, F. Zhang, Multiplexed and portable nucleic acid detection platform with Cas13, Cas12a, and Csm6, Science, 360(2018) 439-44.

[149] J.C. Snyder, M.M. Bateson, M. Lavin, M.J. Young, Use of cellular CRISPR (clusters of regularly interspaced short palindromic repeats) spacer-based microarrays for detection of viruses in environmental samples, Appl Environ Microbiol, 76(2010) 7251-8.

[150] P. Perez-Pinera, D.D. Kocak, C.M. Vockley, A.F. Adler, A.M. Kabadi, L.R. Polstein, et al., RNA-guided gene activation by CRISPR-Cas9-based transcription factors, Nat Methods, 10(2013) 973-6.

[151] D. Balboa, J. Weltner, S. Eurola, R. Trokovic, K. Wartiovaara, T. Otonkoski, Conditionally Stabilized dCas9 Activator for Controlling Gene Expression in Human Cell Reprogramming and Differentiation, Stem Cell Reports, 5(2015) 448-59.

[152] D. Kim, S. Bae, J. Park, E. Kim, S. Kim, H.R. Yu, et al., Digenome-seq: genome-wide profiling of CRISPR-Cas9 off-target effects in human cells, Nat Methods, 12(2015) 237-43, 1 p following 43.

[153] S.Y. Seong, M.S. Choi, I.S. Kim, Orientia tsutsugamushi infection: overview and immune responses, Microbes Infect, 3(2001) 11-21.

[154] Y. Yun, S.T. Heo, G. Kim, R. Hewson, H. Kim, D. Park, et al., Phylogenetic Analysis of Severe Fever with Thrombocytopenia Syndrome Virus in South Korea and Migratory Bird Routes Between China, South Korea, and Japan, Am J Trop Med Hyg, 93(2015) 468-74.

[155] O. Piepenburg, C.H. Williams, D.L. Stemple, N.A. Armes, DNA detection using recombination proteins, PLoS Biol, 4(2006) e204.

[156] Z. Guo, R.A. Guilfoyle, A.J. Thiel, R. Wang, L.M. Smith, Direct fluorescence analysis of genetic polymorphisms by hybridization with oligonucleotide arrays on glass supports, Nucleic Acids Res, 22(1994) 5456-65.

[157] M. Fedurco, A. Romieu, S. Williams, I. Lawrence, G. Turcatti, BTA, a novel reagent for DNA attachment on glass and efficient generation of solid-phase amplified DNA colonies, Nucleic Acids Res, 34(2006) e22.

[158] C. Adessi, G. Matton, G. Ayala, G. Turcatti, J.J. Mermod, P. Mayer, et al., Solid phase DNA amplification: characterisation of primer attachment and amplification mechanisms, Nucleic Acids Res, 28(2000) E87.

[159] J. Shendure, H. Ji, Next-generation DNA sequencing, Nat Biotechnol, 26(2008) 1135-45.

국문요약

연구 목적

암이나 신변종감염병의 빠르고 정확한 진단은 추가 감염 예방 및 환자 모니터링, 신속한 치료를 위하여 매우 중요하다. 특히 암 돌연변이나 감염의 심각성 정도에 따라 개별적인 증상 패턴이 다를 수 있기 때문에 정확한 질병 진단을 통한 최적화된 치료가 필수적이다. 현재 빠르고 정확한 진단을 위해 기존의 진단방법을 보완한 새로운 진단방법이 연구되고 있지만, 실제 현장에서 사용되는 진단방법들은 한정되어 있다. 또한 의료 현장에서 실시되는 의료기술들은 대부분 시간이 오래 걸리고 복잡하며 대형 장비가 필요하다. 또한 민감도가 낮고 다중표적 검출 특이도가 낮은 단점들이 존재한다. 본 연구는 기존에 사용되는 진단방법의 한계를 극복하기 위하여 저비용 기능성 바이오 물질을 이용한 첨단 질병 진단 플랫폼을 개발하였다.

연구 방법

색션 1 에서는 저비용 기능성 바이오 물질을 이용한 샘플 전처리 플랫폼을 제시하였다. 샘플 전처리는 나노바이오합성물과 미세유체 플랫폼을 이용한 빠르고 간단한 cfNA 샘플링과 미세유체 플랫폼을 이용한 병원체 농축 및 핵산 추출 연구를 진행하였다. 샘플 전처리 플랫폼의 검증을 위하여 총 366 개의 임상 검체를 분석하였다. 구체적으로는 나노바이오합성물을 이용한 cfNA 샘플링에는 13 개의 혈장 샘플 (3 대장암, 10 췌장암), 미세유체 플랫폼을 이용한 cfNA 샘플링에는 81 개의 혈장 샘플 (40 결핵, 41 비결핵) 및 미세유체 플랫폼을 이용한 병원체 농축 및 핵산 추출에는 272 개의 경구스왑 샘플 (128 결핵, 144 비결핵)을 이용하였다..

색션 2 에서는 첨단 바이오 광학 센싱 플랫폼을 제시하였다. 바이오 광학 센싱은 실리콘 마이크로링 공진기 센서를 기반으로 한 표지가 필요 없는 실시간 핵산 등온 증폭 및 검출 바이오 광학 센서와 CRISPR/dCas9 을 결합한 개선된 바이오 광학 센서 및 아치형 증폭 기반의 다중 검출 센서 연구를 진행하였다. 바이오 광학 센싱 플랫폼의 검증을 위해 총 61 개의 임상 검체를 분석하였다. 바이오 광학 센서에는 35 개의 혈장 샘플 (16 큐열, 19 다른 열성 질환), CRISPR/dCas9 을 결합한 개선된 바이오 광학

센서에는 6 개의 혈장 샘플 (3 쯔쯔가무시, 3 중증 열성 혈소판감소 증후군), 아치형 증폭 기반의 다중 검출 센서에는 20 개의 비인두 샘플 (11 메르스, 9 인간 코로나 바이러스)을 이용하였다.

연구 결과

나노바이오합성물을 이용하여 genomic DNA 및 DNA 증폭 산물 (777, 525 및 150 bp)과의 핵산결합력을 확인한 결과, 높은 핵산 캡쳐 효율(86.78–90.26%)을 보였으며, cell lysis 단계와 특정 장비 필요 없이 13 개의 암 환자 혈장 샘플에서 고순도 및 고농도의 cfDNA 샘플링이 가능함을 확인하였다. 미세유체 플랫폼을 이용한 cfDNA 샘플링 결과 81 개의 결핵 의심 환자 샘플에서 높은 민감도(80.0%) 및 특이도(78.1%)를 보임을 확인하였으며, 기존에 사용하고 있는 결핵 진단 방법인 항산균 도말검사(31.6%), Xpert MTB/RIF(61.1%) 및 배양 방법(65.8%)보다 높은 민감도를 가짐을 확인하였다. 또한 IGRA 의 민감도(80.6%) 및 특이도 (71.4%)와 비슷하였으며, 두 분석 방법을 같이 사용하였을 때 더 높은 민감도(94.4%)를 보임을 확인하였다. 미세유체 플랫폼을 이용한 병원체 농축 및 DNA 추출 결과 272 개의 결핵 의심 환자 샘플에서 높은 민감도(65.6%)및 특이도(86.1%)를 보임을 확인하였으며, 기존에 사용하고 있는 결핵 진단 방법인 Xpert MTB/RIF(43.4%)보다 높은 민감도를 가짐을 확인하였다. 또한 도말음성, 배양양성 샘플 및 배양음성 샘플에서 미세유체 플랫폼(각각 64.6%, 69.0%)이 Xpert MTB/RIF(각각 53.7%, 7.4%)보다 더 높은 민감도를 보임을 확인하였다.

바이오 광학 센서를 이용하여 16 개의 큐열 환자 샘플 및 19 개의 다른 열성 질환 환자 샘플을 확인하였을 때 높은 민감도(87.5%) 및 특이도(89.5%)를 가지며 10 분 이내에 검출이 가능하였다. CRISPR/dCas9 을 결합한 개선된 바이오 광학 센서를 이용하여 3 개의 쯔쯔가무시 및 3 개의 중증 열성 혈소판감소 증후군 환자 샘플을 확인한 결과 단일 분자 수준의 검출한계 (0.54–0.63 aM)를 가짐을 확인하였으며, 20 분 이내에 두 질병의 명확한 검출도 가능함을 확인하였다. 또한 기존 검출 방법인 real-time PCR 보다 100 배 더 민감함을 확인하였다. 아치형 증폭 기반의 다중 검출 센서를 이용하여 검출한계를 확인한 결과 10–100 copies 의 검출한계를 가짐을 확인하였으며 T7 RNAs (메르스, 지카, 에볼라)를 이용하였을 때 다중 검출이 가능함을 확인하였다.

또한 11 개의 메르스 환자 샘플 및 9 개의 인간코로나바이러스 환자 샘플에서 20 분 이내에 두 질병의 명확한 검출이 가능함을 확인하였다.

결론

본 연구에서는 저비용 기능성 바이오 물질을 이용한 첨단 질병 진단 플랫폼을 제안하였다. 이 플랫폼은 나노바이오합성물과 미세유체 플랫폼을 이용한 샘플 전처리 섹션과 바이오 광학 센서, CRISPR/dCas9 을 결합한 개선된 바이오 광학 센서 및 아치형 증폭 기반의 다중 검출 센서를 이용한 검출 섹션으로 구성되었다. 본 연구를 통해 해당 플랫폼이 임상 응용 분야에서 암 및 신변종 감염병의 빠르고 정확한 진단을 위해 활용될 수 있을 것으로 기대한다.